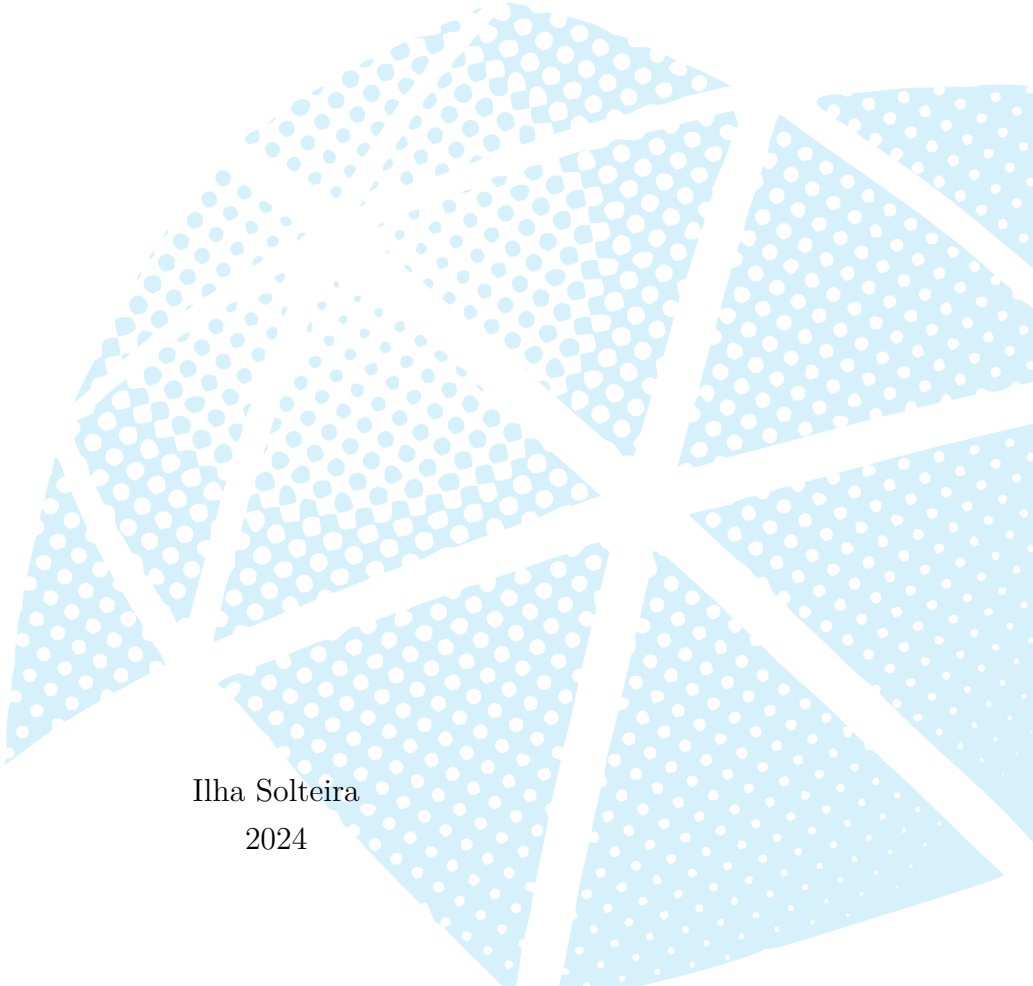
UNIVERSIDADE ESTADUAL PAULISTA "JÚLIO DE MESQUITA FILHO"
CÂMPUS DE ILHA SOLTEIRA
DEPARTAMENTO DE ENGENHARIA MECÂNICA

HENRIQUE CORDEIRO NOVAIS

CO-KRIGING MODELING FOR STRUCTURAL HEALTH MONITORING APPLICATIONS



Ilha Solteira
2024

UNIVERSIDADE ESTADUAL PAULISTA
"JÚLIO DE MESQUITA FILHO"
Campus de Ilha Solteira

HENRIQUE CORDEIRO NOVAIS

CO-KRIGING MODELING FOR STRUCTURAL HEALTH MONITORING APPLICATIONS

Dissertation presented to the São Paulo State University (UNESP), School of Engineering, Ilha Solteira, as part of the requirements for obtaining the Master degree in Mechanical Engineering.

Knowledge Area: Dynamic Systems.

Prof. Dr. Samuel da Silva
Supervisor

Ilha Solteira
2024

FICHA CATALOGRÁFICA
Desenvolvido pelo Serviço Técnico de Biblioteca e Documentação

N936c

Novais, Henrique Cordeiro.
Co-kriging modeling for structural health monitoring applications / Henrique Cordeiro Novais. -- Ilha Solteira: [s.n.], 2024
93 f. : il.

Dissertação (mestrado) - Universidade Estadual Paulista. Faculdade de Engenharia de Ilha Solteira. Área de conhecimento: Mecânica dos Sólidos, 2024

Orientador: Samuel da Silva

Inclui bibliografia

1. Co-kriging. 2. Gaussian process regression. 3. Structural Health Monitoring (SHM). 4. Composite laminates. 5. Damage quantification.

Amanda Sertori dos Santos
Bibliotecária - CRB/8-9061
Seção Técnica de Referência, Atendimento ao Usuário e Documentação
Diretoria Técnica de Biblioteca e Documentação

UNIVERSIDADE ESTADUAL PAULISTA

Câmpus de Ilha Solteira

CERTIFICADO DE APROVAÇÃO

TÍTULO DA DISSERTAÇÃO: CO-KRIGING MODELING FOR STRUCTURAL HEALTH MONITORING APPLICATIONS

AUTOR: HENRIQUE CORDEIRO NOVAIS
ORIENTADOR: SAMUEL DA SILVA

Aprovado como parte das exigências para obtenção do Título de Mestre em Engenharia Mecânica, área: Mecânica dos Sólidos pela Comissão Examinadora:

Prof. Dr. SAMUEL DA SILVA (Participaçao Virtual)
Departamento de Engenharia Mecanica / Faculdade de Engenharia de Ilha Solteira - UNESP

Prof. Dr. VOLNEI TITA (Participaçao Virtual)
Escola de Engenharia de São Carlos / Universidade de São Paulo - USP

Prof. Dr. FLÁVIO DE ANDRADE SILVA (Participaçao Virtual)
Pontifícia Universidade Católica do Rio de Janeiro - PUC

Ilha Solteira, 25 de novembro de 2024

This work is dedicated to my family, whose unwavering support and love have been my greatest strength.

ACKNOWLEDGEMENTS

First and foremost, I would like to express my gratitude to God for being with me throughout every phase of this journey, providing me with the courage and patience to face challenges and persevere in my academic life.

I would also like to thank my family, especially my parents, Edvan and Lucinéia, my grandparents Terezinha and Luiz (wherever he may be), and my brother Leonardo, who has always motivated me to continue my studies and has been my greatest support throughout this entire process. If I have reached this point today, it is because they have always encouraged me to improve each day.

I am grateful to Prof. Samuel for the teachings and support he provided throughout this work, for encouraging me to always give my best, and for his patience, valuable advice, encouragement, and friendship during the completion of this dissertation. This would not have been possible without his support, and I am very thankful for it. I would also like to extend my deepest gratitude to Prof. Jean-François Deü and Prof. Christophe Hoareau for their invaluable contributions to my work and for their support during my time at the Conservatoire National des Arts et Métiers (CNAM) in Paris. It was an incredible experience that greatly enriched this research and my life, offering valuable experiences during my time abroad.

I want to express my gratitude to my lab colleagues at the SHM Lab, whom I am honored and happy to call friends. I will always carry the lessons, discussions, and fun we shared throughout this journey. The process over the past two years has been much easier, thanks to all of you (and the coffee in the break room). I would also like to thank my rock and roll partners from the band "Os Qu4térnî²os". I will always fondly remember the shows and events we performed, which made the academic environment more enjoyable, lively, and, of course, a little noisy.

I also thank the São Paulo Research Foundation (FAPESP) for making all this possible through their financial support under grants 22/12575-7 and 23/14432-1.

Finally, I would like to thank everyone who, in one way or another, whether directly or indirectly, contributed to my education. Thank you very much!

"Don't adventures ever have an end? I suppose not. Someone else always has to carry on the story"

J.R.R. Tolkien

ABSTRACT

Computational modeling plays a crucial role in applied science and engineering, offering valuable insights into the behavior of structures and mechanical systems. However, the complexity and significant execution time required for these models can limit their applicability in real-world scenarios. To mitigate these challenges, metamodeling, or surrogate modeling, provides a practical solution by substituting the complex model with a simplified function that mimics its behavior, thereby substantially reducing evaluation time. One widely applied method is Gaussian Process Regression (GPR), also known as Kriging, which has proven effective in various structural health monitoring applications. However, achieving accurate predictions for damage-sensitive variables often requires extensive historical data or well-calibrated structural models, which can be costly. Thus, this dissertation proposes applying the co-Kriging method, a multivariate extension of ordinary Kriging that leverages the covariance between two or more related datasets, making it particularly advantageous when the co-variable is more economical to measure than the target variable. This work presents two distinct applications: the first focuses on a concrete bridge, using natural frequencies under different temperature conditions to develop the co-Kriging model; the second application pertains to composite structures, where simulated Lamb wave data is combined with experimental tests to detect and quantify delamination in laminates. In both applications, the co-Kriging method showcased its reliability and superiority over Kriging, offering an efficient means of enhancing prediction accuracy while minimizing data acquisition costs.

Keywords: co-Kriging; gaussian process regression; Structural Health Monitoring (SHM); composite laminates; damage quantification

RESUMO

A modelagem computacional desempenha um papel crucial nas áreas de ciência aplicada e engenharia, proporcionando conhecimentos valiosos sobre o comportamento de estruturas e sistemas mecânicos. No entanto, a complexidade e o tempo significativo necessários para a execução desses modelos podem limitar sua aplicabilidade em cenários reais. Para mitigar esses desafios, a metamodelagem, ou modelagem substitutiva, oferece uma solução prática ao substituir o modelo complexo por uma função simplificada que imita seu comportamento, reduzindo substancialmente o tempo de avaliação. Um dos métodos amplamente aplicados é a Regressão po Processo Gaussiano (*Gaussian Process Regression* - GPR), também conhecida como Kriging, que se mostra eficaz em diversas aplicações de monitoramento de integridade estrutural. Entretanto, obter predições precisas para variáveis sensíveis a danos frequentemente requer uma grande quantidade de dados históricos ou modelos estruturais bem calibrados, o que pode ser oneroso. Assim, esta dissertação propõe a aplicação do método de co-Kriging, uma extensão multivariada do Kriging ordinário que aproveita a covariância entre dois ou mais conjuntos de dados relacionados, sendo especialmente vantajoso quando a co-variável é mais econômica de medir do que a variável-alvo. Este trabalho apresenta duas aplicações distintas: a primeira enfoca uma ponte de concreto, utilizando frequências naturais sob diferentes condições térmicas para desenvolver o modelo de co-Kriging; a segunda aplicação refere-se a estruturas em material compósito, onde dados simulados de ondas Lamb são combinados com testes experimentais para detectar e quantificar a delaminação em laminados. Em ambas as aplicações, o método de co-Kriging evidenciou sua confiabilidade e superioridade em comparação ao Kriging, oferecendo um meio eficiente de melhorar a precisão das predições ao mesmo tempo em que minimiza os custos de aquisição de dados.

Keywords: co-Kriging; regressão por processo gaussiano; Monitoramento de Integridade Estrutural; compósitos laminados; quantificação de danos

LIST OF FIGURES

Figure 1 – Variable measurement locations for co-Kriging strategy. 23
Figure 2 – Representation of the confidence interval convergence at known points from the Markov property. 25
Figure 3 – Expensive data of the one variable function example. 29
Figure 4 – Kriging prediction through expensive points y_e. 29
Figure 5 – Kriging prediction increasing the number of y_e points. 30
Figure 6 – Cheap and expensive data of the one variable example. 31
Figure 7 – Comparison of Kriging and co-Kriging predictions through the one variable function example. 31
Figure 8 – Cheap and expensive data of the co-Kriging regression example. 33
Figure 9 – Performance of Kriging regression using expensive observations. 34
Figure 10 – Performance of co-Kriging regression combining both expensive and cheap datasets. 35
Figure 11 – Flowchart illustrating the proposed framework for enhanced bridge structural health variables predictions using a Co-Kriging strategy. . . 39
Figure 12 – Z24 bridge benchmark including the front view (bottom) and a cross-section of the girder, highlighting the locations where temperature measurements were taken (top-right). 40
Figure 13 – Correlation of the first two natural frequencies versus ambient temperature under undamaged conditions. 41
Figure 14 – First two natural frequencies of the Z24 bridge under healthy and damaged conditions. 42
Figure 15 – Hybrid data of the relationship between 2nd natural frequency and ambient temperature in the healthy condition. 44
Figure 16 – Co-Kriging model performance trained with numerical and experimental samples and tested with a database including healthy and damaged scenarios. 44
Figure 17 – Effects of delamination damage on output signals from a composite plate. 51
Figure 18 – Illustration of feature space. 55
Figure 19 – Illustrative example of damage feature extraction using autoregressive models combined with Mahalanobis Distance for damage classification. 56

Figure 20 – Graphical abstract depicting the proposed framework for cost-effective damage detection and quantification in composites utilizing hybrid data in a co-Kriging regression model. 57
Figure 21 – Schematic representation of CONCEPT. 58
Figure 22 – Schematic representation of CONCEPT. 59
Figure 23 – Experimental results for PZT2 signals under different conditions. (a) Healthy signals at different temperature conditions; (b) zoomed-in view of the signal in (a); (c) comparison between healthy and progressive damage signals at the same temperature; and (d) comparison of the same damage condition at different temperatures. 60
Figure 24 – Visualization of the FE model within the PZTs region. 61
Figure 25 – Visualization of the FE model within the excitation signal on PZT1. . . 62
Figure 26 – Sample size for model convergence. 64
Figure 27 – Comparison between experimental and numerical curves in the healthy condition under different temperature conditions. 64
Figure 28 – Comparison between experimental and numerical curves in the same temperature under different damage conditions. 65
Figure 29 – Experimental and numerical output signals available for the proposed methodology. 66
Figure 30 – Baseline measured and predicted experimental signals by AR and autocorrelation of residuals for model's validation. 67
Figure 31 – Damage sensitive features extracted from autoregressive models estimated based on experimental and numerical output signals. 68
Figure 32 – Damage index computed for all temperature conditions for both experimental and numerical datasets. 69
Figure 33 – Performance comparison between Kriging and co-Kriging predictions for damage indices at T = 30°C. 69
Figure 34 – Comparison of Kriging and co-Kriging performance in estimating delamination areas considering temperature effects. 71

LIST OF TABLES

Table 1 – Damage progression scenarios for the Z24 bridge in 1998. 42
Table 2 – Classification performance for damage detection using all four approaches regarding Type I and Type II errors. 45
Table 3 – Structural conditions tested for the carbon-epoxy laminate. 60
Table 4 – Mechanical properties for the materials at T = 30°C. 63
Table 5 – Distribution of training and testing data for Kriging and co-Kriging models. 70

LIST OF SYMBOLS

$\mathrm{A}(\%)$	- Delamination area
A_0	- Anti-symmetric mode
$\mathbf{A_B}$	- AR coefficients vector in the baseline condition
$\mathbf{A}_{\text{ident}}$	- AR coefficients vector identified in an unknown condition
a_r	- AR coefficients
$\beta^T f(x)$	- Mean value of the Gaussian distribution
$\mathcal{C}$	- Co-Kriging covariance matrix
$\mathcal{D}^2$	- Mahalanobis squared distance
$Ds_{i(i=1...7)}$	- Experimental size of delamination damage
$\mathcal{DI}$	- Damage index
Δx	- Maximum element size
Δt	- Integration time step
$e(k)$	- Residual error with zero mean
$\mathbf{e_B}$	- Residual errors vector in the baseline condition
$\mathbf{e}_{\text{ident}}$	- Residual errors vector identified in an unknown condition
E_1	Young's modulus in the fiber direction
E_2	Young's modulus in the direction perpendicular to the fibers
f_c	- Cheap function
f_e	- Expensive function
f_{max}	- Maximum frequency expected in the simulation
G_{12}	- Shear modulus in-plane
G_{23}	- Shear modulus out-of-plane

λ_c - Co-Kriging regression constant associated to the cheap data

λ_e - Co-Kriging regression constant associated to the expensive data

λ_{min} - Shortest wavelength of interest

$\mathcal{M}$ - Model output

n_r - Number of past samples

ψ - Correlation function

$\mathbf{\Psi}$ - Matrix of correlations between the expensive and/or cheap data

p_c - Co-Kriging hyper-parameter associated to the cheap model

p_d - Co-Kriging hyper-parameter associated to the difference model

r^2 - Correlation coefficient between the expensive and cheap datasets

ρ - Composite material density

ρ' - Scaling factor

σ^2 - Variance

Σ - Covariance matrix of the training data in the baseline condition associated with Mahalanobis squared distance

S_0 - Symmetric mode

θ - Hyper-parameter vector of kernel function

θ_c - Co-Kriging hyper-parameter associated to the cheap model

θ_d - Co-Kriging hyper-parameter associated to the difference model

ν_{12} - Poisson's ratio

$x(k)$ - Discretized time series

$\mathbf{X}$ - Test matrix

$\mathcal{X}_1, \mathcal{X}_2$ - Damage-sensitive features

$\mathcal{X}_c$ - Vector containing all the x-coordinate points of the cheap data

$\mathcal{X}_e$ - Vector containing all the x-coordinate points of the expensive data

$\mathcal{Y}_c$ - Vector containing all the y-coordinate points of the cheap data

$\mathcal{Y}_e$ - Vector containing all the y-coordinate points of the expensive data

$\mathcal{Z}(.,.)$ - Zero mean, unit variance and a stationary Gaussian process

$\bar{\mathbf{Z}}$ - Mean vector

CONTENTS

1 INTRODUCTION 16

1.1 MOTIVATION 16

1.2 OBJECTIVE 17

1.3 MAIN CONTRIBUTIONS 17

1.4 OUTLINE 18

2 METAMODELING STRATEGIES FOR FUNCTION APPROXIMATION: KRIGING AND CO-KRIGING 20

2.1 KRIGING 20

2.2 CO-KRIGING 23

2.3 COMPARISON BETWEEN BOTH STRATEGIES USING A ONE-VARIABLE FUNCTION AS AN EXAMPLE 28

2.4 CO-KRIGING REGRESSION 32

2.5 PARTIAL REMARKS 35

3 EXPERIMENTAL APPLICATION OF A CO-KRIGING STRATEGY FOR STRUCTURAL HEALTH MONITORING OF BRIDGES 36

3.1 PROBLEM STATEMENTS AND PROPOSED FRAMEWORK 36

3.2 Z24 BRIDGE CASE STUDY: ANALYSIS OF EXPERIMENTAL AND NUMERICAL DATA AVAILABILITY 40

3.3 CO-KRIGING METHOD FOR DAMAGE DETECTION IN THE Z24 BRIDGE CONSIDERING TEMPERATURE EFFECTS 43

3.4 PARTIAL REMARKS 46

4 CO-KRIGING MODELING FOR DELAMINATION QUANTIFICATION IN LAMINATES 47

4.1 INSIGHTS INTO STRUCTURAL HEALTH MONITORING FOR COMPOSITE MATERIALS: TECHNIQUES AND STOCHASTIC APPROACHES 47

4.2 STRUCTURAL HEALTH MONITORING USING LAMB WAVES FOR DELAMINATION DETECTION IN COMPOSITE STRUCTURES . . 50

4.3 DAMAGE SENSITIVE FEATURE EXTRACTION USING AUTOREGRESSIVE MODELS . . . 53
4.4 DAMAGE INDICES FOR STRUCTURE CONDITION CLASSIFICATION . . . 55
4.5 PROPOSED FRAMEWORK . . . 56
4.6 HYBRID DATASET FOR CO-KRIGING: EXPERIMENTAL AND NUMERICAL DATA . . . 58
4.6.1 Expensive data - experimental setup . . . 58
4.6.2 Cheap data - numerical simulations . . . 60
4.7 DAMAGE DETECTION AND QUANTIFICATION IN LAMINATES . 66
4.8 Partial Remarks . . . 72

5 FINAL REMARKS . . . 73
5.1 Concluding . . . 73
5.2 Future works . . . 74

REFERENCES . . . 75

APPENDIX A – CO-KRIGING REGRESSION CODE IN MATLAB . . . 83
A.1 Main code . . . 83
A.2 Hyper-parameters estimation functions . . . 88
A.2.1 Cheap model . . . 88
A.2.2 Difference model . . . 89
A.3 Co-Kriging regression function . . . 90

1 INTRODUCTION

This chapter outlines the subject of this master's dissertation. Firstly, Section 1.1 presents the motivation for conducting this research. Sections 1.2 and 1.3 address this work's objectives and achieved contributions, respectively. Finally, Section 1.4 indicates the organization of the chapters in this work.

1.1. MOTIVATION

Computational modeling is essential in science and engineering, especially for analyzing the behavior of complex mechanical systems and structures. However, the computational demands associated with high-fidelity models often restrict their practical application, especially in real-time scenarios. Surrogate modeling, or metamodeling, has emerged as a solution to mitigate these challenges by approximating complex models with simplified functions that capture essential behavior and significantly reduce evaluation time. Gaussian Process Regression (GPR), known as Kriging, is a prominent surrogate modeling method extensively applied in structural health monitoring (SHM) to detect and assess structural damage. This probabilistic approach enables confidence interval estimation, facilitating the integration of uncertainties in damage identification applications. For example, Paixão *et al.* (2021) applied the ordinary Kriging method to quantify the delamination area in composite materials. In contrast, Pavlack *et al.* (2022) demonstrated the effectiveness of this strategy in studying debonding defects in composite wind turbine blades by enhancing Kriging through the use of polynomial chaos expansion (Lüthen; Marelli; Sudret, 2021).

While the studies mentioned have been effective in SHM, one of its limitations is its dependency on extensive, high-quality data, which can be costly to acquire. Accurate predictions for target variables in SHM applications often require substantial historical data or a well-calibrated structural model, which can be resource-intensive. For instance, Silva, Figueiredo and Moldovan (2022) highlighted the challenge of gathering sufficient experimental data to capture a bridge's temperature variations over a year. Moreover, constructing a robust model typically demands costly instrumentation and skilled professionals to ensure the reliability of the monitoring data.

In this scenario, we address these challenges by applying the co-Kriging method,

which takes advantage of the covariance between two or more related datasets (Forrester; Sóbester; Keane, 2008). Co-Kriging builds on traditional Kriging by combining data from at least two sources with differing acquisition costs. The more expensive dataset typically originates from laboratory experiments or detailed functional tests, while the more economical data is obtained from simpler and less calibrated numerical or analytical models (Gratiet; Garnier, 2014). By incorporating this additional information from less costly co-variables, co-Kriging can significantly enhance predictions for the primary variable. As the less expensive data is often more readily available in larger quantities (Xiao *et al.*, 2018), co-Kriging addresses data limitations by merging a smaller set of high-cost data with a larger volume of lower-cost data, ultimately improving prediction accuracy and reducing experimental demands (Gratiet; Garnier, 2014).

Therefore, within this work's scope, this dissertation aims to apply a co-Kriging procedure in two practical applications in SHM. The first application involves a regression analysis of a bridge's natural frequency variations in response to climatic changes. In contrast, the second focuses on quantifying delamination damage in a carbon-epoxy composite plate. In both cases, a limited amount of experimental data was combined with a larger set of numerical simulations derived from finite element (FE) models. The results showcase that co-Kriging, by integrating low-cost numerical data with experimental information, substantially enhances both damage detection and quantification accuracy, as well as reliability in SHM applications.

1.2. OBJECTIVE

This study aims to implement and evaluate the co-Kriging approach in structural health monitoring applications while comparing its performance against traditional Kriging models. The research focuses on two specific cases: assessing the natural frequency variations of a bridge due to climatic changes and quantifying delamination damage in a carbon-epoxy composite plate.

1.3. MAIN CONTRIBUTIONS

The key contributions of this dissertation are:

- Exploration of the viability and application of the co-Kriging method in the field of SHM;
- Comprehensive study and review of both Kriging and co-Kriging methods;
- Demonstrative examples of co-Kriging applications across varied scenarios (an article was published in the Structural Health Monitoring Journal - "Co-Kriging strategy for structural health monitoring of bridges" (Novais; Silva; Figueiredo, 2024));
- Introduction of a novel methodology for quantifying delamination in laminates by leveraging the advantages of the co-Kriging approach.

1.4. OUTLINE

The work is organized as follows:

Chapter 1: Introduction - Presents the study's motivation, objectives, and contributions.

Chapter 2: Metamodeling with Kriging and Co-Kriging - Furnishes a thorough overview of Kriging and co-Kriging as metamodeling strategies, emphasizing their versatile applications.

Chapter 3: Experimental Application of co-Kriging for Bridge Monitoring - Presents an overview of techniques that integrate hybrid datasets for SHM in bridge applications. This chapter further showcases the findings of applying a co-Kriging technique to enhance damage detection in a real structure.

Chapter 4: Co-Kriging for Delamination Quantification in Laminates - Provides a literature review and theoretical background on composite materials and SHM methodologies for laminates, emphasizing the importance of these materials and the essential role of SHM techniques. This chapter further details the experimental setup and methodologies employed to evaluate a carbon-epoxy composite plate under various conditions, offering insight into the practical applications of SHM in delamination detection and monitoring.

Chapter 5: Final Remarks - Wraps up the key takeaways, provides insights into potential future research directions, and highlights the main academic contributions.

Appendix A: Implementation of co-Kriging regression in MATLAB - provides an implementation of the co-Kriging regression in MATLAB, featuring a practical example that illustrates the estimation of a mathematical function.

2 METAMODELING STRATEGIES FOR FUNCTION APPROXIMATION: KRIGING AND CO-KRIGING

This chapter provides a comprehensive overview of Kriging and co-Kriging methodologies in metamodeling, highlighting their applications in various fields. Section 2.1 introduces the concept of metamodeling, emphasizing the significance of Kriging as a statistical method for interpolating complex functions and its extension to machine learning tasks. In Section 2.2, the co-Kriging technique is explained, showcasing its ability to enhance interpolation by incorporating additional co-variables and its utility in scenarios involving both expensive and cheap data points. A practical comparison of Kriging and co-Kriging is illustrated with a single-variable function example in Section 2.3, showcasing the improved prediction performance of co-Kriging even with limited, expensive data. In Section 2.4, co-Kriging regression is introduced as an adaptation that accommodates noisy data and regression tasks. Finally, Section 2.5 presents an overview of the chapter's findings. Overall, these sections elucidate the versatility and advantages of Kriging and co-Kriging in modeling different functions across some applications.

2.1. KRIGING

Computational models are essential in applied science and engineering, providing valuable insights. However, their utility is often associated with high complexity and significant execution time requirements. To address these challenges, metamodeling—or surrogate modeling—offers an effective strategy for economizing computational time and resources by replacing a complex model with a metamodel. This simplified function approximates the behavior of the original model while being much faster to evaluate. One widely used method in this field is Kriging, or Gaussian process regression, a statistical technique for interpolating complex functions using Gaussian processes to provide accurate estimates across various functions. Originally developed in the 1950s when Krige applied it to spatial interpolation in geostatistics (Krige, 1951), the method was later formalized by Matheron in the 1960s (Matheron, 1963), and has since evolved beyond geostatistics to encompass metamodeling and computer experiments. Notably, Sacks *et al.* (1989) demonstrated Kriging's effectiveness in modeling input/output relationships for computationally expensive models, cementing its place as a powerful tool in a range of

fields.

Gaussian processes, a component of Kriging, gained renewed attention in the mid-2000s for their applications in machine learning, particularly in regression and classification tasks. This resurgence was driven by the introduction of GP-regression, which accommodates noisy data (Rasmussen; Williams, 2006). For a comprehensive introduction to Kriging as a metamodeling tool, readers can refer to Santner, Williams and Notz (2003), while Rasmussen and Williams (2006) presents a similar exploration of Kriging's use as a regression and classification tool. The Kriging prediction is created from a mean base term $\beta^T f(x)$ (or the mean value of the Gaussian distribution) plus a zero mean, unit-variance, stationary Gaussian process $\mathcal{Z}(x, \Omega)$, as follows (Santner; Williams; Notz, 2003; Forrester; Sóbester; Keane, 2007):

$$\mathcal{Y} = \mathcal{M}^K(x) = \beta^T f(x) + \sigma^2 \mathcal{Z}(x, \Omega) \tag{2.1}$$

where $\mathcal{M}(x)$ is the model output and σ^2 is the variance of the Gaussian process.

The stationary Gaussian process $\mathcal{Z}(x, \Omega)$ represents the local features of f around the n sample points. It is characterized by a correlation function (ψ or $\mathcal{R}(x, x', \theta)$) and its hyper-parameters θ. The correlation function, as it suggests, describes correlations between a random variable from the model output $\mathcal{Y}(x)$ at the point to be predicted ($x^{(n+1)}$) and at the sample data points (Forrester; Sóbester; Keane, 2007). The Gaussian kernel function is the most commonly employed choice for constructing Kriging models in engineering design. However, it is important to emphasize that the choice of the optimal kernel function is closely tied to the problem at hand. Thus, correctly selecting an appropriate kernel is essential in achieving the highest possible approximation accuracy (Palar; Shimoyama, 2018). For example, Stein (2012) suggests using the Matérn kernel function over the Gaussian function, as the excessive smoothness exhibited by the Gaussian function tends to be impractical for numerous real-world processes.

The covariance function generally describes the degree of similarity between existing observations and new data points. Consequently, input points near each other will likely display similar outputs or responses. Several kernel functions are present in the literature, including Linear, Exponential, Gaussian (referred to as squared exponential), and Matérn autocorrelation functions, as follows (Lataniotis *et al.*, 2022):

- Linear:

$$\mathcal{R}(x, x'; \theta) = \max\left(0.1 - \frac{|x - x'|}{\theta}\right) \tag{2.2}$$

- Exponential:

$$\mathcal{R}(x, x'; \theta) = \exp\left[-\frac{|x - x'|}{\theta}\right] \tag{2.3}$$

- Guassian (or squared exponential):

$$\mathcal{R}(x, x'; \theta) = \exp\left[-\frac{1}{2}\left(\frac{|x - x'|}{\theta}\right)^2\right] \tag{2.4}$$

- Mátern:

$$\mathcal{R}(x, x', \theta, v) = \frac{1}{2^{v-1}\Gamma(v)}\left(2\sqrt{v}\frac{|x - x'|}{\theta})\right)^v \mathcal{K}_v\left(2\sqrt{v}\frac{|x - x'|}{\theta})\right) \tag{2.5}$$

where x and x' are a pair of one-dimensional input, θ is the correlation function scale parameter, $v \geq$ is the shape parameter, Γ is the Euler's Gamma function, and $\mathcal{K}_v$ is the modified Bessel function of the second kind.

Forrester, Sóbester and Keane (2007) also introduces the Kriging kernel, which holds significant value in surrogate-based optimization problems:

$$\psi(x^{(i)}, x^{(j)}) = \exp\left(-\sum_{l=1}^{k} \theta_l \left|x_l^{(i)} - x_l^{(j)}\right|^{p_l}\right) \tag{2.6}$$

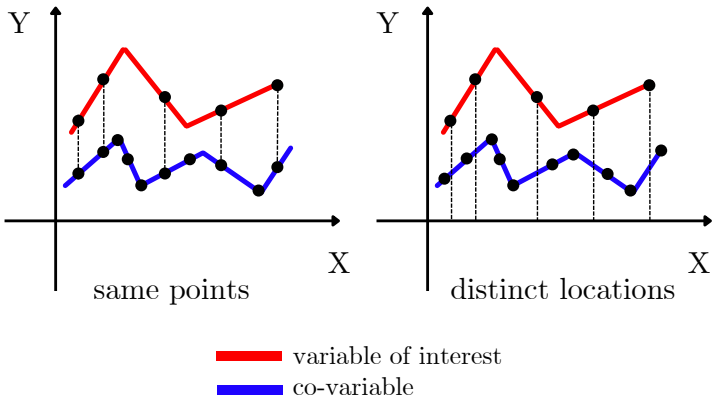
where p_l represents a hyper-parameter that acts as a determining factor for the smoothness level in function approximation, and θ is a hyper-parameter that indicates the rate at which the function changes as a new point deviates from a previous observation. Higher and lower θ values indicate the function's active or inert behavior along dimension j. A more detailed discussion about Kriging and other surrogate models is given by Forrester, Sóbester and Keane (2007) and Rasmussen and Williams (2006).

In this study, the UQLab software was employed to derive Kriging metamodels. In scenarios involving the propagation of uncertainties, UQLab proves to be a robust tool for effectively tackling such challenges. Built upon the Matlab framework, UQLab offers an extensive arsenal of types of analysis and integrated algorithms. It consists of open-source scientific modules that work together with UQLabCore to handle the process of uncertainty propagation. This includes techniques like Monte Carlo sampling, sensitivity analysis, and reliability analysis (which calculates probabilities of rare events). The framework also supports creating surrogate models using methods, including Kriging (Marelli; Sudret, 2014).

2.2. CO-KRIGING

Co-Kriging represents an extension of ordinary Kriging, wherein additional observed variables, known as co-variates, are utilized to enhance the precision of interpolating the primary variable of interest. These co-variates often exhibit correlations with the variable being modeled. Unlike regression and universal Kriging methods, co-Kriging does not necessitate the availability of secondary information at all prediction locations. These co-variates may be measured at the same points as the target variable (co-located samples), at distinct locations, or even at a combination, as shown in Figure 1. A prevalent application of co-Kriging arises when the co-variable is more cost-effective to measure than the target variable (Stein; Corsten, 1991).

Figure 1 – Variable measurement locations for co-Kriging strategy.



Source: Prepared by the author.

A larger volume of this cheap data can be combined with a limited quantity of costly data, thereby enriching the precision of a surrogate model for the higher-cost function. To effectively utilize the less expensive data, it is necessary to develop a corrective procedure that characterizes the disparities between the less expensive and more expensive functions. A complete discussion of this strategy is provided by Forrester, Sóbester and Keane (2007). In this work, co-Kriging will be applied in all cases to correlate two sets of data: cheap data (denoted by $\mathcal{X}_c$) and expensive data (denoted by $\mathcal{X}_e$). Its formulation begins with the concatenation of the sample locations, as follows:

$$\mathcal{X} = \begin{pmatrix} \mathcal{X}_c \\ \mathcal{X}_e \end{pmatrix} = \begin{pmatrix} x_c^{(1)} \\ \vdots \\ x_c^{(n_c)} \\ x_e^{(1)} \\ \vdots \\ x_e^{(n_e)} \end{pmatrix} \tag{2.7}$$

Similar to the concept in Kriging, the value assigned to a specific point within the domain $\mathcal{X}$ is approached as if it were an instance of a Gaussian random variable. Consequently, in the context of co-Kriging, an analogous stochastic field is encountered:

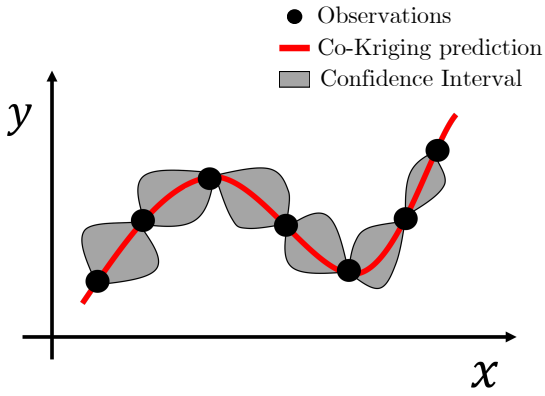
$$\mathcal{Y} = \begin{pmatrix} \mathcal{Y}_c(\mathcal{X}_c) \\ \mathcal{Y}_e(\mathcal{X}_e) \end{pmatrix} = \begin{pmatrix} y_c(x_c^{(1)}) \\ \vdots \\ y_c(x_c^{(n_c)}) \\ y_e(x_e^{(1)}) \\ \vdots \\ y_e(x_e^{(n_e)}) \end{pmatrix} \tag{2.8}$$

When one knows the value of an expensive output interpolation at any new x point being predicted from the method $y_e(x^{(i)})$, it is assumed that no further information can be extracted from the less expensive dataset. In simpler terms, the assumption is that the costly data is entirely accurate, and any inaccuracies are attributed to the cheap data, which is a Markov property (see Equation 2.9) (Kennedy; O'Hagan, 2000). This principle is fundamental to the co-Kriging method, as it enables the effective integration of data with differing levels of fidelity by appropriately modeling their covariance. The assumption of zero covariance between distinct points suggests that the expensive data are conditionally independent of the cheaper data, except at shared sampling locations (Forrester; Sóbester; Keane, 2007). Figure 2 illustrates this concept, showing that the confidence interval goes to zero at points where the actual values of the function, which is being estimated, are known.

$$\operatorname{cov}\left\{y_e(x^{(i)}), y_c(x) | y_c(x^{(i)})\right\} = 0, \quad \forall x \neq x^{(i)} \tag{2.9}$$

In essence, the co-Kriging strategy approximates the expensive code by combining the cheap code multiplied by a scaling factor ρ' with a Gaussian process denoted as $Z_d(\cdot)$,

Figure 2 – Representation of the confidence interval convergence at known points from the Markov property.



Source: Prepared by the author.

which captures the distinction between $\rho' Z_c(\cdot)$ and $Z_e(\cdot)$:

$$Z_e(x) = \rho' Z_c(x) + Z_d(x) \tag{2.10}$$

Due to the correlation of multiple sets of data, co-Kriging involves a more complex covariance matrix in comparison to ordinary Kriging, as follows:

$$\mathcal{C} = \begin{pmatrix} \sigma_c^2 \mathbf{\Psi}_c(\mathcal{X}_c, \mathcal{X}_c) & \rho' \sigma_c^2 \mathbf{\Psi}_c(\mathcal{X}_c, \mathcal{X}_e) \\ \rho' \sigma_c^2 \mathbf{\Psi}_c(\mathcal{X}_e, \mathcal{X}_c) & \rho'^2 \sigma_c^2 \mathbf{\Psi}_c(\mathcal{X}_e, \mathcal{X}_e) + \sigma_d^2 \mathbf{\Psi}_d(\mathcal{X}_e, \mathcal{X}_e) \end{pmatrix} \tag{2.11}$$

Here, $\mathbf{\Psi}$ denotes a correlation matrix between the expensive and cheap datasets (with a similar structure to Equation 2.6). There are four hyperparameters to calculate (θ_c, θ_d, p_c, and p_d) along with a scaling factor ρ', which can be estimated using maximum likelihood estimates (MLEs) (Forrester; Sóbester; Keane, 2007). The subscripts c and d refer to the hyperparameters associated with the cheap dataset and the difference between the cheap and expensive datasets. The hyperparameters θ control the rate at which the function changes as the input x deviates from a known data point, determining the correlation length or the rate of correlation decay with distance. Parameters p_c and p_d influence the smoothness of the function approximation; for instance, a very low p value (e.g., $p = 0.1$) suggests a minimal immediate correlation between two points, implying a near discontinuity between $y(x^{(i)})$ and $y(x)$. Finally, ρ' acts as a scaling factor, adjusting the overall scale of the model (Forrester; Sóbester; Keane, 2007; Forrester; Sóbester; Keane, 2008).

The hyper-parameters associated to the cheap data (θ_c and p_c) can be found by maximizing the following equation:

$$-\frac{n_c}{2}\ln(\widehat{\sigma}_c^2) - \frac{1}{2}\ln|\det(\mathbf{\Psi}_c(\mathcal{X}_c,\mathcal{X}_c))| \tag{2.12}$$

where ($\mathbf{1}$ is an $n \times 1$ column vector of ones)

$$\hat{\mu}_c = \frac{\mathbf{1}\mathbf{\Psi}_c(\mathcal{X}_c,\mathcal{X}_c)^{-1}\mathcal{Y}_c}{\mathbf{1}\mathbf{\Psi}_c(\mathcal{X}_c,\mathcal{X}_c)^{-1}\mathbf{1}} \tag{2.13}$$

and

$$\hat{\sigma}_c^2 = \frac{(\mathcal{Y}_c - \mathbf{1}\hat{\mu}_c)^T\mathbf{\Psi}_c(\mathcal{X}_c,\mathcal{X}_c)^{-1}(\mathcal{Y}_c - \mathbf{1}\hat{\mu}_c)}{n_c} \tag{2.14}$$

Estimating the hyper-parameters for the cheap data is essential to obtain the values of θ_d, p_d, and ρ' (related to the difference model). The scaling factor ρ' can be estimated by:

$$\mathbf{d} = \mathcal{Y}_e - \rho'\mathcal{Y}_c(\mathcal{X}_e) \tag{2.15}$$

where $\mathcal{Y}_c(\mathcal{X}_e)$ are the values of the cheap data at locations common to the expensive data (co-located samples). If the values of $\mathcal{Y}_c$ are unknown at $\mathcal{X}_e$, one needs to calculate the values of $\hat{\mathcal{Y}}_c(\mathcal{X}_e)$ from the Kriging estimator (Equation 2.1) to estimate ρ'. By maximizing the following equation, θ_d and p_d can be found:

$$-\frac{n_e}{2}\ln(\widehat{\sigma}_d^2) - \frac{1}{2}\ln|\det(\mathbf{\Psi}_d(\mathcal{X}_e,\mathcal{X}_e))| \tag{2.16}$$

where

$$\hat{\mu}_d = \frac{\mathbf{1}\mathbf{\Psi}_d(\mathcal{X}_e,\mathcal{X}_e)^{-1}\mathbf{d}}{\mathbf{1}^T\mathbf{\Psi}_d(\mathcal{X}_e,\mathcal{X}_e)^{-1}\mathbf{1}} \tag{2.17}$$

and

$$\hat{\sigma}_d^2 = \frac{(\mathbf{d} - \mathbf{1}\hat{\mu}_d)^T\mathbf{\Psi}_d(\mathcal{X}_e,\mathcal{X}_e)^{-1}(\mathbf{d} - \mathbf{1}\hat{\mu}_d)}{n_e} \tag{2.18}$$

By implementing the co-Kriging strategy, one aims to discover a function that predicts the value of expensive data at any given new point x. Simplifying this concept, a predictive point can be understood as an interpolator of the expensive data, as follows:

$$\hat{y}_e(x) = \hat{\mu} + \mathbf{c}^T \mathcal{C}^{-1}(\mathcal{Y} - \mathbf{1}\hat{\mu}) \tag{2.19}$$

where $\hat{\mu}$ denotes the estimated mean of the process, $\mathbf{c}$ represents the covariance vector between the point x and the sampled points, and $\mathbf{1}$ denotes a column vector of ones, as given below:

$$\hat{\mu} = \mathbf{1}^T \mathcal{C}^{-1} \mathcal{Y} / \mathbf{1}^T \mathcal{C}^{-1} \mathbf{1} \tag{2.20}$$

and

$$\mathbf{c} = \begin{pmatrix} \hat{\rho}' \hat{\sigma}_c^2 \mathbf{\Psi}_c(\mathcal{X}_c, x^{(n+1)}) \\ \hat{\rho}'^2 \hat{\sigma}_c^2 \mathbf{\Psi}_c(\mathcal{X}_e, x^{(n+1)}) + \hat{\sigma}_d^2 \mathbf{\Psi}_d(\mathcal{X}_e, x^{(n+1)}) \end{pmatrix} \tag{2.21}$$

where $\hat{\sigma}_c^2$ represents the variance associated with the cheap data, and $\hat{\sigma}_d^2$ is the variance related to the difference model. Notably, the circumflex symbol indicates estimated or predicted values of variables, specifically marking maximum likelihood estimates, which are approximations of the mean, variance, or other parameters obtained through the MLE approach. This notation distinguishes between the true values of variables and their estimated or predicted counterparts (Forrester; Sóbester; Keane, 2007). For instance, in Equation 2.19, $\hat{y}_e(x)$ denotes an estimate of the expensive dataset, as opposed to the actual value, $y_e(x)$.

Therefore, from Equation (2.19), an interpolator for the expensive data is obtained, which is very similar to the ordinary Kriging interpolator unless the presence of cheap data. The estimated mean-squared error in the predictor is given as follows:

$$s^2(x) = \hat{\rho}'^2 \hat{\sigma}_c^2 + \hat{\sigma}_d^2 - \mathbf{c}^T \mathcal{C}^{-1} \mathbf{c} \tag{2.22}$$

The co-Kriging model functions as an interpolator for $\mathcal{Y}_e$. Consequently, when evaluated at the locations of the expensive samples, its error is anticipated to be zero. In the subsequent section, an illustrative example will be provided, followed by a comparative discussion on the performance of both Kriging and co-Kriging methods.

When implementing this technique, an essential factor is evaluating whether the covariate dataset enhances the prediction of the target variable. Forrester, Sóbester and Keane (2007) recommend calculating a correlation coefficient between the two datasets

involved in the analysis. Practically, this involves testing the model using a test dataset of size n_t along with a corresponding set of predictions, as outlined below:

$$r^2 = \left(\frac{\operatorname{cov}(\mathbf{y}, \widehat{\mathbf{y}})}{\sqrt{\operatorname{var}(\mathbf{y}) \operatorname{var}(\widehat{\mathbf{y}})}} \right)^2 \tag{2.23}$$

$$= \left(\frac{n_t \sum_{i=0}^{n_t} y^{(i)} \widehat{y}^{(i)} - \sum_{i=0}^{n_t} y^{(i)} \sum_{i=0}^{n_t} \widehat{y}^{(i)}}{\sqrt{\left[n_t \sum_{i=0}^{n_t} y^{(i)2} - \left(\sum_{i=0}^{n_t} y^{(i)} \right)^2 \right] \left[n_t \sum_{i=0}^{n_t} \widehat{y}^{(i)2} - \left(\sum_{i=0}^{n_t} \widehat{y}^{(i)} \right)^2 \right]}} \right)^2 \tag{2.24}$$

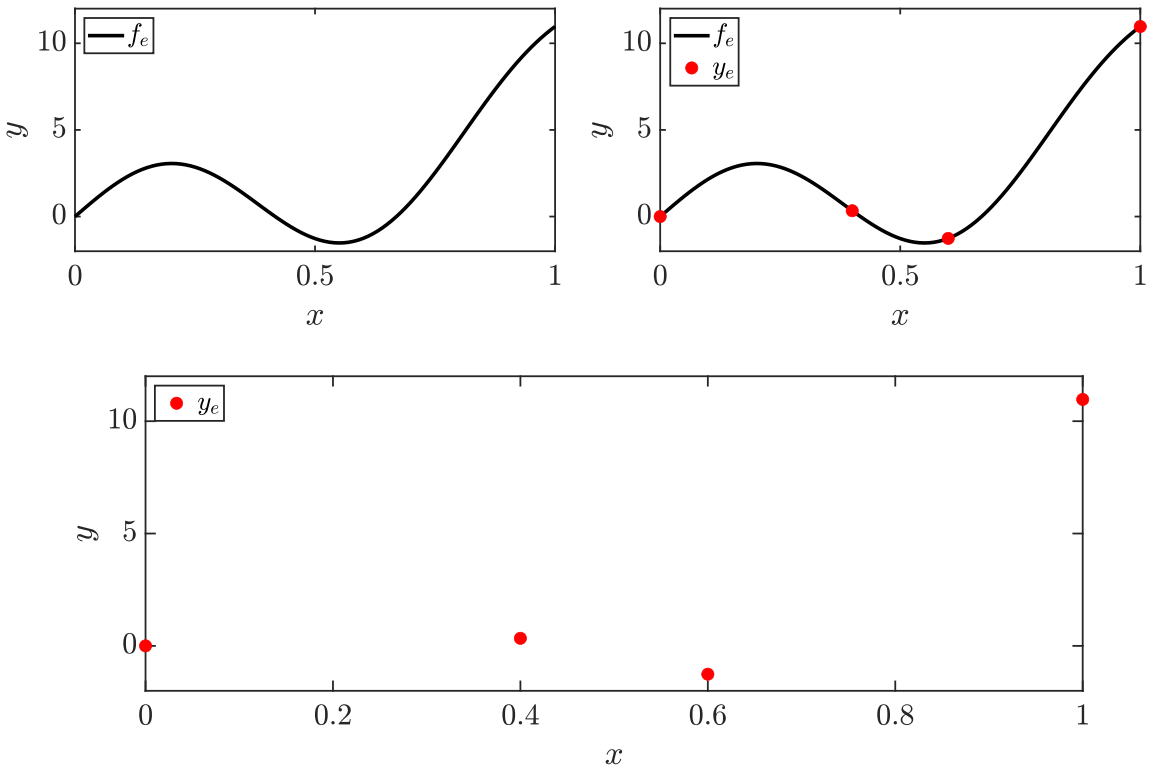
The correlation coefficient is particularly valuable because it assesses the relationship between the two datasets independently of their scale differences. In essence, it emphasizes comparing the shapes or patterns of the data distributions rather than their absolute values. This characteristic is especially advantageous when evaluating models of varying fidelity, where the objective is to identify a low-fidelity model that can reliably predict the location of optima, even if it does not accurately capture the exact values. Generally, an r^2 value greater than 0.8 indicates that the surrogate model possesses good predictive capabilities. In the next section, an example using a mathematical function will be presented to enhance clarity and facilitate the understanding of the method.

2.3. COMPARISON BETWEEN BOTH STRATEGIES USING A ONE-VARIABLE FUNCTION AS AN EXAMPLE

In the provided scenario, a mathematical function represents the expensive estimator for a set of points, denoted as f_e. The expensive function takes the form $f_e(x) = 3\sin(8x) + (2x)^3$ and is evaluated at only four points (simulating a situation with limited information about the variable of interest), resulting in $\mathcal{X}_e = [0, 0.4, 0.6, 1]$. Figure 3 illustrates the target function to be estimated and the four expensive points (y_e) sampled along this curve to train the metamodels.

The UQLab (Marelli; Sudret, 2014) software was used to obtain the Kriging metamodel of the expensive function f_e, and the results are illustrated in Figure 4. A Kriging prediction based on the data points y_e yields an insufficient approximation, due to the limited number of points used to capture the correlations. By increasing the dataset size, Kriging can improve performance, as shown in Figure 5. However, acquiring a comprehensive and representative dataset can be expensive and challenging in numerous real-world

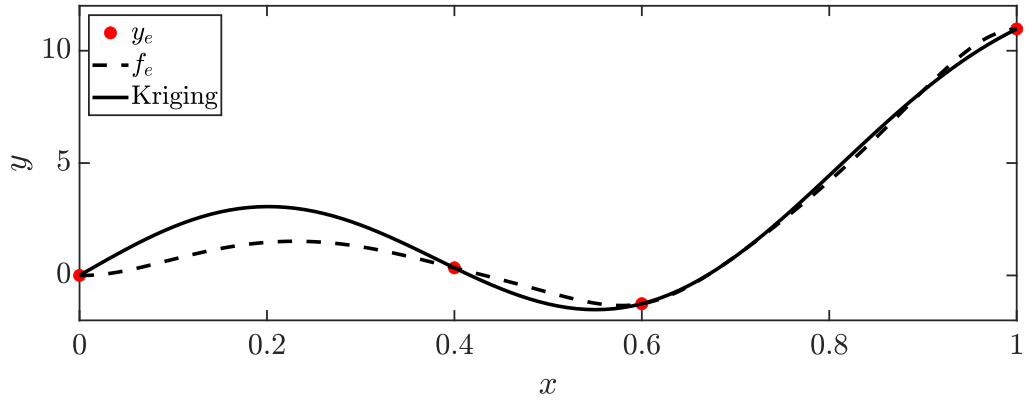
Figure 3 – Expensive data of the one variable function example.



Source: Prepared by the author.

scenarios, as discussed in Section 1.1.

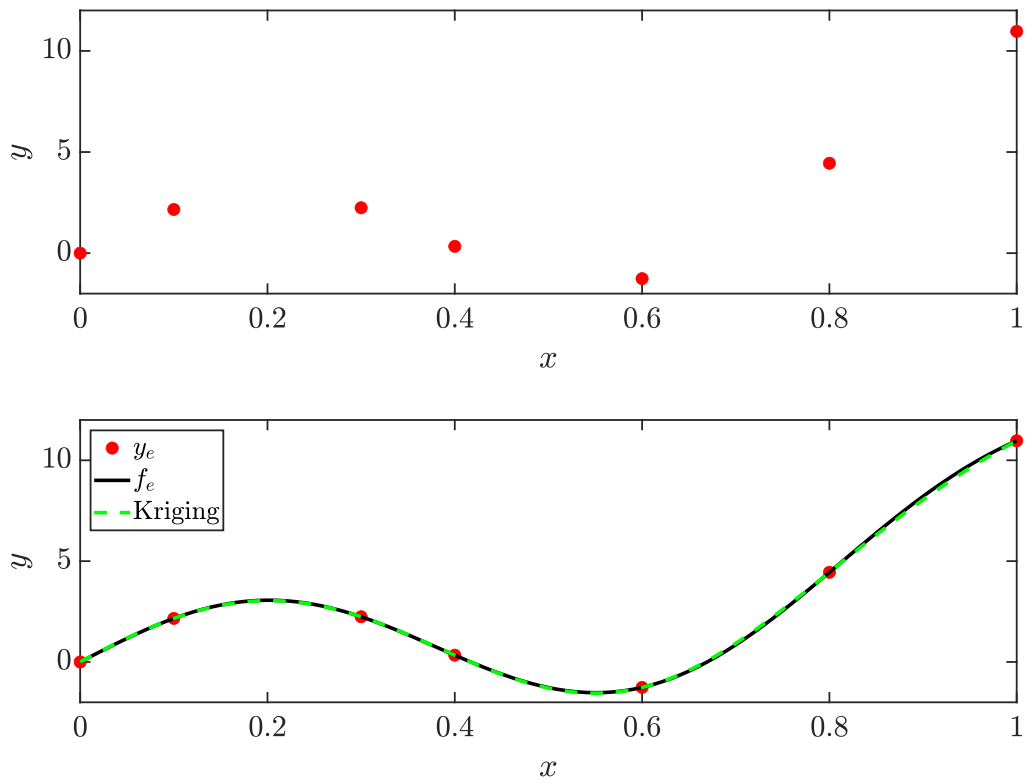
Figure 4 – Kriging prediction through expensive points y_e.



Source: Prepared by the author.

In another scenario, a new mathematical function is introduced into the dataset to exemplify the cheap data, denoted as f_c. The cheap function is defined as $f_c(x) = 0.5f_e + 10(x - 0.5) - 5$, and it is assumed that it can be calculated at a considerably larger

Figure 5 – Kriging prediction increasing the number of y_e points.



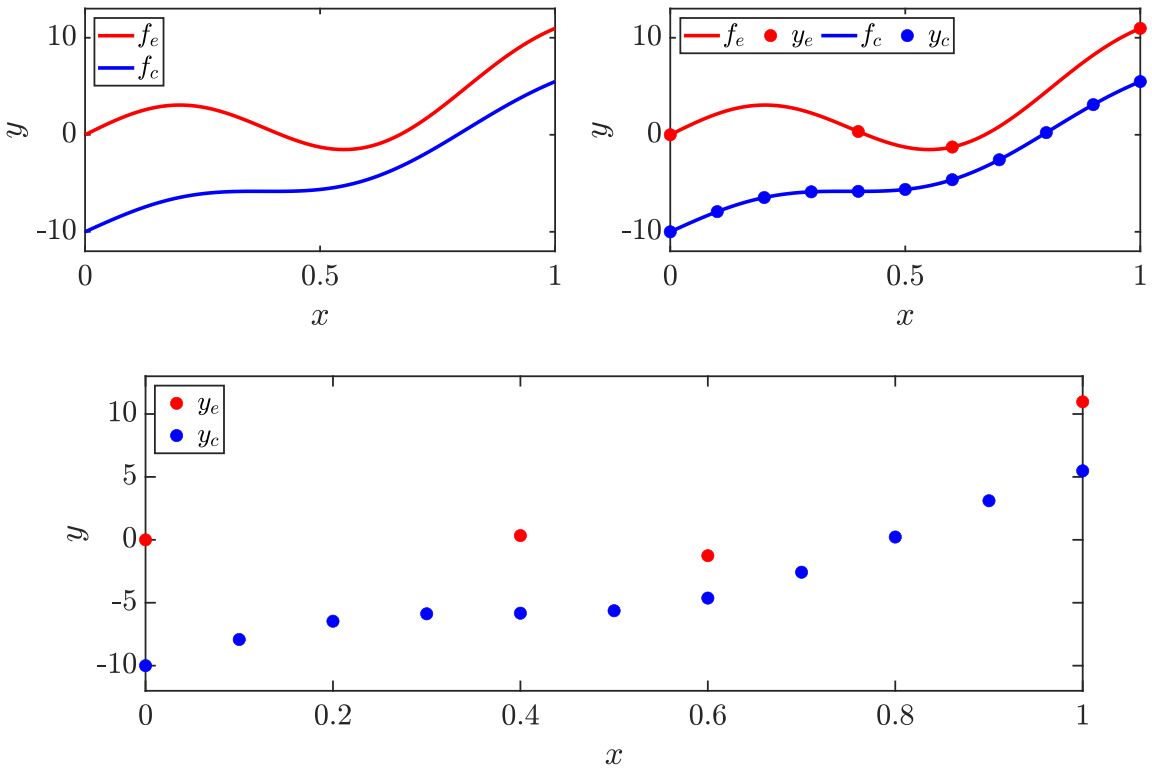
Source: Prepared by the author.

number of points, represented by $\mathcal{X}_c = [0, 0.1, 0.2, 0.3, 0.4, 0.5, 0.6, 0.7, 0.8, 0.9, 1]$. Figure 6 portrays the positions of the expensive and cheap points (y_e and y_c), along with their respective functions.

Compared to the performance of Kriging, co-Kriging predictions remain remarkably closer to the expensive function f_e, even with a small dataset comprising the y_e points. This is achieved by leveraging additional, less accurate points from f_c. Despite the significant differences between the two functions, a straightforward relationship has been identified between the cheap and expensive datasets. As a result, the co-Kriging method effectively approximates the curve, as illustrated in Figure 7.

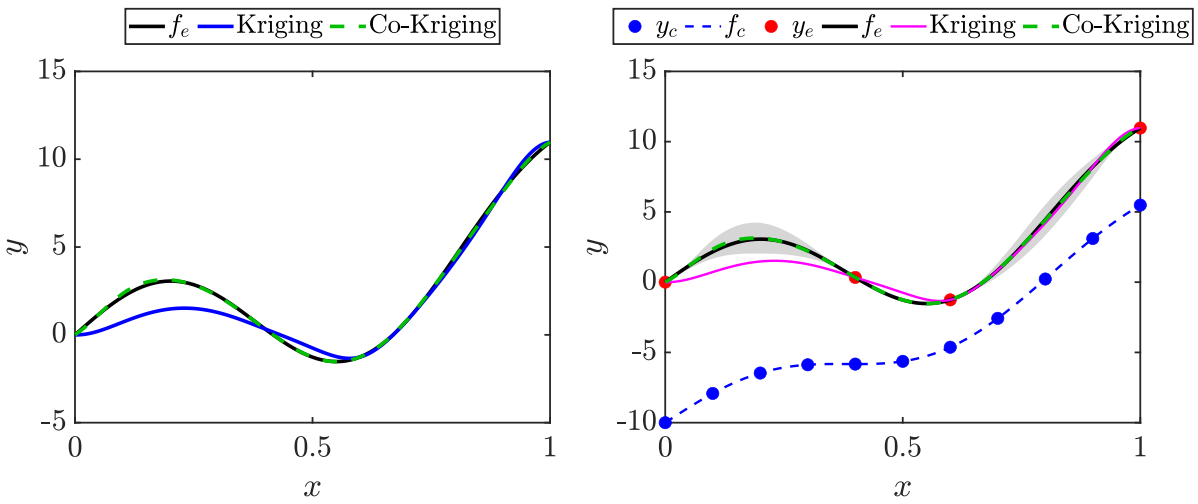
The co-Kriging model operates as an interpolator for $\mathcal{Y}_e$. As a result, when evaluated at the locations of the expensive samples, the expected error is zero, as shown in Figure 7, where the gray-colored area approaches zero. However, this is not entirely valid in a real-world scenario, as uncertainties are inherently present. Rather than obtaining a single, precise value, we observe measurements revealing variations around this value,

Figure 6 – Cheap and expensive data of the one variable example.



Source: Prepared by the author.

Figure 7 – Comparison of Kriging and co-Kriging predictions through the one variable function example.



Source: Prepared by the author.

indicating a range or dispersion rather than an exact point, necessitating adjustments in the co-Kriging model to account for such variability.

2.4. CO-KRIGING REGRESSION

In practical applications, it is essential to recognize that unknown factors often arise when employing experimental methods and other approaches, introducing uncertainties that may result from measurement errors or model simplifications. To account for these uncertainties, the co-Kriging interpolation formulation presented in Section 2.2 can be adapted to regress each analysis, effectively filtering any noise in the data. In noise-free conditions, the predictor captures the mean and variance of a Gaussian process, accurately interpolating the provided design points. Conversely, when noise is present, the predictor operates as a regression model, adapting to the inherent noise in the data and accommodating it effectively (Lataniotis *et al.*, 2022).

Different levels of filtering may be necessary for specific analyses. For instance, information obtained from a basic low-fidelity computer code may exhibit inherent smoothness, reducing the need for regression. In contrast, noise may become evident when combined with a detailed high-fidelity analysis, requiring filtering through regression. Similarly, a simplified model represented on a considerably coarser mesh may necessitate more extensive regression than required for the comprehensive high-fidelity code (Forrester; Sóbester; Keane, 2007).

Forrester, Sóbester and Keane (2007) introduces then an enhanced formulation of co-Kriging, referred to as co-Kriging regression, which incorporates two new regression constants, denoted as λ_c and λ_e, associated with the cheap and expensive datasets, respectively. These constants are added to the leading diagonal of the correlation matrices, resulting in a new covariance matrix $\mathcal{C}$ (Equation 2.11), as follows:

$$\mathcal{C}+\lambda=\begin{pmatrix} \sigma_{\mathrm{c}}^2\left\{\boldsymbol{\Psi}_{\mathrm{c}}(\mathcal{X}_{\mathrm{c}},\mathcal{X}_{\mathrm{c}})+\boldsymbol{I}_{(n_{\mathrm{c}}\times n_{\mathrm{c}})}\lambda_{\mathrm{c}}\right\} & \rho\text{'}\sigma_{\mathrm{c}}^2\left\{\boldsymbol{\Psi}_{\mathrm{c}}(\mathcal{X}_{\mathrm{c}},\mathcal{X}_{\mathrm{e}})+\begin{pmatrix}\mathbf{0}_{(n_{\mathrm{c}}-n_{\mathrm{e}})\times n_{\mathrm{e}}}\\ \boldsymbol{I}_{(n_{\mathrm{e}}\times n_{\mathrm{e}})}\end{pmatrix}\lambda_{\mathrm{c}}\right\} \\ \rho\text{'}\sigma_{\mathrm{c}}^2\left\{\boldsymbol{\Psi}_{\mathrm{c}}(\mathcal{X}_{\mathrm{e}},\mathcal{X}_{\mathrm{c}})\right\} & \rho\text{'}^2\sigma_{\mathrm{c}}^2\left\{\boldsymbol{\Psi}_{\mathrm{c}}(\mathcal{X}_{\mathrm{e}},\mathcal{X}_{\mathrm{e}})+\boldsymbol{I}_{(n_{\mathrm{e}}\times n_{\mathrm{e}})}\lambda_{\mathrm{c}}\right\} \\ +\left(\mathbf{0}_{(n_{\mathrm{e}}\times n_{\mathrm{c}}-n_{\mathrm{e}})}\boldsymbol{I}_{(n_{\mathrm{e}}\times n_{\mathrm{e}})}\right)\lambda_{\mathrm{c}}\right\} & +\sigma_{\mathrm{d}}^2\left\{\boldsymbol{\Psi}_{\mathrm{d}}(\mathcal{X}_{\mathrm{e}},\mathcal{X}_{\mathrm{e}})+\boldsymbol{I}_{(n_{\mathrm{e}}\times n_{\mathrm{e}})}\lambda_{\mathrm{e}}\right\} \end{pmatrix} \tag{2.25}$$

where $\boldsymbol{I}$ is an identity matrix and $\mathbf{0}$ a zero matrix.

The constants λ_c and λ_e are determined alongside the other hyper-parameters by maximizing Equations 2.12 and 2.16. In this new approach, the co-Kriging estimator (regression predictor) and its estimated mean-squared error become:

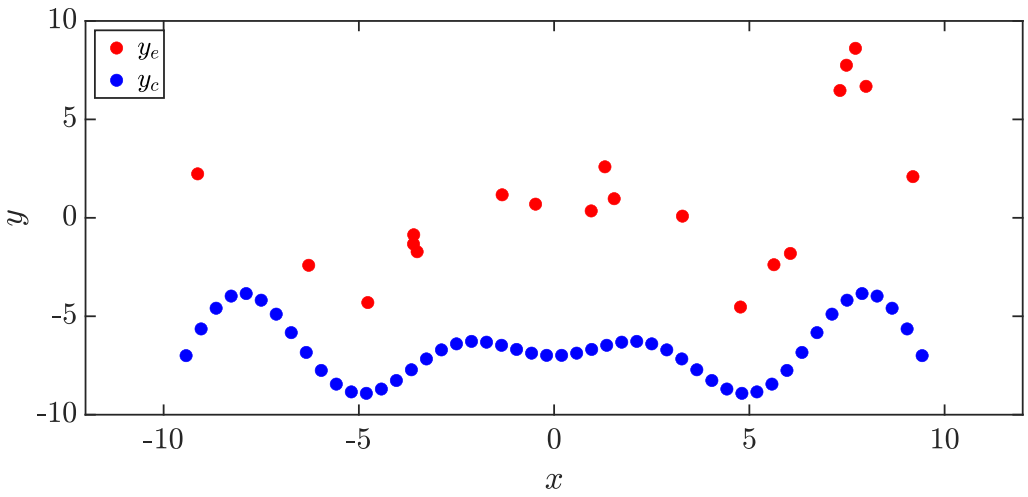
$$\hat{y}_{\mathrm{e,r}}\left(x^{(n_\mathrm{e}+1)}\right) = \hat{\mu} + \boldsymbol{c}^{\mathrm{T}}(\mathcal{C}+\lambda)^{-1}(\mathcal{Y} - \mathbf{1}\hat{\mu}), \tag{2.26}$$

$$s_{\mathrm{r}}^2(x) = \hat{\rho}'^2\hat{\sigma}_{\mathrm{c}}^2\hat{\lambda}_{\mathrm{c}} + \hat{\sigma}_{\mathrm{d}}^2\hat{\lambda}_{\mathrm{e}} - \boldsymbol{c}^{\mathrm{T}}(\mathcal{C}+\lambda)^{-1}\boldsymbol{c} \tag{2.27}$$

It is important to note that the subscript r indicates a regression process. When comparing the new predictor to the previously discussed object (refer to Equation 2.19), the primary distinction lies in the updated covariance matrix $\mathcal{C}$, which now incorporates the two new parameters λ. Unlike the scenario in Equation 2.22, where the interpolation error approaches zero at the sample points, the regression error does not exhibit this behavior. In cases where f_c and f_e are obtained through deterministic computer experiments, it is possible to recover the estimated error and predictor by removing the noise filtering error.

In the following example, an expensive function $f_e = x\,\sin(x)$ is considered, incorporating a noise component to simulate outcomes from a physical experiment. This noise is generated by adding random values from a normal distribution with zero mean and 20% of the original function's standard deviation to the initial results. The cheap function is defined as $f_c(x) = 0.4\,f_e(x) - 7$ and is treated as deterministic, evaluated using a straightforward computer model. Figure 8 illustrates the distribution of observations from both the cheap and expensive functions.

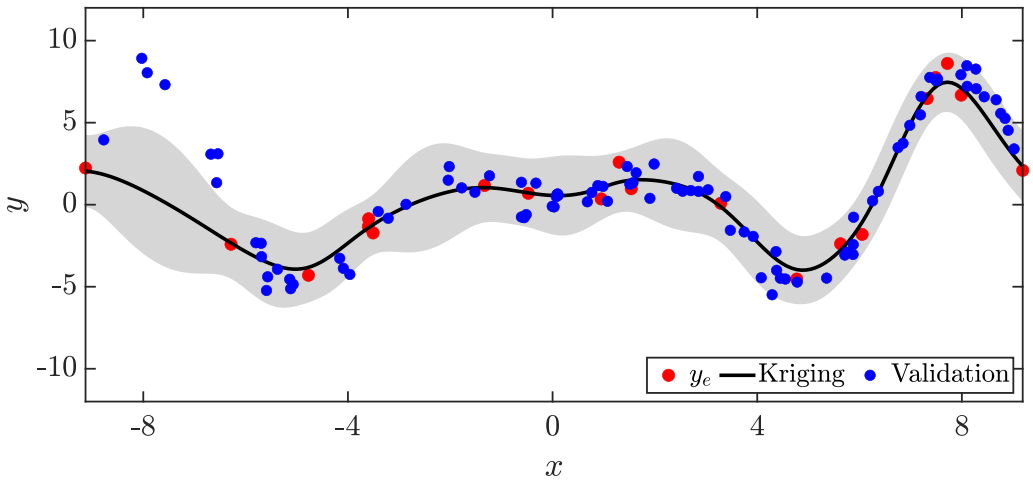
Figure 8 – Cheap and expensive data of the co-Kriging regression example.



Source: Prepared by the author.

In areas with a sufficient density of sampled points, the Kriging prediction performs effectively and aligns with the expensive dataset. However, as previously mentioned, in regions with limited point coverage, the accuracy of the Kriging estimation is compromised. This is illustrated in Figure 9.

Figure 9 – Performance of Kriging regression using expensive observations.

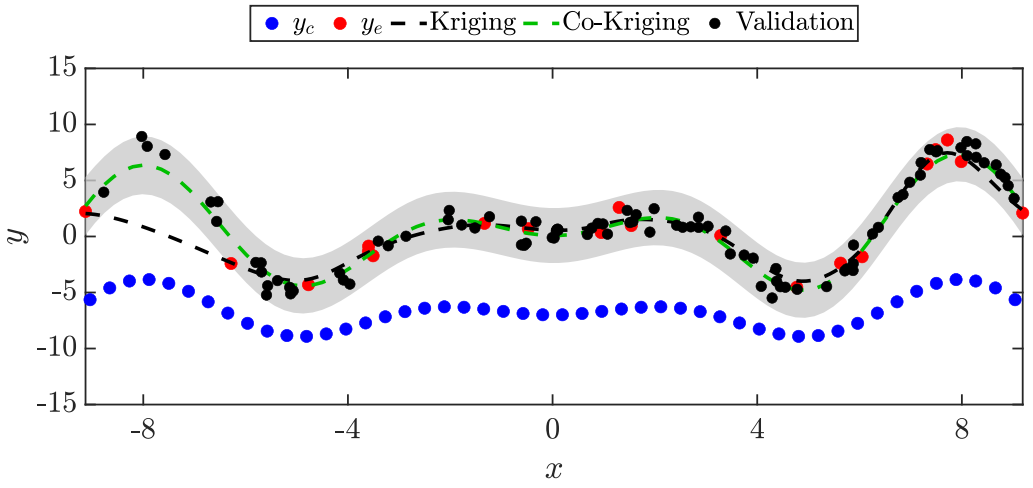


Source: Prepared by the author.

Metamodels were trained using 20 data points from the expensive function f_e and 50 data points from the cheap function f_c, followed by validation with an additional 100 data points (not used in the training phase). Co-Kriging regression leverages information from the cheap dataset, enabling it to produce improved estimates compared to regular Kriging, particularly in regions where there is limited information about the model being estimated, as illustrated in Figure 10. In this scenario, noise was incorporated solely into the outputs of the expensive data, as this error is linked to data quality rather than the model's accuracy. However, this approach can be extended to scenarios where noisy responses are present in the cheap, expensive, or both datasets, as will be discussed in the next chapter of this work, involving the dataset from a concrete bridge.

The MATLAB code used to generate the results presented in this section can be found in Appendix A for readers interested in understanding its operational implementation. It is important to note that, unlike Kriging, the co-Kriging method is not available in UQLab. To integrate co-Kriging with appropriate weighting, a custom code was developed for use within this platform. While co-Kriging is implemented in Forrester, Sóbester and Keane (2007) as an interpolator for the variable of interest, the regression method,

Figure 10 – Performance of co-Kriging regression combining both expensive and cheap datasets.



Source: Prepared by the author.

which accounts for uncertainties in the measured observations by incorporating regression constants, is not part of its implementation and was instead developed by the authors.

2.5. PARTIAL REMARKS

Kriging and co-Kriging formulations were presented in this chapter as powerful techniques for interpolation and regression tasks, offering accurate approximations of functions. Co-Kriging enhances interpolation precision by incorporating additional co-variables, proving particularly beneficial for scenarios with costly evaluations. The co-Kriging regression formulation addresses noise and uncertainty while highlighting its capability to improve predictions by leveraging expensive and cheap model information. It ultimately contributes to more efficient decision-making processes in diverse fields, especially when the co-variable is more cost-effective to measure than the target variable.

3 EXPERIMENTAL APPLICATION OF A CO-KRIGING STRATEGY FOR STRUCTURAL HEALTH MONITORING OF BRIDGES

This chapter presents co-Kriging as a strategy to enhance the structural health monitoring of bridge structures through a hybrid approach. The results discussed in this section were published in the journal Structural Health Monitoring under the title "Co-Kriging strategy for structural health monitoring of bridges" (Novais; Silva; Figueiredo, 2024).

The study focuses on capturing the correlation between natural frequencies and temperature variations. by combining numerical data from a finite element model with experimental data. The development of a co-Kriging model is showcased to improve damage detection performance, yielding superior results compared to traditional approaches and achieving high accuracy even when trained with a smaller subset of experimental data supplemented by abundant numerical data. Section 3.1 presents a brief review of techniques that combine hybrid datasets for structural health monitoring applications in bridges and how the current work proposes a novel approach to enhance data integration and damage detection. Section 3.2 provides insights into the Z24 bridge, a post-tensioned concrete box girder framework in Switzerland, serving as a significant case study in SHM. Section 3.3 presents the outcomes for the Z24 bridge, comparing the results obtained by Silva, Figueiredo and Moldovan (2022) (using a GPR model) with the co-Kriging performance. Finally, Section 3.4 outlines this chapter's remarks, and discussions are initiated regarding possible alternative approaches or future works.

3.1. PROBLEM STATEMENTS AND PROPOSED FRAMEWORK

Bridges play a key role in our society. However, their structural deterioration over time has increased the need for bridge owners and authorities to develop reliable methods for continuous assessment of structural conditions (Wenzel, 2008). Such assessment is crucial for optimizing maintenance and preventing potential bridge collapses. Over the past thirty years, structural health monitoring has emerged as a strategy for identifying damage through statistical pattern recognition (SPR) approaches (Figueiredo; Brownjohn, 2022).

The SPR framework aims to differentiate patterns or structural changes associated

with undamaged conditions—considering operational and environmental variations—from those linked to damage. This process starts with collecting response data and culminates identifying damage to evaluate the bridge's structural state. Within this framework, data-driven approaches have been developed to address the challenges posed by the lack of reliable physics-based methods and the limited availability of long-term experimental datasets necessary to fully characterize bridge behavior (Farrar; Worden, 2013). Unlike physics-based methods, which rely on inverse problem-solving techniques, data-driven approaches use statistical models to directly interpret physical phenomena from response data (Paixão *et al.*, 2021; Pavlack *et al.*, 2022; Vadyala *et al.*, 2022; Fan; Li; Hao, 2021).

One widespread method for these statistical models, which may be particularly relevant in the application of structural health monitoring for bridges, is Kriging. This approach provides a probabilistic framework for damage identification (Rytter, 1993), specifically for detecting damage and estimating its extent in the context of SHM applications. However, as discussed throughout this work, a limitation remains: acquiring a representative data set for understanding correlations through Kriging. Collecting such data can become prohibitively expensive, mainly when there is a lack of prior monitoring data or a clear understanding of the critical damage and its correlation with damage-sensitive feature variations. For example, Silva, Figueiredo and Moldovan (2022) demonstrated the challenge of obtaining enough experimental data to capture a bridge's temperature variations over an entire year, which requires costly instrumentation and the involvement of qualified professionals to collect adequate monitoring data.

Acknowledging the challenges, the SHM community is increasingly adopting hybrid datasets—combinations of numerical and experimental data (Malekzadeh; Atia; Catbas, 2015; Figueiredo *et al.*, 2019; Svendsen *et al.*, 2023). Data derived from numerical models, obtained through analytical methods or finite element models simulating system outputs, offer a promising solution by highlighting modifications in damage-sensitive features that correspond to increasing damage intensity. This approach has shown promise in enhancing the performance of classifiers and regression-based machine learning algorithms, ultimately leading to more precise and cost-effective solutions. However, it is essential to ensure that these models are robust and regularly updated to maintain accuracy, which can be resource-intensive and presents challenges for professionals in structural health monitoring.

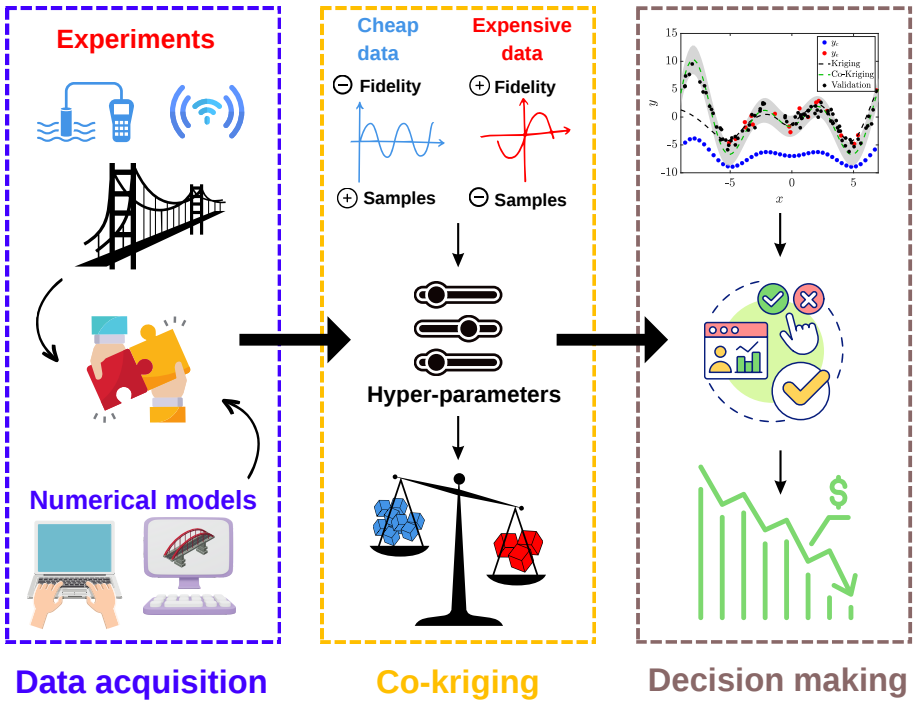
Recently, Silva, Figueiredo and Moldovan (2022) demonstrated the integration of

natural frequencies obtained from a numerical FE model with those derived from experimental data collected from a concrete bridge. This hybrid dataset was utilized to develop a Kriging model to improve regression curve estimation. However, the GPR model applied a single kernel function for estimation and did not account for two distinct probability distributions in the data learning process for regression. In this context, the proposal is to enhance regression curve estimation using the co-Kriging technique. It balances two datasets based on their characteristics (higher and lower fidelity) and quantities (numerical data being more abundant and experimental data being more limited). The primary contribution of this application example is to highlight the effectiveness and practicality of co-Kriging in the field of bridge structural health monitoring, further showcased using benchmark datasets from the Z24 bridge, a prestressed concrete structure that has been extensively monitored over the course of a year. While it shares similarities with other studies that utilize hybrid datasets for training regression models, this work introduces an innovative approach by incorporating a model that captures the differences between numerical and experimental data. This distinction underscores co-Kriging's potential to enhance regression accuracy, particularly in complex scenarios where data sources may be limited or costly. Figure 11 presents the comprehensive framework utilized in this study.

The process begins with data acquisition, which involves collecting costly experimental data from a real bridge structure while generating cheap numerical data from a finite element model. The experimental data, obtained through rigorous testing, offers high fidelity and reliability concerning the structural health of the analyzed bridge. However, the high costs and logistical challenges associated with these tests limit the quantity of experimental data that can be gathered. In contrast, numerical data from simulations can be produced in large quantities at a relatively low cost and effort. Although these numerical data points are generally less reliable and of lower fidelity than experimental data, their abundance provides a wealth of information that can improve the model's overall accuracy.

Following data acquisition, the next phase is data preprocessing, which involves evaluating the quality and compatibility of the datasets. This step is essential to ensure that both the high-fidelity experimental and abundant lower-fidelity numerical data are suitable for integration. Preprocessing may include filtering noise, aligning data to a common temporal or spatial resolution, and addressing gaps or inconsistencies. Effective preprocessing enhances the coherence between the datasets and prepares them for seamless

Figure 11 – Flowchart illustrating the proposed framework for enhanced bridge structural health variables predictions using a Co-Kriging strategy.



Source: Prepared by the author.

integration into the co-Kriging model.

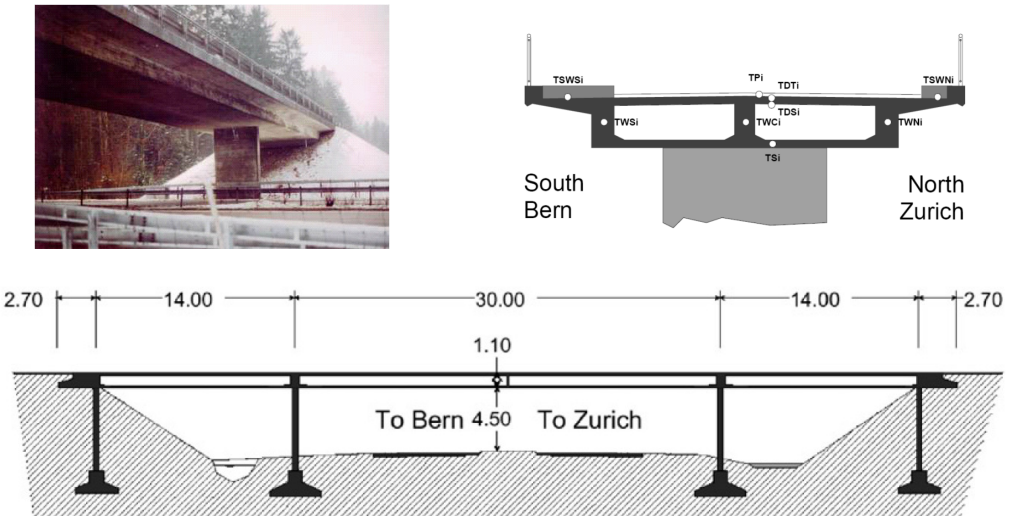
Once the data has been preprocessed, the next step is to optimize the hyperparameters of the co-Kriging model. This tuning process is vital to balancing the influence of the expensive experimental data with the cheaper numerical data, ensuring that the model effectively utilizes the strengths of both data types.

At the heart of this framework is the development of the co-Kriging model. By merging both experimental and numerical datasets, the co-Kriging model considers the covariance between them, significantly improving the prediction of the target variable. This integration allows for more accurate and reliable predictions essential for effective structural health monitoring. Ultimately, the co-Kriging model serves as a tool for making informed decisions regarding the analyzed bridge's structural health and maintenance requirements. The model's superior prediction capabilities enhance the decision-making process, facilitating timely and accurate identification of potential issues and their severity.

3.2. Z24 BRIDGE CASE STUDY: ANALYSIS OF EXPERIMENTAL AND NUMERICAL DATA AVAILABILITY

The Z24 bridge (Figure 12) was a post-tensioned concrete box girder structure in Switzerland, featuring two side spans measuring 14 m each and a central span of 30 m. The Z24 bridge is a noteworthy case in the SHM community, as it represents a structure subjected to realistic progressive damage tests and various environmental conditions before its complete demolition. For further details on the description of this bridge, the reader is referred to the work discussed by Maeck and Roeck (2003).

Figure 12 – Z24 bridge benchmark including the front view (bottom) and a cross-section of the girder, highlighting the locations where temperature measurements were taken (top-right).



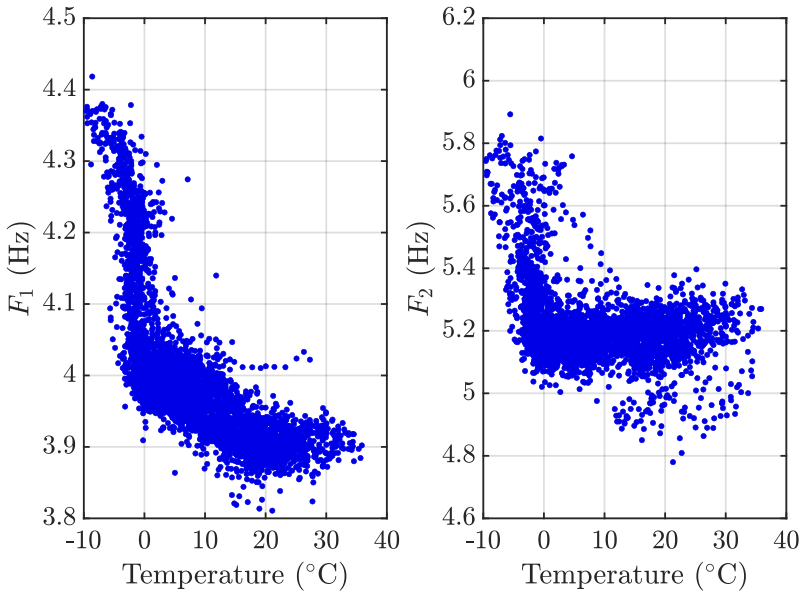
Source: Adapted from Maeck and Roeck (2003).

A continuous long-term monitoring plan was conducted on the bridge from November 11, 1997, to September 10, 1998, during which vibration data were collected. Sensors were strategically installed along the bridge span to monitor environmental parameters like temperature, humidity, and wind speed. Concurrently, eight accelerometers recorded structural responses hourly for 11 minutes. In the final month (August 4 to September 10, 1998), progressive damages were intentionally introduced to the bridge in preparation for its demolition (Peeters; Roeck, 2001; Reynders; Roeck, 2009).

Feature extraction was conducted to estimate the Z24 bridge's natural frequencies hourly, using these as sensitive indicators of structural integrity. Between November 11, 1997, and August 10, 1998, the bridge was undamaged, influenced by operational and

environmental conditions with temperatures spanning from −10°C to 35°C. Throughout this period, 4,955 hourly frequency samples were recorded, with peaks in natural frequencies observed at low temperatures, likely due to changes in the asphalt layer that increased the bridge's stiffness and altered its dynamic properties (Reynders; Roeck, 2009). In the final monitoring phase, from August to September 10, 1998, progressive damage was intentionally introduced to the bridge. Figure 13 illustrates the dataset for the first two natural frequencies over the entire monitoring period.

Figure 13 – Correlation of the first two natural frequencies versus ambient temperature under undamaged conditions.



Source: Prepared by the author.

Starting on August 4, 1998, a controlled campaign was initiated to progressively damage the bridge. This process included installing hydraulic jacks into the Koppigen pier to induce settlement and tilting by removing approximately 0.4 meters of concrete (Maeck; Roeck, 2003). Throughout the tests, the pier was supported by steel sections designed to mimic the stiffness of the original concrete. Hourly measurements were collected using a network of accelerometers (Bud *et al.*, 2022). Additional scenarios were simulated to assess various potential conditions, including concrete spalling, abutment landslides, hinge failures, anchor head malfunctions, and tendon ruptures. However, these scenarios are not discussed here, as they had minimal or negligible impact on bending stiffness (Maeck; Roeck, 2003) (the testing procedures followed the sensor network paradigms described by Figueiredo *et al.* (2011)). Table 1 provides an overview of the first six scenarios in the

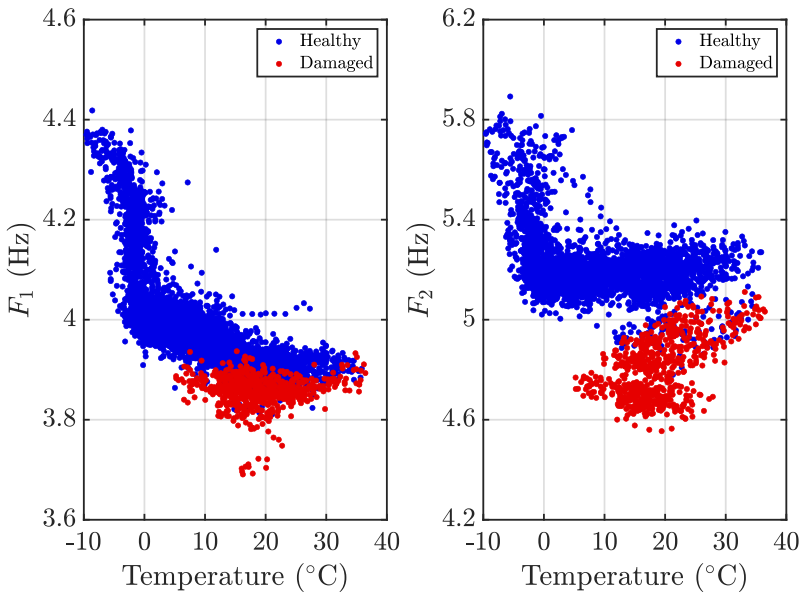
monitoring program (Silva; Figueiredo; Moldovan, 2022), and Figure 14 shows the dataset of the first two natural frequencies, comparing the bridge in healthy and damaged states.

Table 1 – Damage progression scenarios for the Z24 bridge in 1998.

Reference	Date	Scenario
1	04.08	Undamaged
2	09.08	Settlement system installation
3	10.08	Settlement of pier, 20 mm
4	12.08	Settlement of pier, 40 mm
5	17.08	Settlement of pier, 80 mm
6	18.08	Settlement of pier, 95 mm

Source: Prepared by the author.

Figure 14 – First two natural frequencies of the Z24 bridge under healthy and damaged conditions.



Source: Prepared by the author.

To enhance and complement the experimental data, a finite element model of the Z24 bridge was developed using CSi Bridge, a commercial finite element software. This model produced numerical samples of the bridge's natural frequencies across a temperature range from -10°C to 40°C. The design focused on simplicity and computational efficiency, primarily using beam elements for the structural components, although shell finite elements were employed for the abutment slabs and foundation blocks. Rigid links connected these elements, and elastic supports represented the soil-structure interface

under the foundations. The model also explicitly incorporated the asphalt layer, which significantly affects stiffness and natural frequencies, represented as beam elements linked to the girder with rigid connections. This modeling approach aimed to align experimental findings with numerical simulations. For further details about the numerical model, readers can refer to Silva, Figueiredo and Moldovan (2022) and Bud *et al.* (2022).

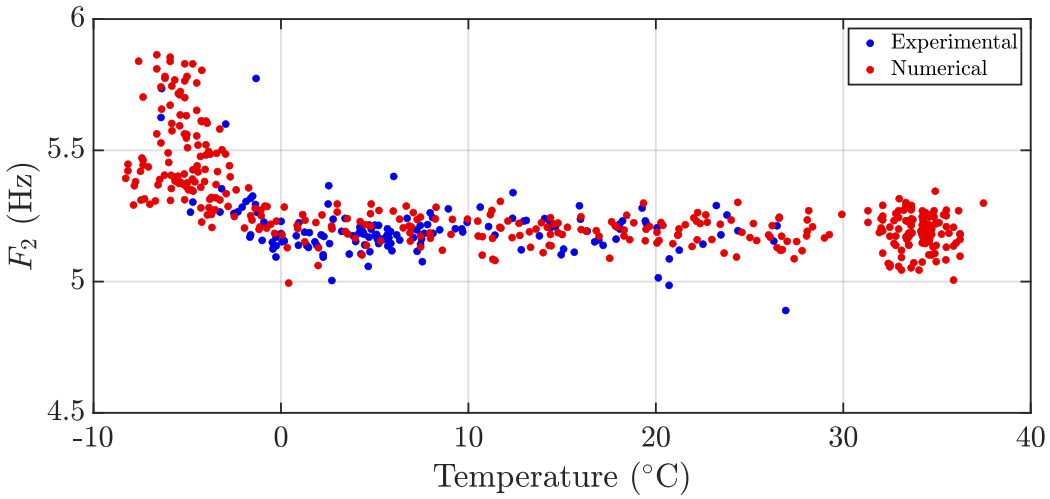
3.3. CO-KRIGING METHOD FOR DAMAGE DETECTION IN THE Z24 BRIDGE CONSIDERING TEMPERATURE EFFECTS

The analysis presented in this section builds upon the research conducted by Silva, Figueiredo and Moldovan (2022), which focused on examining the correlation between the natural frequencies and temperature variations of the Z24 bridge. This study created a hybrid dataset by integrating numerical data from a finite element model with experimental measurements. The implemented model provided supplementary data for the undamaged structure across a wide range of temperature variations that were not captured experimentally. A Kriging metamodel was developed to facilitate damage detection using three different training strategies: the first utilized only experimental data, the second relied solely on numerical data, and the third combined both experimental and numerical observations. The findings indicated that the hybrid approach yielded the best results in terms of binary classification, as measured by the number of false positives and false negatives. However, the GPR model constructed by the authors performed the integration of the hybrid datasets without differentiating between them. In this way, this new approach enhances classification performance for damage detection in the Z24 bridge by employing a co-Kriging method, treating the experimental data as the more costly, high-quality data, while the data derived from the FE model is considered the less expensive, lower-quality data.

The one-year monitoring of the Z24 bridge yielded 4,955 frequency samples, while the finite element model produced 14,096 samples (for simplicity, this analysis focuses on the second natural frequency). However, only 150 samples were randomly selected from the total to represent the expensive data, while 400 samples were chosen to represent the more abundant, cheaper data. Figure 15 displays both the cheap (numerical) and expensive (experimental) data used to implement the co-Kriging strategy.

To evaluate the classifier's performance, the model was tested with 200 new healthy

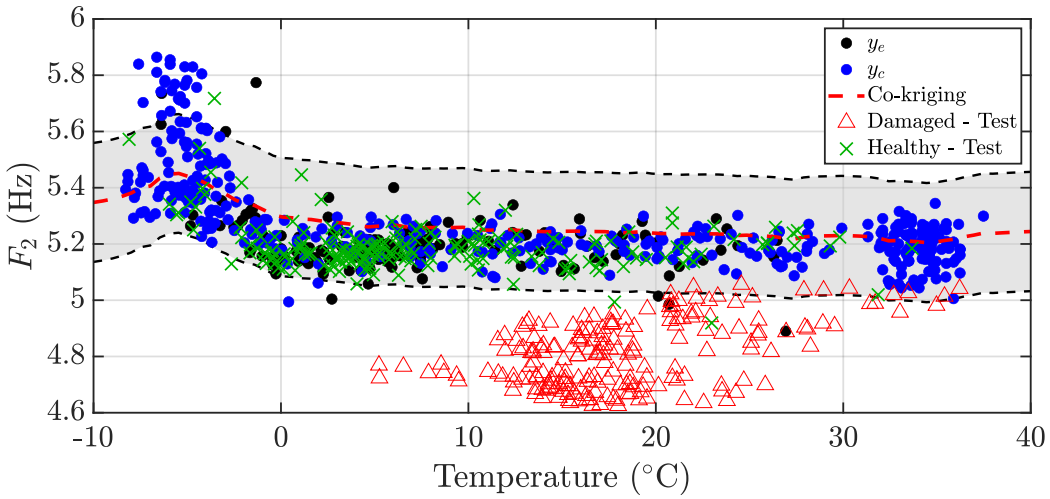
Figure 15 – Hybrid data of the relationship between 2nd natural frequency and ambient temperature in the healthy condition.



Source: Prepared by the author.

samples not part of the training phase, alongside 200 damaged samples sourced from the experimental data (the FE model was not employed to generate damaged samples for training). Figure 16 shows the classification performance of the co-Kriging model trained with hybrid training data.

Figure 16 – Co-Kriging model performance trained with numerical and experimental samples and tested with a database including healthy and damaged scenarios.



Source: Prepared by the author.

As noted by Silva, Figueiredo and Moldovan (2022), the hybrid approach outperformed models trained solely on numerical or experimental data regarding binary classification, particularly regarding the number of false positives and false negatives. The

co-Kriging method further improved these results, achieving even better outcomes in binary classification, as shown in Table 2. Specifically, it reduced the Type II error from 4% to 2.5%. It is important to emphasize that this classification considers two types of errors: Type I error, which occurs when a test incorrectly indicates the presence of a condition or attribute (commonly referred to as the false alarm or false positive rate - FPR), and Type II error, which arises when a test incorrectly suggests the absence of a condition or attribute (known as the miss rate or false negative rate - FNR), as follows (Fawcett, 2006; Taha; Hanbury, 2015):

$$\mathrm{FPR} = \frac{\mathrm{FP}}{\mathrm{FP} + \mathrm{TN}} \tag{3.1}$$

$$\mathrm{FNR} = \frac{\mathrm{FN}}{\mathrm{FN} + \mathrm{TP}} \tag{3.2}$$

where FP represents the number of false positives (instances where the test mistakenly identifies the presence of a condition), TN denotes the number of true negatives (instances where the test accurately identifies the absence of a condition), FN signifies the number of false negatives (instances where the test incorrectly identifies the absence of a condition), and TP indicates the number of true positives (instances where the test correctly identifies the presence of a condition). In this study, these classifiers focus on determining the presence or absence of damage in the structure being analyzed.

Table 2 – Classification performance for damage detection using all four approaches regarding Type I and Type II errors.

Training Strategy	Type I error (%)	Type II error (%)
Experimental data	8	3
Numerical data	19.5	0
Hybrid data: Kriging	5.5	4
Hybrid data: co-Kriging	5.5	2.5

Source: Prepared by the author.

The co-Kriging method offers advantages that extend beyond improved binary classification performance. For instance, co-Kriging was trained using only 150 experimental samples, compared to 400 samples for training the traditional Kriging model. This efficiency is particularly significant, as obtaining experimental samples can be costly and labor-intensive. The co-Kriging method's ability to perform effectively with limited data-

sets makes it well-suited for real-world applications where data collection is constrained, positioning it as a practical solution in scenarios with limited training data.

3.4. PARTIAL REMARKS

The Z24 bridge in Switzerland was the subject of study in this chapter, examining its natural frequencies in correlation with temperature variations throughout the year. Co-Kriging has demonstrated superior performance to ordinary Kriging, reducing the Type II error from 5.5% to 2.5%, even when trained with a smaller subset of experimental data, complemented by abundant numerical data from a finite element model. This approach represents an economical and effective solution, especially when collecting experimental data is resource-intensive and challenging. Additionally, it is suggested to implement the co-Kriging method to compare various numerical models with varying levels of calibration and fidelity. The aim is to explore how this approach could improve regression accuracy by incorporating data from a simpler, more efficiently evaluated model as co-variables.

4 CO-KRIGING MODELING FOR DELAMINATION QUANTIFICATION IN LAMINATES

This chapter provides a theoretical background on structural health monitoring methodologies for damage quantification in composite materials, specifically laminates. Section 4.1 emphasizes the significance of composite materials in engineering, their vulnerability to damage, and the importance of SHM techniques. Various SHM methods are discussed, including GPR, with co-Kriging proposed for damage quantification. Next, Section 4.2 addresses delamination damage in composites, focusing on the role of Lamb waves in detecting this effect within such structures. Following this, Section 4.3 provides an overview of autoregressive models and their utility in extracting damage-sensitive features, and Section 4.4 discusses the proposed Mahalanobis Squared Distance for structural condition classification. Then, Section 4.5 outlines the methodology employed for damage detection and quantification in a composite plate using co-Kriging. Further, Section 4.6 details the hybrid dataset used in this work, integrating experimental and numerical data under various conditions, including delamination. Section 4.7 showcases the results achieved in detecting and quantifying delamination through co-Kriging. Finally, Section 4.8 concludes with key insights and opens a discussion on potential alternative approaches and directions for future work.

4.1. INSIGHTS INTO STRUCTURAL HEALTH MONITORING FOR COMPOSITE MATERIALS: TECHNIQUES AND STOCHASTIC APPROACHES

Composite materials have become essential in modern engineering and manufacturing. They are created by combining different phases at the macroscopic level, leading to enhanced performance compared to their components. As a result, these synthesized materials frequently exceed traditional materials' mechanical, thermal, and electrical properties (Daniel; Ishai, 2006). Over the past few decades, the utilization of composite materials has experienced significant growth, driven by industries such as aerospace, automotive, agriculture, civil engineering, and renewable energy. The request for composites lies in their superior properties to metallic materials, such as high strength, stiffness, low density, and excellent corrosion resistance (Ghrib *et al.*, 2019). Notably, materials like carbon fiber-reinforced polymers offer exceptional mechanical properties.

However, due to their complex internal structure, often anisotropic, and their vulnerability to various types of damage, such as matrix cracking, delamination, debonding, etc., identifying and predicting failure in composite materials has become challenging. Consequently, structures are often over-designed to avoid catastrophic failures, leading to increased costs (Saxena *et al.*, 2011). Effective damage detection and prediction techniques, like structural health monitoring, ensure composite structures' safe and reliable performance, enable timely maintenance and repair strategies, and maximize their cost-efficiency in various engineering and industrial sectors. Numerous SHM techniques for composite materials have been documented in the literature, employing various technologies such as ultrasonic inspection, imaging methods, acoustic emission, fiber optic sensors, piezoelectric lead zirconate titanates (PZTs), and laser vibrometry (David-West *et al.*, 2017; Yuan; Wang; Chen, 2020). In the past two decades, special SHM techniques based on active-sensing guided waves have garnered considerable attention, particularly for composite structures, owing to their heightened sensitivity to early-stage damage. On the other hand, these active-sensing SHM methods still encounter significant challenges due to their susceptibility to operating and environmental conditions.

It is important to highlight that most damage quantification techniques are deterministic, lacking confidence intervals for estimating damage size and relying on extensive data from a population of identical structures to accommodate varying conditions (Amer; Kopsaftopoulos, 2019). However, this limitation can be overcome by adopting a stochastic approach to estimate damage size, offering a more precise and robust prediction while minimizing the data requirements in this context (Corbetta *et al.*, 2018). A stochastic procedure that can address this issue is the construction of surrogate models, a widely employed strategy in science and engineering to describe physical phenomena (Franzoi *et al.*, 2022).

One prominent and widely used method is Kriging, which allows for incorporating uncertainties in the model, enabling the quantification of confidence intervals for the predictions (Fuentes *et al.*, 2014). This strategy has proven effective in many SHM approaches in composites, as discussed by Paixão *et al.* (2021) and Pavlack *et al.* (2022), for example. In the first one, the authors proposed a data-driven approach using stochastic modeling and GPR to quantitatively assess delamination damage in composite materials. The main objective was to determine whether there is an imminent structural failure or if the system can continue to operate under monitoring to track the damage progression and

its impact on structural safety. Auto-regressive models were applied to extract damage-sensitive features from Lamb wave signals, while the Mahalanobis squared distance was used to compute damage indices. The GPR effectively accommodated uncertainties associated with the damage indices and the affected area, resulting in smooth and accurate predictions for both simulated and actual delamination damage. In the second one, Pavlack *et al.* (2022) showcased the potential of using GPR in the complex geometry of wind turbine composite blades with debonding defects, improving Kriging with polynomial chaos expansion (PCE) (Lüthen; Marelli; Sudret, 2021). The study demonstrated that the PCE method effectively captures the global behavior of the computational model, while Kriging captures local variations, resulting in a more robust PC-Kriging approach for obtaining metamodels. Additionally, the PC-kriging trend curve consistently reflected a monotonic increase in damage indices, indicating promising outcomes for damage quantification.

However, while the studies mentioned have brought significant insights, the same limitation remains (refer to Section 3.1). In practice, conducting experimental tests to study damage mechanisms such as fiber breaking, matrix micro-cracking, delamination, and adjacent layers, debonding can be costly. This issue could be addressed by implementing the co-Kriging strategy. By integrating a co-variable that encloses information regarding the damage, researchers can construct a relevant model that simulates fracture mechanisms in laminates and correlates with the target variable. This incorporation allows for numerical simulations to assemble co-variable data, which can then be utilized in the prediction process.

Building upon the damage modeling methodology for composite materials established by Ladevèze *et al.* (2000), which introduced a mesoscale model to accurately depict interlaminar damage and delamination under dynamic loading using an explicit method, this study proposes a simplified approach to simulate delamination scenarios of varying extents using a composite plate model. However, the innovation of this work lies in its ability to simulate these delamination damage scenarios in a simplified manner. The model is not calibrated and produces approximate signal patterns corresponding to different levels of delamination without necessarily providing precise measurements. It aims to balance low-cost numerical simulation data with a small amount of experimental data by considering the kernels in Kriging. Specifically, the goal is to enhance delamination area estimation by integrating experimental data, which can be challenging to quantify, with

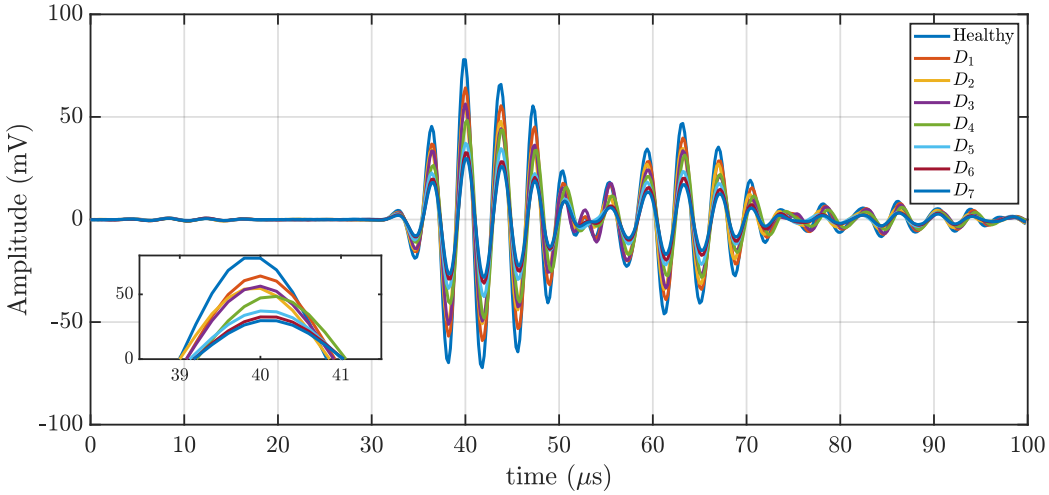
numerical data from a finite element model. The following section will address delamination more effectively by investigating its effects on composites and exploring detection and monitoring techniques.

4.2. STRUCTURAL HEALTH MONITORING USING LAMB WAVES FOR DELAMINATION DETECTION IN COMPOSITE STRUCTURES

Delamination is a critical issue in composite structures, as it severely compromises their strength and is often a primary factor in structural failure (Larrosa; Lonkar; Chang, 2014). This failure mode is particularly concerning due to the relatively weak interfaces between the layers of composite laminates (Latifi; van der Meer; Sluys, 2015). Delamination occurs when the layers within a composite separate, typically triggered by matrix cracking, bending cracks, and shear cracks. This type of damage significantly reduces the compressive strength of the laminate, ultimately leading to failure through buckling. Therefore, effective management and understanding of delamination are essential for maintaining the structural integrity and reliability of composite materials subjected to impacts (Safri; Sultan; Jawaid, 2019).

Paixão *et al.* (2021) demonstrated that delamination damage in composites, simulated by the application of an industrial adhesive putty to the surface of a composite plate, reduces the signal amplitude and causes a shift in the phase during guided wave propagation. An even more pronounced attenuation of the amplitudes was observed as the area covered by the adhesive increased, as illustrated in Figure 17. Similarly, Lee *et al.* (2011) reported that the addition of localized mass introduces changes in the damping characteristics of the plate, which are associated with energy dissipation effects. In real delamination scenarios, the separation between layers leads to interlayer displacement, accompanied by contact and friction between the detached regions, resulting in dissipative effects. In this work, the adhesive mass was intentionally used to simulate these dissipative effects caused by delamination, providing a controlled way to study the impact of such damage on guided wave propagation in composite structures. The experimental results showcased in Figure 17, which serve as a foundational reference for this study, are derived from the CONCEPT dataset (CarbON-epoxy CompositE PlaTe) (Silva *et al.*, 2021; Paixão *et al.*, 2021; Paixão; Silva; Figueiredo, 2020; Silva, 2018). For a detailed overview of the experimental setup and data processing, please refer to Section 4.6.

Figure 17 – Effects of delamination damage on output signals from a composite plate.



Source: Prepared by the author.

Numerous researchers have extensively studied and validated the use of active sensing with Lamb waves for diagnosing delamination in composite structures, often employing PZT sensors. These sensors, attached to the structure, propagate Lamb waves through the material being analyzed, and damage identification is achieved by analyzing the waves captured by multiple PZT sensors. Several studies have confirmed the effectiveness of this method for damage detection and localization (Yuan, 2016; Tian; Yu; Leckey, 2015; Figueiredo *et al.*, 2011; Mitra; Gopalakrishnan, 2016). Lamb waves, also known as plate waves, are guided waves that propagate between two parallel surfaces in plate-like structures (Ihn; Chang, 2004). They are particularly prevalent in thin, plate-like materials, where they are confined and channeled by their upper and lower free surfaces. In finite bodies, various wave modes exist, and their propagation characteristics are influenced by factors such as entry angle, frequency, and the structure's geometry (Su; Ye, 2009). Building on this, active structural health monitoring systems that utilize interrogative Lamb waves offer an effective solution, combining cost efficiency with the ability to monitor large areas from a single position (Gresil *et al.*, 2013). The inherent properties of Lamb waves—such as their capacity for long-distance propagation and high sensitivity to changes in structural integrity—make them particularly valuable for SHM methodologies (Dworakowski *et al.*, 2015). A wealth of literature illustrates how changes in the received Lamb wave signals, affected by structural damage, can be utilized for monitoring purposes (Dworakowski *et al.*, 2015).

Toyama, Noda and Okabe (2003) demonstrated that transverse cracking and de-

lamination reduce the structure's stiffness and influence the propagation velocity of the symmetric mode S_0 in cross-ply laminates. In another study, Ramadas *et al.* (2009) investigated the interaction of the anti-symmetric mode A_0 with symmetric delamination, observing a mode conversion from A_0 to S_0 as the wave passed through the damaged region. They suggested estimating the delamination size by measuring the time-of-flight between the through-transmitted mode-converted signals. Nevertheless, it is worth noting that Lamb waves present multiple modes of propagation and are influenced by various interference sources, including high-frequency ambient noise, low-frequency structural vibration, temperature fluctuations, operational variability, and material inhomogeneity and anisotropy (Su; Ye, 2009). Consequently, constructing a robust SHM method relies on extracting damage features with reduced sensitivity to interference sources or implementing sophisticated compensation techniques, considering the intricate complexity of Lamb wave propagation.

Numerous damage features have been documented in the literature, leveraging variations in wave attenuation, time-of-flight, reflection, time-frequency analysis, and other time-domain characteristics (Dworakowski *et al.*, 2015; Figueiredo *et al.*, 2012). For instance, Dworakowski *et al.* (2015) introduced an innovative structural health monitoring approach tailored to aircraft structures utilizing Lamb waves. This method involved integrating piezoelectric sensors within the aircraft sheathing to generate Lamb waves, facilitating the monitoring of the integrity of complex parts. Various damage indices were successfully computed by analyzing the ultrasonic signals captured from these sensors. Similarly, in their research on damage detection in composite plates, Figueiredo *et al.* (2012) employed autoregressive models with exogenous inputs in the time domain to model the data gathered by piezoelectric active sensors, using the parameters of these models as damage-sensitive features. Furthermore, Silva (2018) demonstrated that a simple autoregressive model, identified using Lamb waves, could effectively predict wave propagation under varying temperature conditions for composite structures. In a recent study, Paixão *et al.* (2021) investigated the detection and localization of damage in a carbon-fiber epoxy laminated composite plate, specifically focusing on the progressive propagation of delamination under varying temperature conditions. To accomplish this, autoregressive models were employed to extract damage-sensitive features from Lamb wave signals, while the Mahalanobis squared distance was utilized to calculate damage indices. Additionally, the researchers trained and applied a GPR model within the same structure to predict

intermediaries' delamination areas.

4.3. DAMAGE SENSITIVE FEATURE EXTRACTION USING AUTOREGRESSIVE MODELS

In recent years, vibration-based damage identification methods have gained significant attention due to their simplicity of operation and clear physical interpretation (Spencer; Ruiz-Sandoval; Kurata, 2004; Alvandi; Cremona, 2006; Chao; Loh, 2013). These methods aim to extract damage-sensitive features from the structural vibration response, enabling the identification, localization, and evaluation of damage severity (Tang *et al.*, 2020). One popular approach for extracting damage-sensitive features is the autoregressive model (AR). Lynch (2004) demonstrated that the AR coefficients are associated with the inherent characteristics of a structure, achieved by implementing Z-transformation on the AR model equation. This significant advancement has provided a solid basis for utilizing AR model-based methods in damage identification.

Autoregressive models are a linear predictive modeling technique designed to forecast a signal sample based on previous samples, using the AR parameters as coefficients. Typically, the modeling of an AR model involves three primary steps: a) determining the model order, b) estimating the model parameters, and c) evaluating the model's validity (Jonathan; Kung-Silk, 2008). When a model expresses a time series $x(k)$ as a linear combination of past n_r-th samples and a white noise or residual error with zero mean $e(k)$, it is called an AR model (Kitagawa, 2010; Gandhi, 2015),

$$x(k) = e(k) + \sum_{r=1}^{n_r} a_r x(k-r) \tag{4.1}$$

where a_r are the AR coefficients. The residual error in an AR model represents the portion of the signal that remains unexplained by the linear combination of the model's explanatory variables. It is assumed to be an independent random variable. When the AR model is properly identified, the residual error follows a normal distribution with a mean of 0 and a variance of σ^2 (Kitagawa, 2010).

In SHM applications, AR models can be employed as a damage-sensitive feature extractor through two approaches: a) using the residuals errors $e(k)$, and b) using the AR parameters a_r. The first approach involves utilizing the AR model, with parameters

estimated from the baseline condition, to forecast the response of data acquired from a potentially damaged structural condition. The residual error is calculated as the difference between the measured and predicted signals. This approach assumes that damage can cause either linear deviations or nonlinear effects in the signal. Consequently, the baseline linear model may no longer accurately predict the response of the damaged structure. The second approach involves fitting an AR model to signals obtained from undamaged and damaged structural conditions. In this particular approach, the AR model parameters are used as the damage-sensitive features, and a multivariate classifier is then employed to distinguish between different damage classes. (Figueiredo, 2010).

To identify an appropriate AR model, it is necessary to first select its order, which is initially unknown. Several techniques to address this problem can be found in the literature. Still, two of them gain prominence in SHM approaches: the Akaike information criterion (AIC) and Bayesian information criterion (BIC). The AIC (Akaike, 1974) is a well-known technique used for model selection based on in-sample fit to estimate the likelihood of a model to predict or estimate future values. A good model is characterized by having the minimum AIC among all the other models. The BIC (Stone, 1977) is an alternative criterion for model selection that provides a measure that considers both model fit and model complexity. Lower values of AIC or BIC indicate a better fit of the model while taking into account its complexity (Mohammed; Naugler; Far, 2015).

Autoregressive models can be mainly employed as damage-sensitive features in two distinct ways: by utilizing the residual errors $e(k)$ and the AR coefficients a_r (Figueiredo, 2010). Numerous statistical features are available in the literature, which are employed to capture alterations in the distribution of coefficients and residual errors. In a healthy structural condition, an AR model will identify a measured signal from the Lamb wave propagation, which will represent the baseline condition. Suppose a new signal from a baseline condition is accurately identified, and the signal has no significant changes. In that case, the AR coefficients ($\mathbf{A_B}$) should remain almost constant, and the residual errors in this baseline condition ($\mathbf{e_B}$) should exhibit a white noise process. On the other hand, if the AR model identifies a new, different, and unknown condition using the same previously selected order n_r, the new AR coefficients ($\mathbf{A}_{\text{ident}}$) and the residual errors will consequently be different. This is because the signal carries new information, indicating that the structure is no longer in the initial condition. The two damage-sensitive features utilized in this work were proposed by Sohn and Farrar (2001) and later implemented by

Paixão *et al.* (2021), which are given by: a) the ratio between the variance of the residual errors,

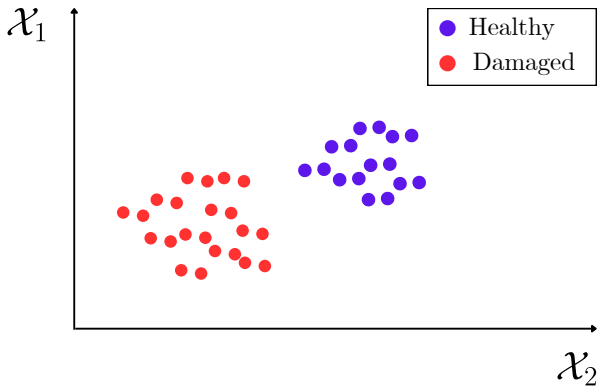
$$\mathcal{X}_1 = \frac{\sigma^2(\mathbf{e}_{\text{ident}})}{\sigma^2(\mathbf{e}_{\text{B}})} \tag{4.2}$$

where $\mathbf{e}_{\text{ident}}$ and $\mathbf{e}_{\text{B}}$ are the vectors that include all samples of residual errors obtained from the AR models identified under both the unknown and baseline conditions, respectively; b) the ratio between the variance of the AR coefficients,

$$\mathcal{X}_2 = \frac{\sigma^2(\mathbf{A}_{\text{ident}})}{\sigma^2(\mathbf{A}_{\text{B}})} \tag{4.3}$$

where $\mathbf{A}_{\text{ident}}$ and $\mathbf{A}_{\text{B}}$ are the vectors that include all samples of the coefficients obtained from the AR models identified under both the unknown and baseline conditions, respectively. With this feature space constructed using both damage-sensitive features $\mathcal{X}_1$ and $\mathcal{X}_2$, as depicted in Figure 18, a new procedure can be implemented to calculate damage indices for classifying the structural conditions.

Figure 18 – Illustration of feature space.



Source: Prepared by the author.

4.4. DAMAGE INDICES FOR STRUCTURE CONDITION CLASSIFICATION

The proposed damage index in this work is based on the Mahalanobis Squared Distance ($\mathcal{D}^2$ or MSD), a scalar measure used for detecting outliers in multivariate data (WORDEN; MANSON; FIELLER, 2000). Mahalanobis distance is a well-defined distance metric that quantifies the distance between two points in a feature space that consists of two or more variables (Zhou *et al.*, 2015). This distance serves multiple purposes,

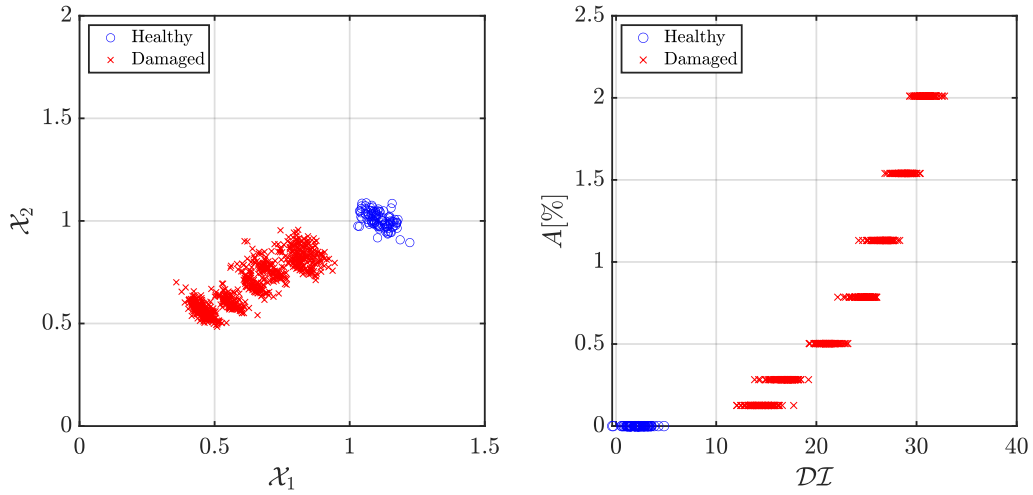
including spectral matching, outlier detection during calibration or prediction, and identification of extrapolation issues during analyses (Mark; Workman, 2018). This approach combines two damaged features into a bi-variate feature space. The MSD is then utilized with a machine-learning algorithm to measure the distance from the centroid of a well-known cluster of points to any other point in the bi-variate space. The Mahalanobis Squared Distance is defined as follows (Zhou *et al.*, 2015):

$$\mathcal{D}^2 = \mathcal{DI} = (\mathbf{X} - \bar{\mathbf{Z}})^T \Sigma^{-1} (\mathbf{X} - \bar{\mathbf{Z}}) \tag{4.4}$$

where $\mathbf{X}$ is the test matrix containing a percentage of features associated with a baseline condition in conjunction with the damage conditions, $\bar{\mathbf{Z}}$ is the mean vector, and Σ is the covariance matrix of the training matrix from the features in the baseline condition.

This approach establishes a relationship between the proposed index and another parameter (specifically the delamination area in this study), as shown in Figure 19. Subsequently, a regression process can be implemented to quantify the damage's extent and obtain a confidence interval for the assessment.

Figure 19 – Illustrative example of damage feature extraction using autoregressive models combined with Mahalanobis Distance for damage classification.



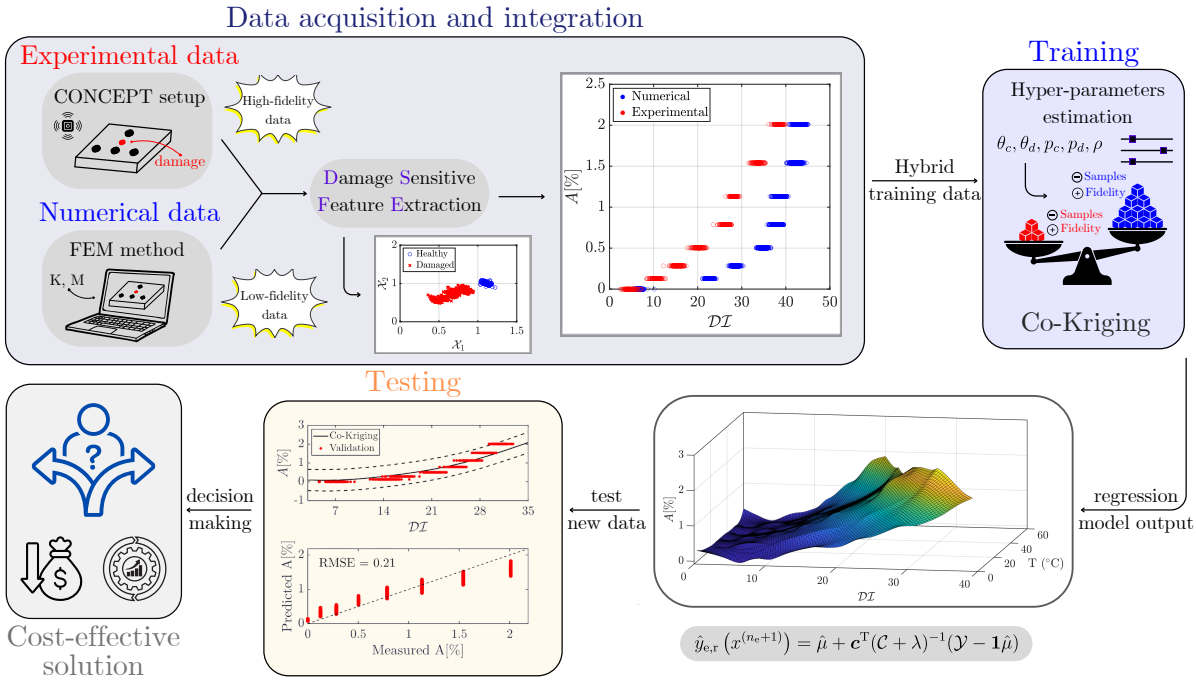
Source: Prepared by the author.

4.5. PROPOSED FRAMEWORK

This work introduces a co-Kriging model that integrates a hybrid dataset for detecting and quantifying damage in a laminated composite structure. Figure 20 illustrates

the comprehensive framework employed in this study.

Figure 20 – Graphical abstract depicting the proposed framework for cost-effective damage detection and quantification in composites utilizing hybrid data in a co-Kriging regression model.



Source: Prepared by the author.

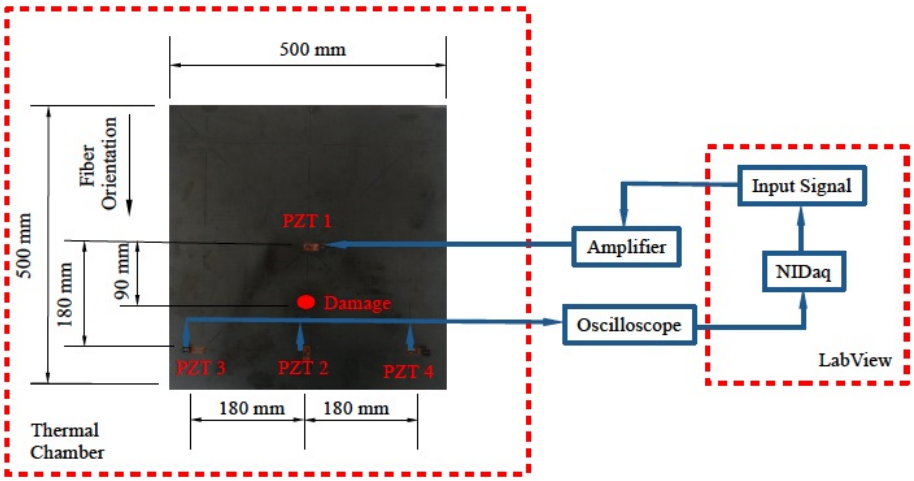
The process begins with integrating experimental data from a composite material plate, regarded as high fidelity, alongside numerical simulations derived from a finite element model, considered low fidelity. Damage-sensitive features are extracted from these datasets using autoregressive models, generating damage indices based on variations in the amplitude and phase of the measured signals. The co-Kriging model is then employed to correlate high- and low-fidelity data, enhancing predictions related to the delamination area. Following this, the predictive model is validated with new input data to assess its effectiveness in detecting and quantifying the extent of damage. With the established damage indices, this method lays the foundation for informed decision-making regarding the structural integrity of the analyzed component, facilitating reliable and cost-effective monitoring of composite structures.

4.6. HYBRID DATASET FOR CO-KRIGING: EXPERIMENTAL AND NUMERICAL DATA

4.6.1 Expensive data - experimental setup

The experimental setup in this work involves a carbon-epoxy composite plate from the CONCEPT dataset[1] (CarbON-epoxy CompositE PlaTe) (CarbON-epoxy CompositE PlaTe) (Silva *et al.*, 2021; Paixão *et al.*, 2021; Paixão; Silva; Figueiredo, 2020; Silva, 2018). This laminated plate consists of ten layers with fibers oriented along the plate borders directions (0° and 90°). The plate dimensions are 500 × 500 × 2 mm³. It was mounted with free boundary conditions to enhance consistency and minimize operational variability. Figure 21 presents a schematic overview of the experimental setup.

Figure 21 – Schematic representation of CONCEPT.



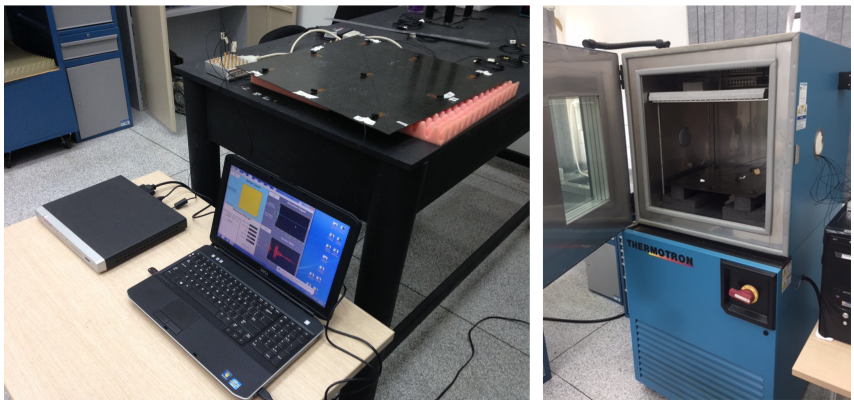
Source: Adapted from Paixão *et al.* (2021).

Four PZT transducers, known as *SMART Layer* from *Accelent Technologies*, were integrated into the composite plate for instrumentation purposes. Each transducer measures 6.35 mm in diameter and 0.25 mm in thickness. Among these transducers, PZT 1 was employed as the actuator. It applied a tone burst input signal consisting of five cycles at 35 V amplitude and a central frequency of 250 kHz. Then, the outputs are collected at PZT 2, PZT 3, and PZT 4 at a sampling rate of 5 MHz, with all channels measured in synchronization. Data acquisition was controlled by *LabVIEW* using a *National Instruments NI USB 6353*N (NIDaq) and a *Keysight* DSO7034B oscilloscope. The plate

[1] https://github.com/shm-unesp/DATASET_PLATEUN01

was subjected to controlled temperature testing inside a *Thermotron* thermal chamber. Seven temperature levels ranging from 0°C to 60°C with a 10°C variation were evaluated. Figure 22 illustrates the experimental setup used in the experiment.

Figure 22 – Schematic representation of CONCEPT.



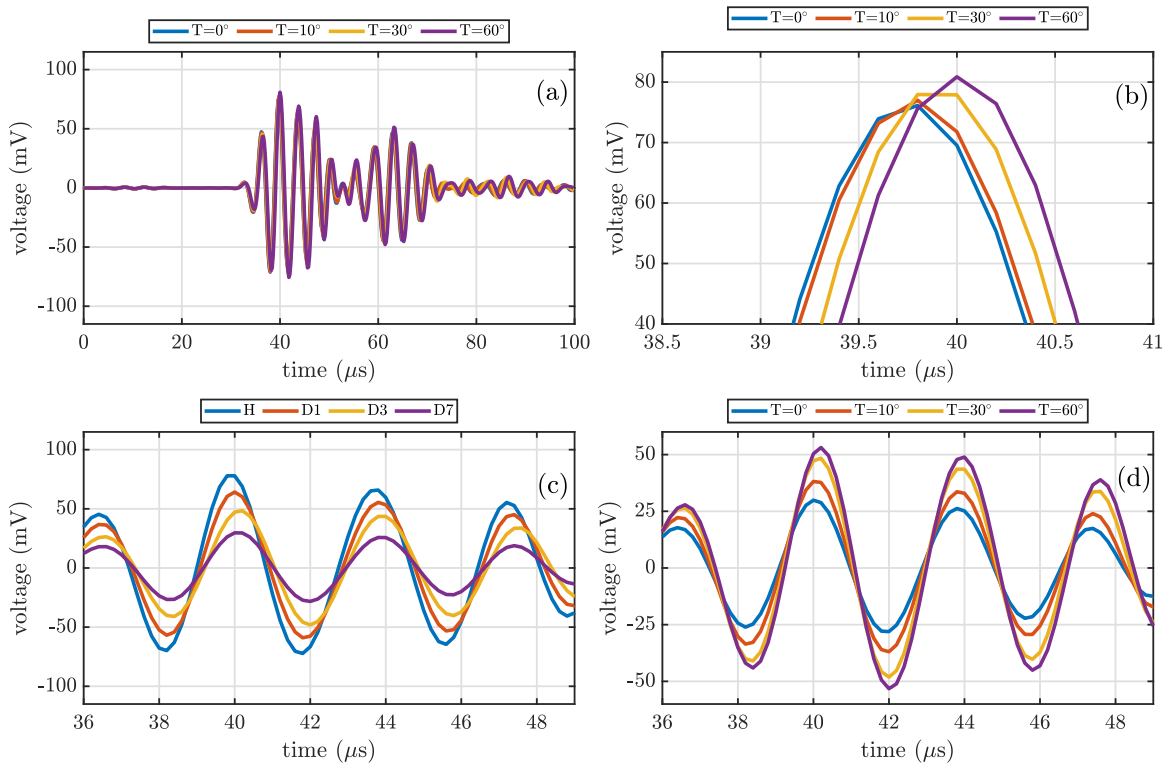
Source: Prepared by the author.

To simulate damage, an industrial adhesive putty was applied to the plate surface, introducing a localized mass change that mimics variations in plate damping, similar to delamination observed in composite structures (Lee *et al.*, 2011). The putty-covered area was incrementally expanded for progressive damage representation while maintaining a consistent circular shape and weight. For each damage state, 100 consecutive output signals were collected. Figure 23 presents experimental signals recorded under undamaged and damaged conditions for different temperature values.

As discussed in Section 4.2, the impact of simulated damage on a composite material plate affects wave propagation by causing a decrease in signal amplitude as the damaged area increases. This also leads to increased local damping, resulting in greater wave attenuation (Lee *et al.*, 2011). Additionally, researchers in the scientific community have examined the impact of temperature changes on guided wave propagation. A common outcome is that temperature variations lead to both phase shifts and amplitude variations in the signal compared to the baseline condition (Salamone *et al.*, 2009). Seven different damage conditions were tested, and the delamination area was computed based on the ratio between the industrial adhesive putty and the plate areas. Table 3 presents an example of how the results are used to quantify the delamination area numerically.

The baseline condition chosen for this study is the healthy state of the plate at a temperature of 30°C, representing the structure's typical behavior under normal ambient

Figure 23 – Experimental results for PZT2 signals under different conditions. (a) Healthy signals at different temperature conditions; (b) zoomed-in view of the signal in (a); (c) comparison between healthy and progressive damage signals at the same temperature; and (d) comparison of the same damage condition at different temperatures.



Source: Prepared by the author.

Table 3 – Structural conditions tested for the carbon-epoxy laminate.

Condition	Healthy	Ds_1	Ds_2	Ds_3	Ds_4	Ds_5	Ds_6	Ds_7
A [%]	0	0.13	0.28	0.50	0.79	1.13	1.54	2.01

Source: Prepared by the author.

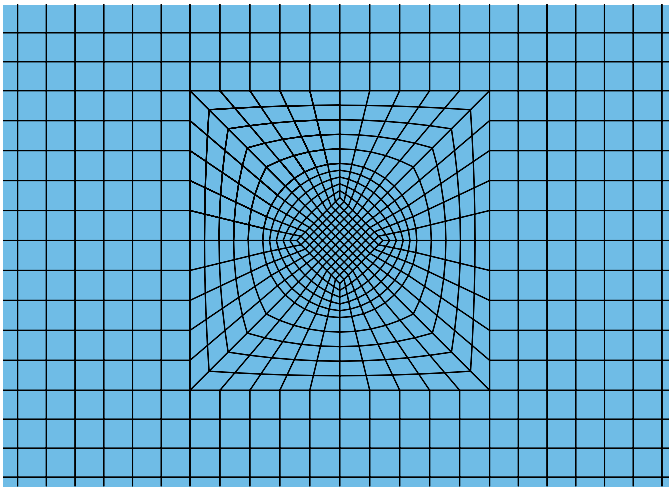
conditions. This information is essential, as it is the foundation for applying autoregressive methods and computing damage indices accordingly.

4.6.2 Cheap data - numerical simulations

A finite element model was developed in the commercial software Ansys LS-DYNA, which utilizes explicit simulations to capture material responses under short-duration, high-intensity loads. LS-DYNA has been successfully applied in previous studies to model fast dynamic events in damaged composites, particularly for simulating complex interla-

minar damage and delamination effects in laminated structures, as detailed by Ladevèze *et al.* (2000). This study modeled the plate with fully integrated shell elements following the first-order shear deformation theory (LSTC, 2012). The FE model defines the composite material properties at each ply level, with orthotropic laminate properties representing the layup and three integration points per lamina. Figure 24 illustrates the implemented model, highlighting the region covered by PZT sensors. The PZT actuators and sensors were simulated by modeling the area where they are attached to the plate using a circular mesh, sharing the same element type, material properties and boundary conditions as the rest of the plate under the healthy conditions of the structure. This simplification assumes that the interaction between the PZT and the plate is idealized, without explicitly including piezoelectric properties or coupling effects.

Figure 24 – Visualization of the FE model within the PZTs region.



Source: Prepared by the author.

Explicit integration methods are particularly suited for dynamic problems of short duration or systems involving wave propagation, such as impact-loaded structures. These methods solve equilibrium equations at time t to determine the response at $t + \Delta t$. By using a diagonal mass matrix, explicit integration avoids the need for matrix storage, leading to a lower computational cost per time step than implicit methods. However, the effectiveness of explicit methods is highly dependent on the spatial and temporal resolution of the model and often necessitates very short steps to maintain numerical stability (Dokainish; Subbaraj, 1989; Moser; Jacobs; Qu, 1999). To achieve both high efficiency and accuracy, it is recommended in the literature that the maximum element size Δx and integration time step Δt comply with the conditions in Equations 4.5 and

4.6.

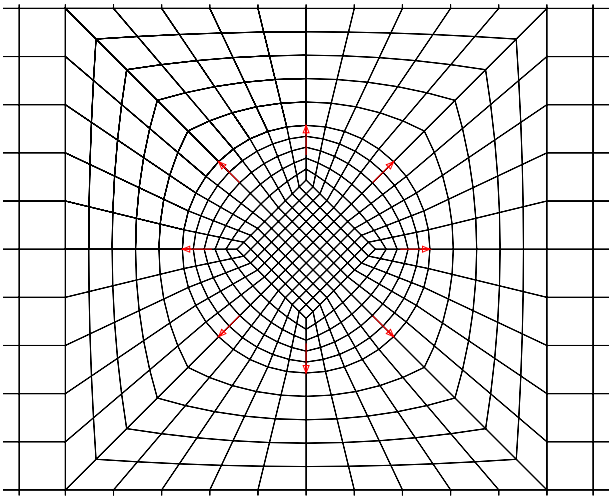
$$\Delta x \leq \frac{\lambda_{min}}{20} \tag{4.5}$$

$$\Delta t \leq \frac{1}{20 f_{max}} \tag{4.6}$$

where λ_{min} represents the shortest wavelength of interest, and f_{max} is the maximum frequency expected in the simulation. For the setup configured to match the CONCEPT experiment, with an excitation signal at 250 kHz, the calculated values yield an element size of approximately 2 mm and a time step around 0.2 μs.

It is important to note that, despite the relatively simple geometry designed to meet the specified parameters, the resulting mesh comprised 174,712 elements. Each numerical simulation conducted using LS-DYNA software took approximately 2 minutes to complete[2]. This aligns with the fundamental concept of co-Kriging, which creates co-variables to enhance phenomena' estimation cost-effectively. For a circular PZT, the excitation signal proposed by Gresil *et al.* (2013) involves strategically applying eight self-balancing forces around the region, as illustrated in Fig. 25. The output signal is then obtained by converting the integrated strain results from within the sensor region into voltage (Sirohi; Chopra, 2000).

Figure 25 – Visualization of the FE model within the excitation signal on PZT1.



Source: Prepared by the author.

The mechanical properties of the composite used in the simulations were sourced from the study conducted by Ferreira *et al.* (2024). Table 4 presents these under the

[2] AMD Ryzen 7 6800H 3.20 GHz 16GB

baseline condition. For simplification, it was assumed that Young's modulus in the two perpendicular in-plane directions (E_1 and E_2) for a plain weave fiber configuration is equal.

Table 4 – Mechanical properties for the materials at T = 30°C.

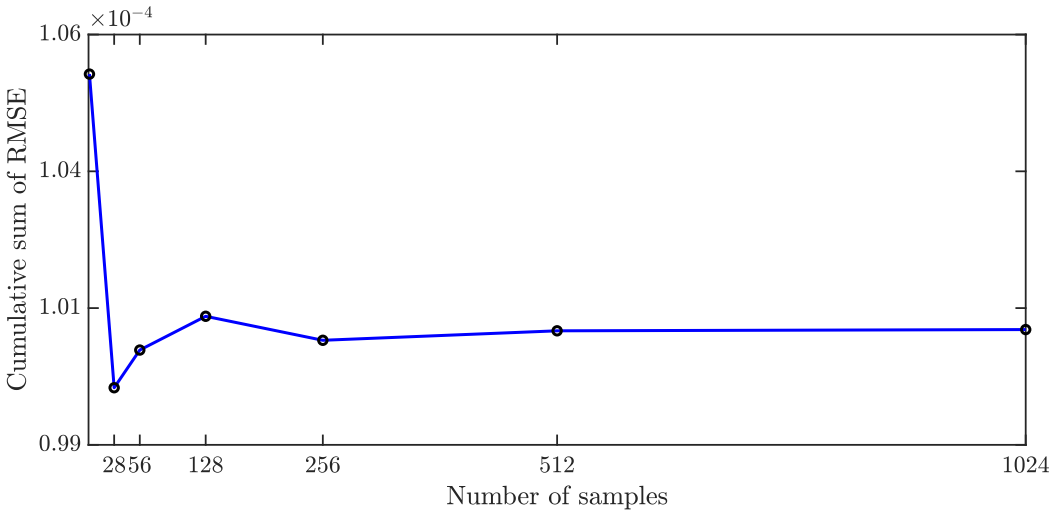
Mechanical Property	Value
E_1 [GPa]	61.06
E_2 [GPa]	61.06
ν_{12}	0.075
ρ [kg/m^3]	1620
G_{12} [GPa]	10.06
G_{23} [GPa]	5.00

Source: Prepared by the author.

As proposed by Ferreira *et al.* (2024), a sensitivity analysis utilizing Sobol indices was conducted to assess the influence of each property on the model's final response across various temperature conditions. The analysis revealed that Young's modulus E_1 and the in-plane shear modulus G_{12} were the primary parameters exerting significant influence. Consequently, these properties were varied to simulate different temperature conditions on the plate while the remaining properties were held constant. Ferreira *et al.* (2024) also employed a stochastic updating framework within Markov-Chain Monte Carlo simulations, providing posterior distributions for E_1 and G_{12} over a temperature range from 0°C to 60°C, including mean and standard deviation values for both properties. However, for model simplification and to test the co-Kriging technique within a simpler, not necessarily well-calibrated model, the properties were treated as random variables following a uniform distribution around 10% of the mean, giving equal weight to all values within this range. Figure 26 illustrates the cumulative RMSE calculated across iterations, which was used to evaluate the model's convergence as a function of varying sample sizes. The results indicate that a minimum data size of 256 samples is necessary for effective modeling.

Figure 27 compares experimental and numerical curves for the healthy conditions under various temperature settings. Notable differences can be seen between the experimental and numerical curves, particularly regarding the amplitude and phase of the signals under identical conditions. Nevertheless, the numerical model effectively captures the behavior exhibited by the experimental data, successfully reproducing the temperature effects on the output signals highlighting increased magnitude and a rightward shift.

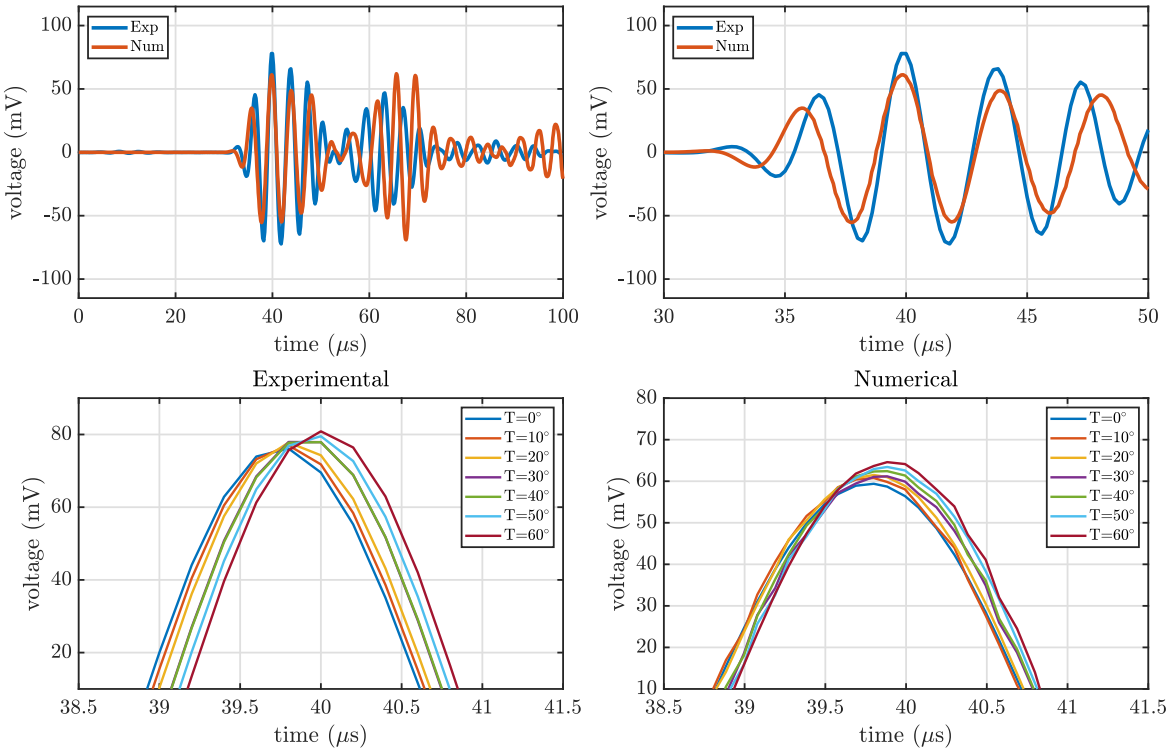
Figure 26 – Sample size for model convergence.



Source: Prepared by the author.

This aligns well with the implementation of the co-Kriging method, which aims to generate co-variables that enhance the estimation of a quantity of interest while being readily obtainable, even if they are not necessarily well-calibrated.

Figure 27 – Comparison between experimental and numerical curves in the healthy condition under different temperature conditions.

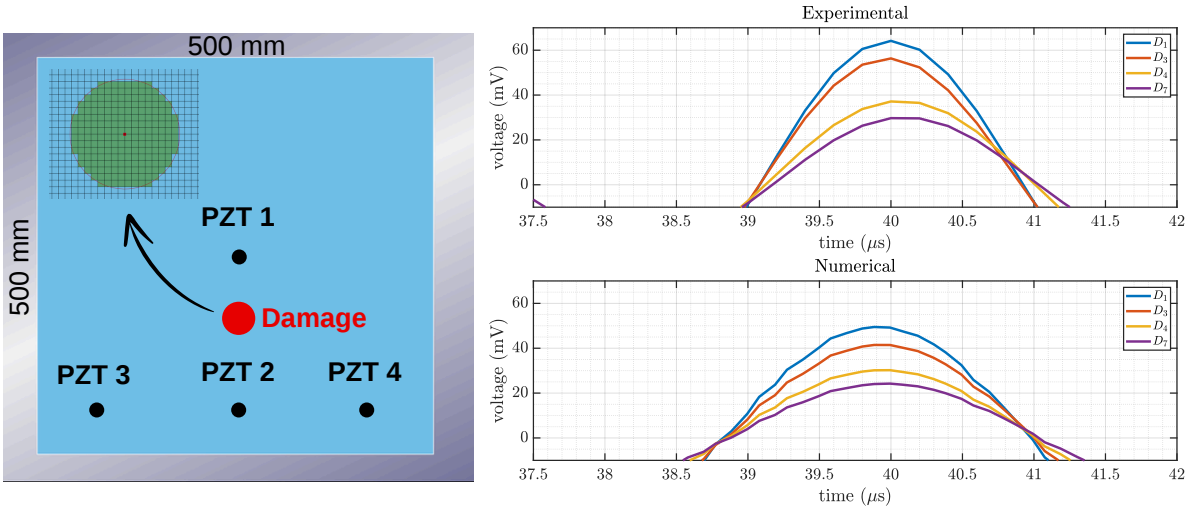


Source: Prepared by the author.

As discussed earlier (Section 4.6.1), the delamination effect in the CONCEPT experiment is simulated by applying an industrial adhesive putty to the plate surface. This added localized mass induces changes in the plate's damping, which resembles delamination behavior in composite structures (Lee *et al.*, 2011).

To replicate the adhesive's effect in the numerical model, the best approach was found to locally change the plate's damping within the region covered by the adhesive, similar to placing a dashpot in the designated region, as illustrated in Figure 28. For this purpose, the stiffness weighted damping method was used in LS-Dyna, with a unitless damping coefficient of 0.25. This coefficient is applied to each element in the specified region, with the damping effect being proportional to the element's stiffness. The value of 0.25 was chosen because it is within the recommended range (0.01 to 0.25) for explicit dynamic analysis, providing sufficient damping without causing numerical instability LSTC (2012). Although simplified, this constructed delamination model successfully emulates the amplitude reduction and phase shift in the output signals as damage progresses, effects close to actual delamination. Consequently, the numerical model's ability to mirror experimental data supports the co-Kriging approach's effectiveness, enhancing the estimation of the variable of interest—here, the delamination area—by incorporating co-variables derived from numerical simulations. For the sake of simplification, it is assumed that the behavior of the polymeric film used to simulate delamination remains constant, without variations due to temperature.

Figure 28 – Comparison between experimental and numerical curves in the same temperature under different damage conditions.

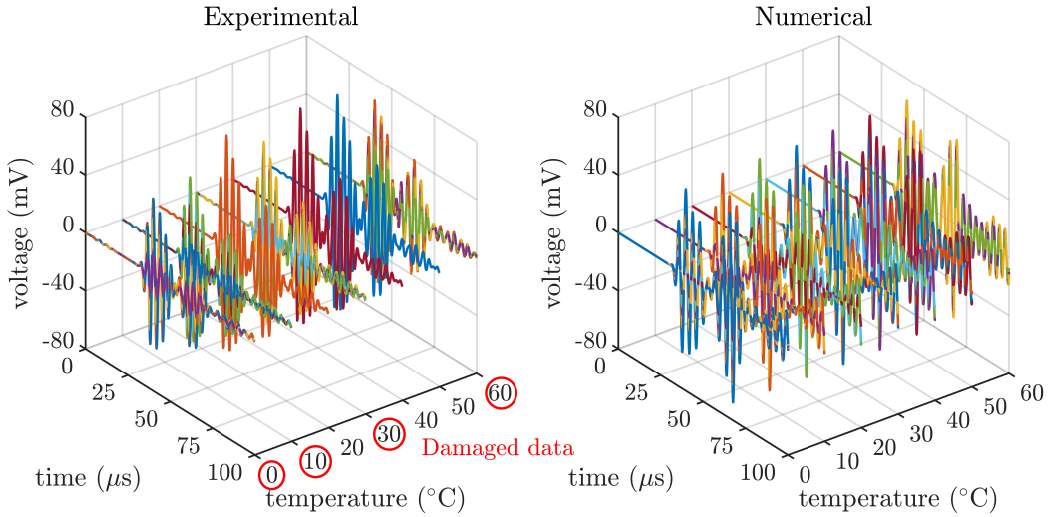


Source: Prepared by the author.

4.7. DAMAGE DETECTION AND QUANTIFICATION IN LAMINATES

Figure 29 illustrates the available data for applying the methodology depicted in Figure 20, showing healthy and damaged conditions captured both experimentally and through the numerical model. Notably, experimental damage conditions were recorded only at temperatures of 0°C, 10°C, 30°C, and 60°C, while the numerical model included a more comprehensive range, covering 0°C, 10°C, 20°C, 30°C, 40°C, 50°C, and 60°C. This expanded dataset allows co-Kriging to estimate delamination areas across a broader temperature range, even in regions lacking experimental measurements.

Figure 29 – Experimental and numerical output signals available for the proposed methodology.

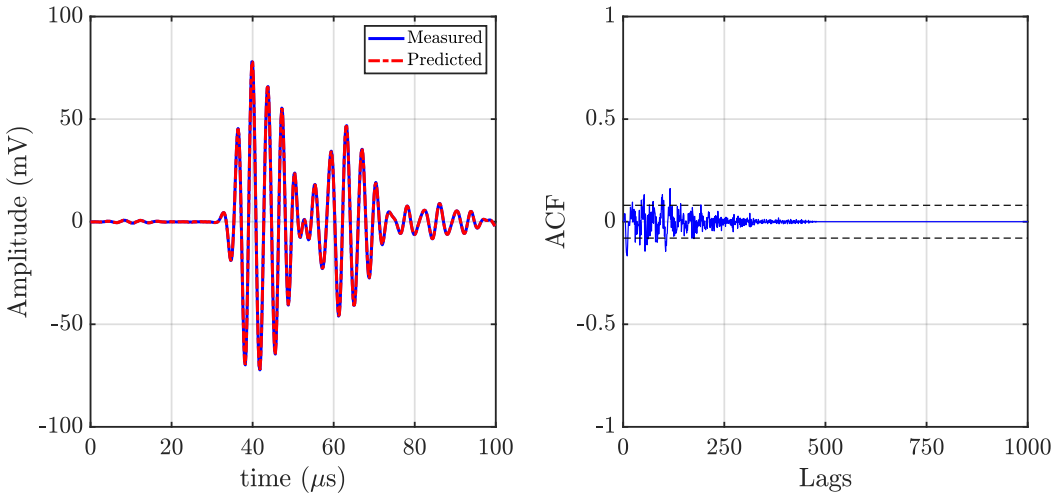


Source: Prepared by the author.

Following the procedure outlined in Section 4.3, the damage-sensitive features used in this study were derived through AR model identification, beginning with selecting the optimal model order for characterizing the output signals. Model validation involved comparing the model's predictive values with actual signal measurements, complemented by an autocorrelation analysis of residuals within the baseline condition (Ljung, 1998). As mentioned, the baseline condition used was the healthy-state signals at a temperature of 30°C, which served as the reference for both experimental and numerical data to determine the optimal model order. Based on the BIC (Figueiredo *et al.*, 2011), a model order of 20 was selected for the experimental dataset and 15 for the numerical dataset. Figure 30 compares the measured signal with the AR model's predicted signal under the baseline condition for the experimental data. As shown, the prediction errors resembling a white

noise process suggest accurate model identification, observed across all cases, including numerical simulations.

Figure 30 – Baseline measured and predicted experimental signals by AR and autocorrelation of residuals for model's validation.



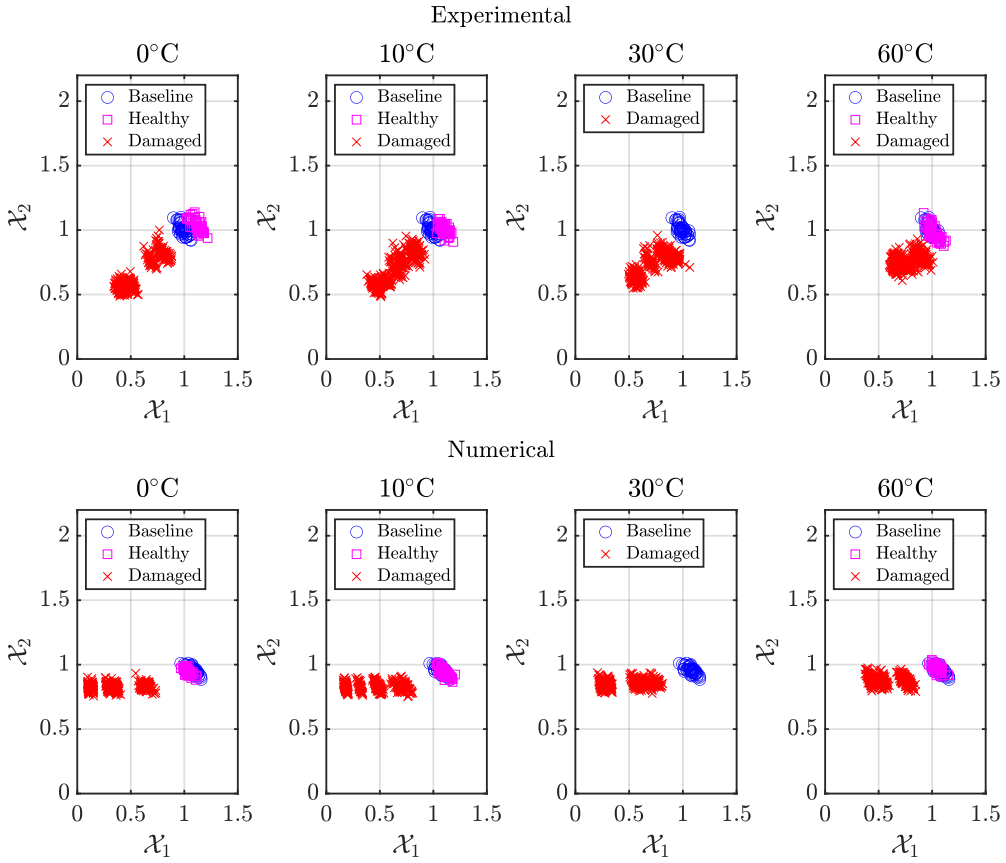
Source: Prepared by the author.

Following the methodology described in Section 4.4, two damage-sensitive features were calculated from the autoregressive models based on both experimental and numerical results, which are presented in Figure 31. As temperature increases, the damage states begin to approximate those observed in the baseline condition more closely. Specifically, the reduction in amplitude and phase shift caused by damage (refer to Figure 23) is gradually offset by the temperature-driven amplitude increase, which tends to bring the system's response closer to the baseline condition. This effect is depicted in Figure 31 by the convergence of the point clouds as temperature rises, highlighting the influence of temperature on the overall system behavior.

Figure 32 displays the Mahalanobis distance across all temperature conditions, where A denotes the ratio of the area covered by the industrial putty on the plate's surface to the plate's total area (refer to Table 3). This distance metric supports the computation of $\mathcal{DI}$s, which are subsequently used for detecting and quantifying damage.

As shown in Fig. 32, the adopted damage index effectively differentiates between healthy and delaminated conditions, regardless of temperature effects. Additionally, it demonstrates sensitivity to the extent of damage, enabling its use for quantitative applications such as regression methods. Initially, Kriging and Co-Kriging metamodels were implemented for each temperature to regress the damage indices as a function of the dela-

Figure 31 – Damage sensitive features extracted from autoregressive models estimated based on experimental and numerical output signals.

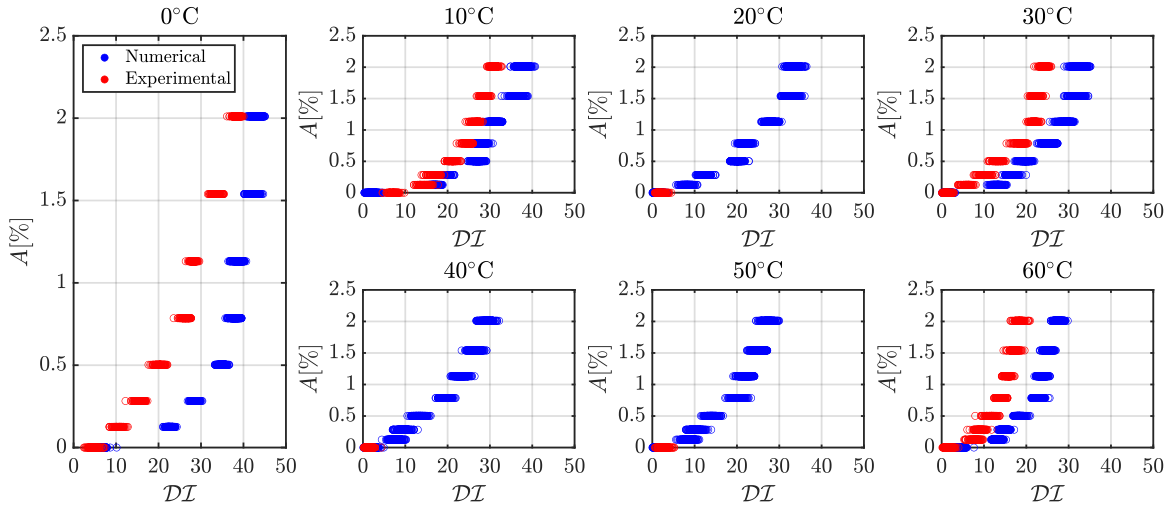


Source: Prepared by the author.

mination area. It is important to note that, to simulate real-world scenarios where there are typically more observations available for less expensive data than for costly data, only a subset of damage conditions was used to train the metamodels, while the remaining conditions were reserved for validation. An example of this is presented in Figure 33 for a temperature of T = 30°C. The root mean squared error (RMSE) was computed to evaluate and compare the predictive performance of each technique.

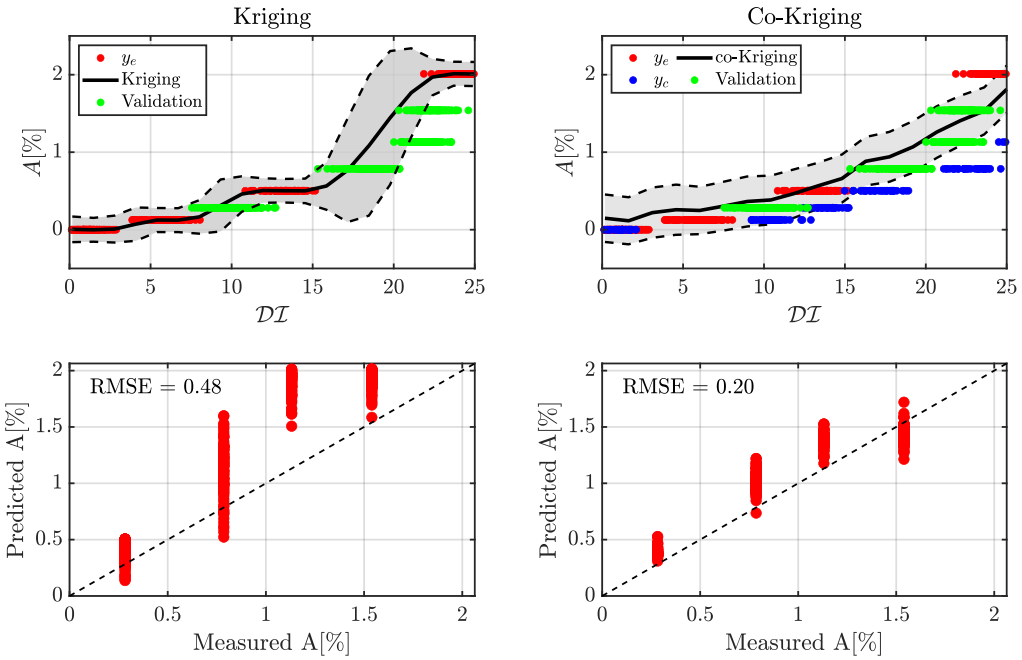
It is important to highlight that the same experimental dataset was utilized to train both the Kriging and co-Kriging models across all temperature levels. Although the number of experimental observations was limited, the co-Kriging model benefits from the additional information provided by co-variables derived from the numerical model, which enhances its predictive capability at all temperatures. This improvement is evident in the reduced root mean squared error (RMSE) between the estimated delamination areas and the experimentally measured values. While increasing the number of experimental observations would undoubtedly improve the Kriging model, the strengths of the co-

Figure 32 – Damage index computed for all temperature conditions for both experimental and numerical datasets.



Source: Prepared by the author.

Figure 33 – Performance comparison between Kriging and co-Kriging predictions for damage indices at T = 30°C.



Source: Prepared by the author.

Kriging approach become particularly apparent in situations where obtaining a large amount of experimental data is challenging or costly, as it allows for supplementation with more easily obtainable variables.

A similar approach was adopted to incorporate the effect of temperature on regres-

sion curves for estimating delamination at intermediate temperatures ranging from 0°C to 60°C, as illustrated in Figure 34. To evaluate the performance of both regression techniques across an unknown temperature range, data collected at 10°C, despite indicating damage, were excluded from the training set and used for validation of the metamodels. For temperatures of 20°C, 40°C, and 50°C, where no experimental damage data were available, numerical results were employed to construct the Kriging metamodel, assigning them equal weight alongside the experimental observations. In the case of the co-Kriging model, numerical data were treated as low-fidelity data due to the lack of experimental damage data at these temperatures. Table 5 presents the distribution of data used for training the Kriging and co-Kriging models, where Exp denotes experimental data and Num indicates numerical data, with HF and LF signifying high-fidelity and low-fidelity data, respectively.

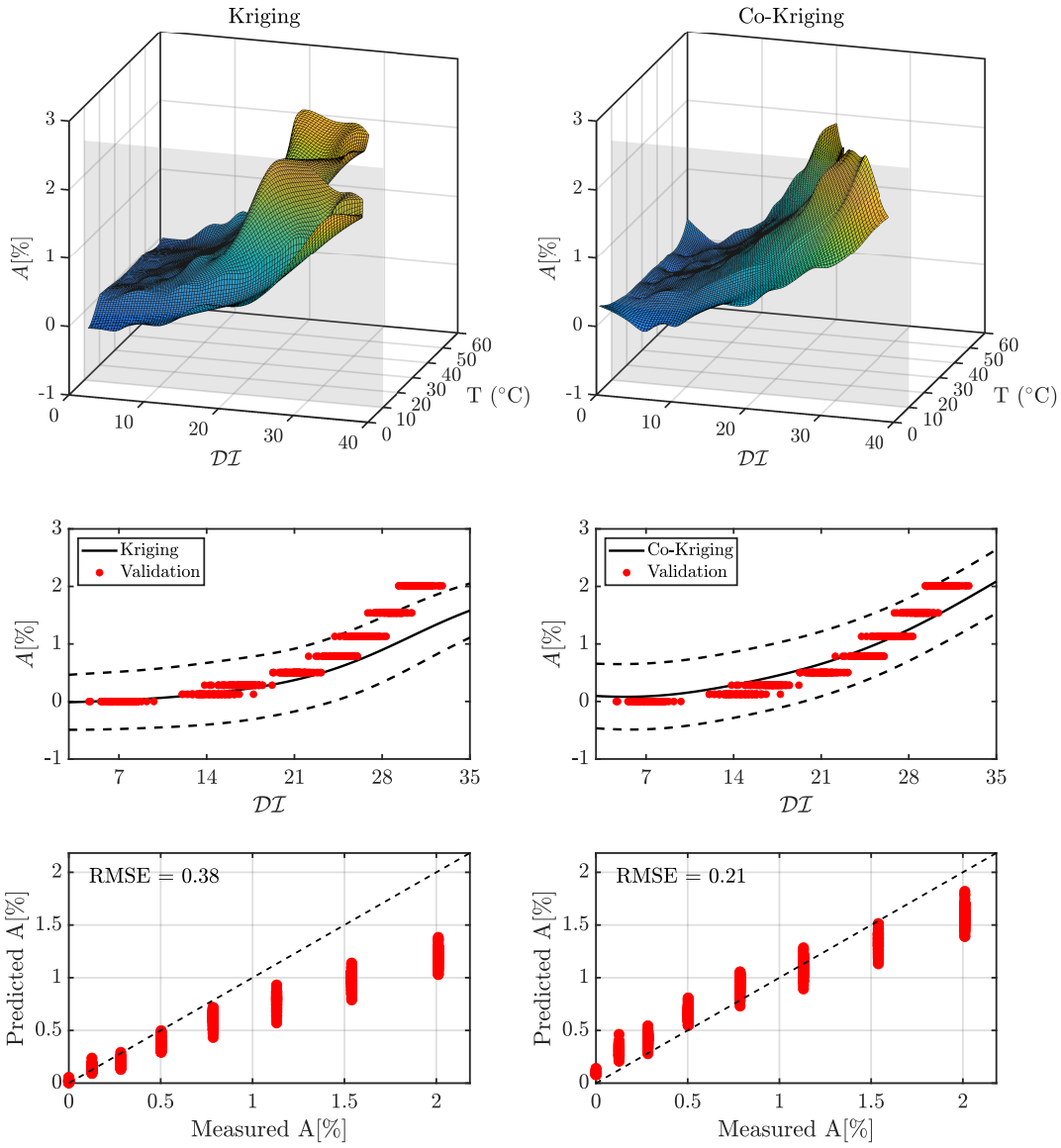
Table 5 – Distribution of training and testing data for Kriging and co-Kriging models.

Temperature	0°C	10°C	20°C	30°C	40°C	50°C	60°C
Classification	Train	Test	Train	Train	Train	Train	Train
Conditions	[1 4 6 8]	all	[1 2 6 8]	[1 2 4 8]	[1 3 5 8]	[1 4 6 8]	[1 2 4 8]
Kriging	Exp - HF	-	Num - HF	Exp - HF	Num - HF	Num - HF	Exp - HF
Co-Kriging	Exp - HF Num - LF	-	Exp - HF Num - LF	Exp - HF Num - LF	Exp - HF Num - LF	Exp - HF Num - LF	Exp - HF Num - LF

Source: Prepared by the author.

Even in scenarios with limited observations regarding a phenomenon of interest, utilizing a numerical dataset to complement the original dataset is an effective strategy. A notable advantage of the co-Kriging model in this context is that the numerical model does not need to be highly calibrated or robust, which simplifies and streamlines data acquisition. Additionally, this technique allows the co-variable data to assume lower importance in the model (low-fidelity data). In the example presented, when numerical data were incorporated into the training phase of the Kriging regression models, they were treated as having the same reliability level as the experimental data from other temperature ranges. However, despite their relative similarity, the distributions of experimental and numerical data exhibit differences, and assuming they belong to the same set may have contributed to the Kriging model's inferior performance compared to the co-Kriging model. The co-Kriging approach effectively addresses this challenge by appropriately weighting the contributions of both experimental and numerical data, facilitating

Figure 34 – Comparison of Kriging and co-Kriging performance in estimating delamination areas considering temperature effects.



Source: Prepared by the author.

a more nuanced understanding of the underlying phenomenon. This capability enhances the overall predictive accuracy and robustness of the model, highlighting the benefits of integrating diverse data sources, especially in situations where experimental observations are limited.

4.8. PARTIAL REMARKS

This chapter focused on the CONCEPT experimental setup to detect and quantify delamination damage within a composite structure using a co-Kriging model. In terms of performance, co-Kriging showcased a clear advantage over Kriging in all tests conducted. The RMSE values for co-Kriging were consistently lower across various temperature ranges, indicating more accurate predictions of delamination areas. This improvement underscores the method's effectiveness in integrating numerical and experimental data to enhance predictive capabilities, especially when only limited experimental data is available. By leveraging additional information from the numerical model, the co-Kriging approach significantly reduces estimation errors, further validating its practical value in damage quantification. This capability notably lessens the need for costly or hard-to-obtain experimental data, making it particularly advantageous in applications such as damage detection and quantification in composite structures. The main challenge in using co-variable data is determining whether a simple, poorly calibrated model can accurately improve the estimation of a variable of interest. This way, future research should focus on evaluating the accuracy of such models to ensure they effectively represent the underlying physics and enhance understanding of the phenomenon, even in a straightforward manner.

5 FINAL REMARKS

5.1. CONCLUDING

This study conducted a thorough literature review and examined the theoretical background of computational modeling techniques in structural health applications, focusing on Kriging and co-Kriging metamodels.

The co-Kriging method presented in this work offers several advantages, most notably a significant increase in predictive accuracy through the effective integration of high- and low-fidelity datasets. By merging various data sources, co-Kriging reduces reliance on expensive or difficult-to-obtain experimental data, making it especially useful for applications when only limited experimental data is available. Another significant advantage of co-Kriging is its robustness against uncertainty. It addresses potential noise and model defects by incorporating regression techniques that filter inaccuracies from lower-fidelity datasets. This leads to more accurate estimates even when the numerical models are not perfectly calibrated.

To validate the effectiveness of co-Kriging, two experimental studies were conducted: one focused on assessing the natural frequency variations of a bridge due to climatic changes, and the other on quantifying delamination damage in a carbon-epoxy composite. In both cases, co-Kriging predictions outperformed those of Kriging, even when utilizing a smaller subset of experimental data (considered high-fidelity). This approach provides a cost-effective solution, mainly when collecting experimental data, which is resource-intensive. In the examples presented, co-kriging emerges as an interesting tool, mainly because obtaining substantial experimental observations can be challenging. For instance, monitoring a bridge often requires specialized equipment and teams over an entire year, while conducting experimental tests on composite structures to investigate damage mechanisms, such as delamination, can be expensive and logistically complex. This way, the application showcased co-Kriging's real-world relevance, underscoring its potential as an efficient tool for enhancing regression accuracy in structural health monitoring approaches.

The main challenge in utilizing this technique is twofold: first, determining whether a set of co-variable data can effectively enhance the estimation of a variable of interest—an aspect that can be mathematically verified, and second, evaluating the extent to which a

simple and poorly calibrated model accurately represents the actual results under analysis. Depending on the circumstances, such a model may fail to improve the estimation and introduce inaccuracies that misrepresent the observed phenomenon. Consequently, this could lead to misleading conclusions, as the errors in the numerical representation may skew results and undermine overall prediction reliability.

5.2. FUTURE WORKS

Therefore, based on the key points raised in the previous section, future research should prioritize evaluating how well simple and poorly calibrated numerical models can accurately represent the underlying physics of the problem. Striking a balance between model complexity and accuracy is essential to ensure that integrated data effectively enhances our understanding of the phenomenon. Furthermore, it is proposed that the co-Kriging method be implemented by comparing different numerical models with varying levels of calibration and fidelity. The goal is to investigate how this strategy can improve interpolation accuracy when utilizing information from simple and quickly evaluated models as co-variables.

REFERENCES

AKAIKE, H. A new look at the statistical model identification. **IEEE Transactions on Automatic Control**, Institute of Electrical and Electronics Engineers (IEEE), London, v. 19, n. 6, p. 716–723, dez. 1974. Disponível em: https://doi.org/10.1109/tac.1974.1100705.

ALVANDI, A.; CREMONA, C. Assessment of vibration-based damage identification techniques. **Journal of Sound and Vibration**, Elsevier BV, London, v. 292, n. 1-2, p. 179–202, abr. 2006. Disponível em: https://doi.org/10.1016/j.jsv.2005.07.036.

AMER, A.; KOPSAFTOPOULOS, F. Probabilistic damage quantification via the integration of non-parametric time-series and gaussian process regression models. In: **International Workshop on Structural Health Monitoring (IWSHM), 12.** Stanford: DEStech Publications, 2019. p. 100. Disponível em: https://doi.org/10.12783/shm2019/32379.

BUD, M. A.; MOLDOVAN, I.; RADU, L.; NEDELCU, M.; FIGUEIREDO, E. Reliability of probabilistic numerical data for training machine learning algorithms to detect damage in bridges. **Structural Control and Health Monitoring**, Oxford, v. 29, n. 7, p. e2950, 2022. Disponível em: https://onlinelibrary.wiley.com/doi/abs/10.1002/stc.2950.

CHAO, S.-H.; LOH, C.-H. Vibration-based damage identification of reinforced concrete member using optical sensor array data. **Structural Health Monitoring**, SAGE Publications, London, v. 12, n. 5-6, p. 397–410, set. 2013. Disponível em: https://doi.org/10.1177/1475921713501109.

CORBETTA, M.; SBARUFATTI, C.; GIGLIO, M.; SAXENA, A.; GOEBEL, K. A bayesian framework for fatigue life prediction of composite laminates under co-existing matrix cracks and delamination. **Composite Structures**, London, v. 187, p. 58–70, 2018. ISSN 0263-8223. Disponível em: https://www.sciencedirect.com/science/article/pii/S0263822317324030.

DANIEL, I.; ISHAI, O. **Engineering Mechanics of Composite Materials**. Oxford University Press, 2006. (Engineering mechanics of composite materials, v. 13). ISBN 9780195150971. Disponível em: https://books.google.com.br/books?id=x5S_QgAACAAJ.

DAVID-WEST, O.; AMAFABIA, D.-a.; HARITOS, G.; MONTALVãO, D. A review of structural health monitoring techniques as applied to composite structures. **SDHM Structural Durability and Health Monitoring**, Henderson, v. 11, p. 91–147, 02 2017.

DOKAINISH, M.; SUBBARAJ, K. A survey of direct time-integration methods in computational structural dynamics—i. explicit methods. **Computers & Structures**, London, v. 32, n. 6, p. 1371–1386, 1989. ISSN 0045-7949. Disponível em: https://www.sciencedirect.com/science/article/pii/0045794989903143.

DWORAKOWSKI, Z.; AMBROZINSKI, L.; PACKO, P.; DRAGAN, K.; STEPINSKI, T. Application of artificial neural networks for compounding multiple damage indices in lamb-wave-based damage detection. **Structural Control and Health Monitoring**,

Oxford, v. 22, n. 1, p. 50–61, 2015. Disponível em: https://onlinelibrary.wiley.com/doi/abs/10.1002/stc.1659.

FAN, X.; LI, J.; HAO, H. Review of piezoelectric impedance based structural health monitoring: Physics-based and data-driven methods. **Advances in Structural Engineering**, London, v. 24, n. 16, p. 3609–3626, 2021. Disponível em: https://doi.org/10.1177/13694332211038444.

FARRAR, C. R.; WORDEN, K. **Structural Health Monitoring: A Machine Learning Perspective**. Hoboken, NJ: John Wiley & Sons, Ltd, 2013. ISBN 9781119994336.

FAWCETT, T. An introduction to roc analysis. **Pattern Recognition Letters**, London, v. 27, n. 8, p. 861–874, 2006. ISSN 0167-8655. Disponível em: https://www.sciencedirect.com/science/article/pii/S016786550500303X.

FERREIRA, L. de P. S.; TELOLI, R. de O.; da Silva, S.; FIGUEIREDO, E.; MOLDOVAN, I. D.; MAIA, N.; CIMINI, C. A. Bayesian calibration for lamb wave propagation on a composite plate using a machine learning surrogate model. **Mechanical Systems and Signal Processing**, London, v. 208, p. 111011, 2024. ISSN 0888-3270. Disponível em: https://www.sciencedirect.com/science/article/pii/S0888327023009196.

FIGUEIREDO, E.; BROWNJOHN, J. Three decades of statistical pattern recognition paradigm for shm of bridges. **Structural Health Monitoring**, London, v. 21, n. 6, p. 3018–3054, 2022. Disponível em: https://doi.org/10.1177/14759217221075241.

FIGUEIREDO, E.; FIGUEIRAS, J.; PARK, G.; FARRAR, C. R.; WORDEN, K. Influence of the autoregressive model order on damage detection. **Computer-Aided Civil and Infrastructure Engineering**, Hoboken, v. 26, n. 3, p. 225–238, 2011. Disponível em: https://onlinelibrary.wiley.com/doi/abs/10.1111/j.1467-8667.2010.00685.x.

FIGUEIREDO, E.; MOLDOVAN, I.; SANTOS, A.; CAMPOS, P.; COSTA, J. C. W. A. Finite element–based machine-learning approach to detect damage in bridges under operational and environmental variations. **Journal of Bridge Engineering**, Reston, v. 24, n. 7, p. 04019061, 2019. Disponível em: https://ascelibrary.org/doi/abs/10.1061/%28ASCE%29BE.1943-5592.0001432.

FIGUEIREDO, E.; PARK, G.; FARINHOLT, K. M.; FARRAR, C. R.; LEE, J.-R. Use of Time-Series Predictive Models for Piezoelectric Active-Sensing in Structural Health Monitoring Applications. **Journal of Vibration and Acoustics**, New York, v. 134, n. 4, p. 041014, 06 2012. ISSN 1048-9002. Disponível em: https://doi.org/10.1115/1.4006410.

FIGUEIREDO, E.; PARK, G.; FARRAR, C. R.; WORDEN, K.; FIGUEIRAS, J. Machine learning algorithms for damage detection under operational and environmental variability. **Structural Health Monitoring**, Hoboken, v. 10, n. 6, p. 559–572, 2011. Disponível em: https://doi.org/10.1177/1475921710388971.

FIGUEIREDO, E. J. F. **Damage identification in civil engineering infrastructure under operational and environmental conditions**. Tese (Doutorado) — Universidade do Porto (Portugal), 2010.

FORRESTER, A. I.; SÓBESTER, A.; KEANE, A. J. Multi-fidelity optimization via surrogate modelling. **Proceedings of the Royal Society A: Mathematical, Physical and Engineering Sciences**, The Royal Society, London, v. 463, n. 2088, p. 3251–3269, out. 2007. Disponível em: https://doi.org/10.1098/rspa.2007.1900.

FORRESTER, A. I. J.; SóBESTER, A.; KEANE, A. J. **Engineering Design via Surrogate Modelling - A Practical Guide**. London: Wiley, 2008.

FRANZOI, R. E.; MENEZES, B. C.; KELLY, J. D.; SWARTZ, C. L. Adaptive least-squares surrogate modeling for reaction systems. In: YAMASHITA, Y.; KANO, M. (Ed.). **14th International Symposium on Process Systems Engineering**. Elsevier, London, 2022, (Computer Aided Chemical Engineering, v. 49). p. 1705–1710. Disponível em: https://www.sciencedirect.com/science/article/pii/B9780323851596502840.

FUENTES, R.; CROSS, E.; HALFPENNY, A.; BARTHORPE, R.; WORDEN, K. Autoregressive gaussian processes for structural damage detection. In: KU LEUVEN - DEPARTMENT OF MECHANICAL ENGINEERING. **Proceedings of the International Conference on Noise and Vibration Engineering, 26.** Leuven, 2014. p. 469–483. ISBN 9789073802919. Disponível em: http://past.isma-isaac.be/downloads/isma2014/papers/isma2014_0711.pdf.

GANDHI, V. Chapter 2 - interfacing brain and machine. In: GANDHI, V. (Ed.). **Brain-Computer Interfacing for Assistive Robotics**. San Diego: Academic Press, 2015. p. 7–63. ISBN 978-0-12-801543-8. Disponível em: https://www.sciencedirect.com/science/article/pii/B9780128015438000028.

GHRIB, M.; RéBILLAT, M.; Vermot des Roches, G.; MECHBAL, N. Automatic damage type classification and severity quantification using signal based and nonlinear model based damage sensitive features. **Journal of Process Control**, London, v. 83, p. 136–146, 2019. ISSN 0959-1524. Disponível em: https://www.sciencedirect.com/science/article/pii/S0959152418301975.

GRATIET, L. L.; GARNIER, J. Recursive co-kriging model for design of computer experiments with multiple levels of fidelity. **International Journal for Uncertainty Quantification**, New York, v. 4, n. 5, p. 365–386, 2014. ISSN 2152-5080.

GRESIL, M.; GIURGIUTIU, V.; SHEN, Y.; PODDAR, B. Guidelines for using the finite element method for modeling of guided lamb wave propagation in shm processes. In: **6th European Workshop on Structural Health Monitoring (EWSHM 2012)**. Dresden, Germany: [s.n.], 2013. p. 0. Disponível em: https://www.ndt.net/?id=14011.

IHN, J.-B.; CHANG, f.-k. Detection and monitoring of hidden fatigue crack growth using a built-in piezoelectric sensor/actuator network: I. diagnostics. **Smart Materials and Structures**, Bristol, v. 13, p. 609, 05 2004.

JONATHAN, D. C.; KUNG-SILK, C. **Time Series Analysis with Applications in R**. 2nd. ed. New York, NY, USA: Springer, 2008. 109-188 p.

KENNEDY, M.; O'HAGAN, A. Predicting the output from a complex computer code when fast approximations are available. **Biometrika**, Oxford, v. 87, n. 1, p. 1–13, 03 2000. ISSN 0006-3444. Disponível em: https://doi.org/10.1093/biomet/87.1.1.

KITAGAWA, G. **Introduction to Time Series Modeling**. 1st. ed. New York: Chapman and Hall/CRC, 2010. 296 p. ISBN 9780429142116.

KRIGE, D. G. **A statistical approach to some mine valuation and allied problems on the Witwatersrand**. Dissertação (Master's thesis) — University of the Witwatersrand, South Africa, 1951.

LADEVèZE, P.; ALLIX, O.; DEü, J.-F.; LéVêQUE, D. A mesomodel for localisation and damage computation in laminates. **Computer Methods in Applied Mechanics and Engineering**, London, v. 183, n. 1, p. 105–122, 2000. ISSN 0045-7825. Disponível em: https://www.sciencedirect.com/science/article/pii/S0045782599002145.

LARROSA, C.; LONKAR, K.; CHANG, F.-K. In situ damage classification for composite laminates using gaussian discriminant analysis. **Structural Health Monitoring**, London, v. 13, n. 2, p. 190–204, 2014. Disponível em: https://doi.org/10.1177/1475921713517288.

LATANIOTIS, C.; WICAKSONO, D.; MARELLI, S.; SUDRET, B. **UQLab user manual – Kriging (Gaussian process modeling)**. [S.l.], 2022. Report UQLab-V2.0-105.

LATIFI, M.; van der Meer, F.; SLUYS, L. A level set model for simulating fatigue-driven delamination in composites. **International Journal of Fatigue**, London, v. 80, p. 434–442, 2015. ISSN 0142-1123. Disponível em: https://www.sciencedirect.com/science/article/pii/S0142112315002121.

LEE, J.-S.; PARK, G.; KIM, C.-G.; FARRAR, C. R. Use of relative baseline features of guided waves for in situ structural health monitoring. **Journal of Intelligent Material Systems and Structures**, London, v. 22, n. 2, p. 175–189, 2011. Disponível em: https://doi.org/10.1177/1045389X10395643.

LJUNG, L. **System Identification: Theory for the User**. 2nd. ed. London: Pearson Education, 1998. ISBN 9780132440530.

LSTC, L. S. T. C. **LS-DYNA Keyword User's Manual: Version 971 R6.1.0**. [S.l.]: Livermore Software Technology Corporation, 2012.

LüTHEN, N.; MARELLI, S.; SUDRET, B. Sparse polynomial chaos expansions: Literature survey and benchmark. **SIAM/ASA Journal on Uncertainty Quantification**, Zurich, v. 9, n. 2, p. 593–649, 2021. Disponível em: https://doi.org/10.1137/20M1315774.

LYNCH, J. Linear classification of system poles for structural damage detection using piezoelectric active sensors. **Proceedings of SPIE - The International Society for Optical Engineering**, Oxford, v. 5391, 07 2004.

MAECK, J.; ROECK, G. D. Description of z24 benchmark. **Mechanical Systems and Signal Processing**, London, v. 17, n. 1, p. 127–131, 2003. ISSN 0888-3270. Disponível em: https://www.sciencedirect.com/science/article/pii/S0888327002915487.

MALEKZADEH, M.; ATIA, G.; CATBAS, N. Performance-based structural health monitoring through an innovative hybrid data interpretation framework. **Journal of Civil Structural Health Monitoring**, New York, v. 5, 07 2015.

MARELLI, S.; SUDRET, B. UQLab: A framework for uncertainty quantification in Matlab. In: UNIVERSITY OF LIVERPOOL. **Proceedings of the 2nd International Conference on Vulnerability and Risk Analysis and Management - ICVRAM**. Liverpool, 2014. p. 2554–2563.

MARK, H.; WORKMAN, J. The statistics of spectral searches. In: **Chemometrics in Spectroscopy (Second Edition)**. Second edition. Academic Press, London, 2018. p. 507–511. ISBN 978-0-12-805309-6. Disponível em: https://www.sciencedirect.com/science/article/pii/B9780128053096000751.

MATHERON, G. Principles of geostatistics. **Economic Geology**, McLean, v. 58, n. 2, p. 1246–1266, 1963.

MITRA, M.; GOPALAKRISHNAN, S. Guided wave based structural health monitoring: A review. **Smart Materials and Structures**, IOP Publishing, Bristol, v. 25, n. 5, p. 053001, mar 2016. Disponível em: https://dx.doi.org/10.1088/0964-1726/25/5/053001.

MOHAMMED, E. A.; NAUGLER, C.; FAR, B. H. Chapter 32 - emerging business intelligence framework for a clinical laboratory through big data analytics. In: TRAN, Q. N.; ARABNIA, H. (Ed.). **Emerging Trends in Computational Biology, Bioinformatics, and Systems Biology**. Boston: Morgan Kaufmann, 2015, (Emerging Trends in Computer Science and Applied Computing). p. 577–602. ISBN 978-0-12-802508-6. Disponível em: https://www.sciencedirect.com/science/article/pii/B9780128025086000326.

MOSER, F.; JACOBS, L. J.; QU, J. Modeling elastic wave propagation in waveguides with the finite element method. **NDT & E International**, London, v. 32, n. 4, p. 225–234, 1999. ISSN 0963-8695. Disponível em: https://www.sciencedirect.com/science/article/pii/S0963869598000450.

NOVAIS, H. C.; SILVA, S. da; FIGUEIREDO, E. Co-kriging strategy for structural health monitoring of bridges. **Structural Health Monitoring**, London, v. 0, n. 0, p. 14759217241265375, 2024. Disponível em: https://doi.org/10.1177/14759217241265375.

PAIXÃO, J. A. S.; SILVA, S. da; FIGUEIREDO, E. Damage quantification in composite structures using autoregressive models. In: WAHAB, M. A. (Ed.). **Proceedings of the 13th International Conference on Damage Assessment of Structures**. Singapore: Springer Singapore, 2020. p. 804–815.

PAIXãO, J.; SILVA, S. da; FIGUEIREDO, E.; RADU, L.; PARK, G. Delamination area quantification in composite structures using gaussian process regression and auto-regressive models. **Journal of Vibration and Control**, London, v. 27, n. 23-24, p. 2778–2792, 2021. Disponível em: https://doi.org/10.1177/1077546320966183.

PALAR, P. S.; SHIMOYAMA, K. Ensemble of kriging with multiple kernel functions for engineering design optimization. In: KOROŠEC, P.; MELAB, N.; TALBI, E.-G. (Ed.). **Bioinspired Optimization Methods and Their Applications**. Cham: Springer International Publishing, 2018. p. 211–222. ISBN 978-3-319-91641-5.

PAVLACK, B.; PAIXãO, J.; SILVA, S. da; CUNHA, J. A.; CAVA, D. G. Polynomial chaos-kriging metamodel for quantification of the debonding area in large wind turbine blades. **Structural Health Monitoring**, London, v. 21, n. 2, p. 666–682, 2022. Disponível em: https://doi.org/10.1177/14759217211007956.

PEETERS, B.; ROECK, G. D. One-year monitoring of the z24-bridge: environmental effects versus damage events. **Earthquake Engineering & Structural Dynamics**, New York, v. 30, n. 2, p. 149–171, 2001.

RAMADAS, C.; BALASUBRAMANIAM, K.; JOSHI, M.; KRISHNAMURTHY, C. V. Interaction of the primary anti-symmetric lamb mode (ao) with symmetric delaminations: numerical and experimental studies. **Smart Materials and Structures**, Bristol, v. 18, n. 8, p. 085011, jun 2009. Disponível em: https://dx.doi.org/10.1088/0964-1726/18/8/085011.

RASMUSSEN, C.; WILLIAMS, C. **Gaussian processes for machine learning**. Cambridge, Massachusetts: MIT Press, 2006. (Adaptive Computation and Machine Learning).

REYNDERS, E.; ROECK, G. D. Continuous vibration monitoring and progressive damage testing on the z 24 bridge. **Encyclopedia of structural health monitoring**, Wiley Online Library, Hoboken, 2009. Disponível em: https://onlinelibrary.wiley.com/doi/abs/10.1002/9780470061626.shm165.

RYTTER, A. **Vibration Based on Inspections of Civil Engineering Structures**. Tese (Doutorado) — Department of Building Technology and Structural Engineering, Aalborg University, Denmark, 1993.

SACKS, J.; WELCH, W. J.; MITCHELL, T. J.; WYNN, H. P. Design and analysis of computer experiments. **Statistical Science**, New York, v. 4, p. 409–435, 1989.

SAFRI, S. N. A. B.; SULTAN, M.; JAWAID, M. 7 - damage analysis of glass fiber reinforced composites. In: JAWAID, M.; THARIQ, M.; SABA, N. (Ed.). **Durability and Life Prediction in Biocomposites, Fibre-Reinforced Composites and Hybrid Composites**. Woodhead Publishing, 2019, (Woodhead Publishing Series in Composites Science and Engineering). p. 133–147. ISBN 978-0-08-102290-0. Disponível em: https://www.sciencedirect.com/science/article/pii/B9780081022900000076.

SALAMONE, S.; BARTOLI, I.; SCALEA, F. L. D.; COCCIA, S. Guided-wave health monitoring of aircraft composite panels under changing temperature. **Journal of Intelligent Material Systems and Structures**, London, v. 20, n. 9, p. 1079–1090, 2009. Disponível em: https://doi.org/10.1177/1045389X08101634.

SANTNER, T.; WILLIAMS, B.; NOTZ, W. **The design and analysis of computer experiments**. [*S.l.*]: Springer, 2003. (Springer Series in Statistics).

SAXENA, A.; GOEBEL, K.; LARROSA, C.; JANAPATI, V.; ROY, S.; CHANG, F. Accelerated aging experiments for prognostics of damage growth in composite materials. In: **Proceedings of the 8th International Workshop on Structural Health Monitoring**. [*S.l.*]: DEStech Publications Inc., 2011. v. 2, p. 1283–1291.

SILVA, S. da. Data-driven model identification of guided wave propagation in composite structures. **Journal of the Brazilian Society of Mechanical Sciences and Engineering**, Springer Science and Business Media LLC, [*S.l.*], v. 40, n. 11, out. 2018. ISSN 1806-3691. Disponível em: http://dx.doi.org/10.1007/s40430-018-1462-4.

SILVA, S. da; FIGUEIREDO, E.; MOLDOVAN, I. Damage detection approach for bridges under temperature effects using gaussian process regression trained with hybrid data. **Journal of Bridge Engineering**, Reston, v. 27, n. 11, p. 04022107, 2022. Disponível em: https://ascelibrary.org/doi/abs/10.1061/%28ASCE%29BE.1943-5592.0001949.

SILVA, S. da; PAIXãO, J.; RéBILLAT, M.; MECHBAL, N. Extrapolation of ar models using cubic splines for damage progression evaluation in composite structures. **Journal of Intelligent Material Systems and Structures**, London, v. 0, n. 0, p. 1045389X20963171, 2021. Disponível em: https://doi.org/10.1177/1045389X20963171.

SIROHI, J.; CHOPRA, I. Fundamental understanding of piezoelectric strain sensors. **Journal of Intelligent Material Systems and Structures**, London, v. 11, n. 4, p. 246–257, 2000. Disponível em: https://doi.org/10.1106/8BFB-GC8P-XQ47-YCQ0.

SOHN, H.; FARRAR, C. R. Damage diagnosis using time series analysis of vibration signals. **Smart Materials and Structures**, Bristol, v. 10, n. 3, p. 446, jun 2001. Disponível em: https://dx.doi.org/10.1088/0964-1726/10/3/304.

SPENCER, B. F.; RUIZ-SANDOVAL, M. E.; KURATA, N. Smart sensing technology: opportunities and challenges. **Structural Control and Health Monitoring**, Hindawi Limited, Cairo, v. 11, n. 4, p. 349–368, 2004. Disponível em: https://doi.org/10.1002/stc.48.

STEIN, A.; CORSTEN, L. Universal kriging and cokriging as a regression procedure. **Biometrics**, Wiley, [*S.l.*], v. 47, p. 575–587, 1991. ISSN 0006-341X.

STEIN, M. L. **Interpolation of Spatial Data: A Theoretical Approach to Kriging**. Heidelberg: Springer Science & Business Media, 2012.

STONE, M. An asymptotic equivalence of choice of model by cross-validation and akaike's criterion. **Journal of the Royal Statistical Society B**, Wiley, Oxford, v. 39, p. 44–47, 1977.

SU, Z.; YE, L. **Identification of Damage Using Lamb Waves**: From fundamentals to applications. 1. ed. Springer London, 2009. X, 346 p. (Lecture Notes in Applied and Computational Mechanics). Disponível em: https://link.springer.com/book/10.1007/978-1-84882-784-4.

SVENDSEN, B. T.; ØISETH, O.; FRøSETH, G. T.; RøNNQUIST, A. A hybrid structural health monitoring approach for damage detection in steel bridges under simulated environmental conditions using numerical and experimental data. **Structural Health Monitoring**, London, v. 22, n. 1, p. 540–561, 2023. Disponível em: https://doi.org/10.1177/14759217221098998.

TAHA, A. A.; HANBURY, A. Metrics for evaluating 3d medical image segmentation: analysis, selection, and tool. **BMC Medical Imaging**, Springer Science and Business Media LLC, [*S.l.*], v. 15, n. 1, ago. 2015. ISSN 1471-2342. Disponível em: http://dx.doi.org/10.1186/s12880-015-0068-x.

TANG, Q.; ZHOU, J.; XIN, J.; ZHAO, S.; ZHOU, Y. Autoregressive model-based structural damage identification and localization using convolutional neural networks. **KSCE Journal of Civil Engineering**, Springer Science and

Business Media LLC, [*S.l.*], v. 24, n. 7, p. 2173–2185, jun. 2020. Disponível em: https://doi.org/10.1007/s12205-020-2256-7.

TIAN, Z.; YU, L.; LECKEY, C. Delamination detection and quantification on laminated composite structures with lamb waves and wavenumber analysis. **Journal of Intelligent Material Systems and Structures**, London, v. 26, n. 13, p. 1723–1738, 2015. Disponível em: https://doi.org/10.1177/1045389X14557506.

TOYAMA, N.; NODA, J.; OKABE, T. Quantitative damage detection in cross-ply laminates using lamb wave method. **Composites Science and Technology**, Oxford, v. 63, n. 10, p. 1473–1479, 2003. ISSN 0266-3538. Disponível em: https://www.sciencedirect.com/science/article/pii/S0266353803001635.

VADYALA, S. R.; BETGERI, S. N.; MATTHEWS, J. C.; MATTHEWS, E. A review of physics-based machine learning in civil engineering. **Results in Engineering**, London, v. 13, p. 100316, 2022. ISSN 2590-1230. Disponível em: https://www.sciencedirect.com/science/article/pii/S2590123021001171.

WENZEL, H. **Health Monitoring of Bridges**. [*S.l.*]: Wiley, 2008. ISBN 9780470740187.

WORDEN, K.; MANSON, G.; FIELLER, N. Damage detection using outlier analysis. **Journal of Sound and Vibration**, London, v. 229, n. 3, p. 647–667, 2000. ISSN 0022-460X. Disponível em: https://www.sciencedirect.com/science/article/pii/S0022460X99925142.

XIAO, M.; ZHANG, G.; BREITKOPF, P.; VILLON, P.; ZHANG, W. Extended co-kriging interpolation method based on multi-fidelity data. **Applied Mathematics and Computation**, London, v. 323, p. 120–131, 2018. ISSN 0096-3003. Disponível em: https://www.sciencedirect.com/science/article/pii/S0096300317307646.

YUAN, F.-G. **Structural Health Monitoring (SHM) in Aerospace Structures**. Sawston: Woodhead Publishing, 2016. ISBN 978-0-08-100148-6. Disponível em: https://doi.org/10.1016/C2014-0-00994-X.

YUAN, S.; WANG, H.; CHEN, J. A pzt based on-line updated guided wave - gaussian process method for crack evaluation. **IEEE Sensors Journal**, Piscataway, v. 20, n. 15, p. 8204–8212, 2020.

ZHOU, Y.; FIGUEIREDO, E.; MAIA, N.; SAMPAIO, R.; PERERA, R. Damage detection in structures using a transmissibility-based mahalanobis distance. **Structural Control and Health Monitoring**, Oxford, v. 22, 02 2015.

APPENDIX A – CO-KRIGING REGRESSION CODE IN MATLAB

The code presented in this appendix implements the co-Kriging regression method, which was used to generate the results shown in Section 2.4.

Initially, the code defines a seed to ensure repeatability of the results. It then generates the input data, which includes two distinct sources: expensive data y_e and cheap data y_c. The expensive dataset represents samples from a complex and costly target function, while the cheap data represents a simplified and less accurate version of the function.

For Kriging, the UQLab interface is used to construct the model. The input points x_e and their corresponding evaluations y_e are provided to UQLab to generate a Kriging metamodel. A uniform distribution is used to define the input space, and the target function is evaluated at points sampled uniformly within this range. A test sample is also generated for validation purposes.

Next, the code optimizes the hyperparameters for the co-Kriging model using an optimization algorithm, employing the functions *likelihoodc* and *likelihoodd* to evaluate the likelihoods for hyperparameter estimation of the cheap and difference models, respectively. With the optimized hyperparameters, the code then calls a custom function, *cokriging_regression*, for co-Kriging regression, which is implemented in a separate file.

Finally, plots are created to visualize the expensive and cheap data, the Kriging and co-Kriging predictions. These plots show the observed points, predictions, and confidence intervals, providing a visual assessment of the Kriging and co-Kriging model performances.

A.1. MAIN CODE

```
%-------------------------------------------------------------------
% Title: Co-kriging estimator (regression)
% Authors: Henrique Cordeiro Novais, Samuel da Silva
% Date: August 15, 2023
%
% Description:
% This script demonstrates an example application of the
% co-kriging regression method using a mathematical function.
%-------------------------------------------------------------------
clc; clear; close all;
%-------------------------------------------------------------------
% Seed definition to guarantee repeatability of random processes
%-------------------------------------------------------------------
mySeed = 626303;
rng_stream = RandStream('mt19937ar', 'Seed', mySeed);
```

```
RandStream.setGlobalStream(rng_stream);

% Configuration of plot appearance
nfonte = 25; % Font size for plots
marker = 20; % Marker size for plots

global ModelInfo % Declare global structure for model information

%% Step 1: Define Model Parameters and Input Distributions
%--------------------------------------------------------------------

% Load UQLab and configure the mathematical model
uqlab
ModelOpts.mString = 'X.*sin(X)'; % Model equation: X*sin(X)
ModelOpts.isVectorized = true;

myModel = uq_createModel(ModelOpts); % Create model in UQLab

% Define uniform input distribution in the range [-3*pi, 3*pi]
InputOpts.Marginals.Type = 'Uniform';
InputOpts.Marginals.Parameters = [-3*pi 3*pi];
myInput = uq_createInput(InputOpts);

% Define training sample size for the expensive model
Ntrain = 20;
Xe = uq_getSample(myInput, Ntrain);
Ye = uq_evalModel(myModel, Xe);
Ye = Ye + 0.2*std(Ye)*randn(size(Ye,1),1);

% Define testing sample size for validation
Ntest = 100;
Xe_test = uq_getSample(myInput, Ntest);
Ye_test = uq_evalModel(myModel, Xe_test);
Ye_test = Ye_test + 0.2*std(Ye_test)*randn(size(Ye_test,1),1);

% Define data for cheaper model
Xc = linspace(-3*pi,3*pi,50);
Yc = 0.4*Xc.*sin(Xc) - 7;

%% Step 2: Plot Training and Cheaper Model Data
%--------------------------------------------------------------------

figure;
plot(Xe, Ye, 'r.', 'MarkerSize', 35); hold on;
plot(Xc, Yc, 'b.', 'MarkerSize', 35);

% Add legend and labels
```

```
l = legend('$y_e$', '$y_c$', 'Location', 'Northwest');
set(l, 'interpreter', 'latex', 'fontsize', marker);
xlabel('$x$', 'FontSize', nfonte, 'interpreter', 'latex');
ylabel('$y$', 'FontSize', nfonte, 'interpreter', 'latex');
set(gca, 'FontSize', nfonte, 'TickLabelInterpreter', 'latex', ...
    'LineWidth', 1.5);
box on
xlim([-12 12]);
grid off

%% Step 3: Store Data for Co-Kriging Model
%--------------------------------------------------------------------

% Transpose cheaper model data for compatibility
Xc = Xc';
Yc = Yc';

% Store expensive and cheaper model data in a global structure
ModelInfo.Xe = Xe;
ModelInfo.Xc = Xc;
ModelInfo.ye = Ye;
ModelInfo.yc = Yc;

%% Step 4: Optimize Parameters for Co-Kriging Model
%--------------------------------------------------------------------

% Optimize parameters for the cheaper model
Paramsc = ga(@likelihoodc, 3, [], [], [], [], [0.1 2 0.1], [5 2 10]);
thetac = Paramsc(1);
pc = Paramsc(2);
lambda_c = Paramsc(3);

% Optimize parameters for the difference model
Paramsd = ga(@likelihoodd, 4, [], [], [], [], [0 2.5 2 5], [10 3 2 10]);
thetad = Paramsd(1);
rho = Paramsd(2);
pd = Paramsd(3);
lambda_e = Paramsd(4);

%% Step 5: Kriging Model for Expensive Data
%--------------------------------------------------------------------

% Set up the kriging model with training data
MetaOpts.ExpDesign.X = Xe;
MetaOpts.ExpDesign.Y = Ye;
MetaOpts.ExpDesign.Sampling = 'User';
MetaOpts.Type = 'Metamodel';
```

```
MetaOpts.MetaType = 'Kriging';
MetaOpts.Regression.SigmaNSQ = 'auto';

% Create the kriging model and evaluate over a fine grid
myKriging = uq_createModel(MetaOpts);
Xc_kriging = linspace(min(Xe), max(Xe), 200);
[Yc_kriging, stdV, ~] = uq_evalModel(myKriging, Xc_kriging');

% Calculate the 95% confidence interval (Kriging)
u_band = Yc_kriging + 1.96*sqrt(stdV);
l_band = Yc_kriging - 1.96*sqrt(stdV);

%% Step 6: Plot Kriging Results with Validation Data
%--------------------------------------------------------------------

figure;
fill([Xc_kriging, fliplr(Xc_kriging)], [u_band', fliplr(l_band')], ...
    [0.8 0.8 0.8], 'facealpha', 0.8, 'EdgeColor', 'none')
hold on; grid off;
plot(Xe, Ye, 'r.', 'MarkerSize', 35);
plot(Xc_kriging, Yc_kriging, '-k', 'LineWidth', 3);
plot(Xe_test, Ye_test, 'b.', 'MarkerSize', 30);

% Add legend and labels
l = legend('', '$y_e$', 'Kriging', 'Validation');
set(l, 'interpreter', 'latex', 'fontsize', marker, 'location', ...
    'southeast', 'NumColumns', 3);
xlabel('$x$', 'FontSize', nfonte, 'interpreter', 'latex');
ylabel('$y$', 'FontSize', nfonte, 'interpreter', 'latex');
set(gca, 'FontSize', nfonte, 'TickLabelInterpreter', 'latex', ...
    'LineWidth', 1.5);
box on
xlim([min(Xe) max(Xe)]);
xticks(-12:4:12);
ylim([-12 12]);
grid on;

%% Step 7: Co-Kriging Prediction and Visualization
%--------------------------------------------------------------------

% Compute cheap model values at expensive model points
yc_xe = 0.4*Xe.*sin(Xe) - 7;

% Generate co-Kriging predictions
xplot = linspace(min(Xe), max(Xe), 100);
[ye_co, s] = cokriging_regression(Xc', Yc', pc, thetac, lambda_c, ...
    Xe, Ye, pd, thetad, rho, lambda_e, yc_xe', xplot);
```

```
sup = ye_co + s;
inf = ye_co - s;

% Plot co-Kriging results
figure
plot(Xc, Yc, 'b.', 'MarkerSize', 35); hold on; grid off;
fill([xplot, fliplr(xplot)], [sup, fliplr(inf)], [0.8 0.8 0.8], ...
    'facealpha', 0.8, 'EdgeColor', 'none');
plot(Xe, Ye, 'r.', 'MarkerSize', 35);
plot(Xc_kriging, Yc_kriging, '--k', 'LineWidth', 3);
plot(xplot, ye_co', 'color', [0 0.75 0], 'LineWidth', 3, ...
    'LineStyle', '--');
plot(Xe_test, Ye_test, 'k.', 'MarkerSize', 30);

% Add legend and labels
l = legend('$y_c$', '', '$y_e$', 'Kriging', 'Co-Kriging', ...
    'Validation', 'Location', 'Northoutside', ...
    'Orientation', 'horizontal');
set(l, 'interpreter', 'latex', 'fontsize', marker);
xlabel('$x$', 'FontSize', nfonte, 'interpreter', 'latex');
ylabel('$y$', 'FontSize', nfonte, 'interpreter', 'latex');
set(gca, 'FontSize', nfonte, 'TickLabelInterpreter', 'latex', ...
    'LineWidth', 1.5);
box on
xlim([min(Xe) max(Xe)]);
xticks(-12:4:12);
ylim([-15 15]);
yticks(-15:5:15);
grid on;

% Display optimized parameters
fprintf('pc = %f \n', pc);
fprintf('pd = %f \n', pd);
fprintf('thetac = %f \n', thetac);
fprintf('thetad = %f \n', thetad);
fprintf('rho = %f \n', rho);
fprintf('lambda_c = %f \n', lambda_c);
fprintf('lambda_d = %f \n', lambda_e);
```

A.2. HYPER-PARAMETERS ESTIMATION FUNCTIONS

A.2.1 Cheap model

```
function NegLnLikec=likelihoodc(x)
% NegLnLikec=likelihoodc(x)
%
% Calculates the negative of the concentrated ln-likelihood
% of the cheap data
%
% Inputs:
%   x - vector of log(theta) parameters
%
% Global variables used:
%   ModelInfo.Xc - n x k matrix of sample locations
%   ModelInfo.yc - n x 1 vector of observed data
%
% Outputs:
%   NegLnLike - concentrated log-likelihood *-1 for minimising
%
% Copyright 2007 A I J Forrester
%
global ModelInfo
Xc=ModelInfo.Xc;
yc=ModelInfo.yc;
nc=size(Xc,1);
thetac=10.^x(1);
pc=x(2);
lambda_c = x(3);
one=ones(nc,1);
PsicXc=zeros(nc,nc);
for i=1:nc
    for j=i+1:nc
        PsicXc(i,j)=exp(-sum(thetac.*abs(Xc(i,:)-Xc(j,:)).^pc));
    end
end
PsicXc=PsicXc+PsicXc'+eye(nc)+eye(nc).*eps;
PsicXc = PsicXc + lambda_c * eye(nc);
[U,p]=chol(PsicXc);
if p>0
    NegLnLikec=100;
else
LnDetPsicXc=2*sum(log(abs(diag(U))));
muc=(one'*(U\(U'\yc)))/(one'*(U\(U'\one)));
```

```
41 SigmaSqrc=(yc-one.*muc)'*(U\(U'\(yc-one.*muc)))/nc;
42 NegLnLikec=-1*(-(nc/2)*log(SigmaSqrc)-0.5*LnDetPsicXc);
43 end
```

A.2.2 Difference model

```
1  function NegLnLiked=likelihoodd(x)
2  % NegLnLiked=likelihoodd(x)
3  %
4  % Calculates the negative of the concentrated ln-likelihood of the
5  % difference model
6  %
7  % Inputs:
8  %   x - vetor of log(thetad) parameters
9  %
10 % Global variables used:
11 %   ModelInfo.Xe - ne x k matrix of expensive sample locations
12 %   ModelInfo.ye - ne x 1 vector of expensive observed data
13 %   ModelInfo.yc - nc x 1 vector of cheap observed data
14 %
15 % Outputs:
16 %   NegLnLiked - concentrated ln-likelihood *-1 for minimising
17 %
18 % Copyright 2007 A I J Forrester
19 %
20 global ModelInfo
21 Xe=ModelInfo.Xe;
22 ye=ModelInfo.ye;
23 yc=ModelInfo.yc;
24 ne=size(Xe,1);
25 k=size(Xe,2);
26 thetad=10.^x(1);
27 rho=x(2);
28 pd = x(3);
29 lambda_e = x(4);
30 one=ones(ne,1);
31
32 % Pre-allocate memory
33 PsidXe=zeros(ne,ne);
34
35 % Build upper half of correlation matrix
36 for i=1:ne
37     for j=i+1:ne
38         PsidXe(i,j)=exp(-sum(thetad.*abs(Xe(i,:)-Xe(j,:)).^pd));
```

```
    end
end

% Add upper and lower halves and diagonal of ones plus
% small number to reduce ill-conditioning
PsidXe=PsidXe+PsidXe'+eye(ne)+eye(ne).*eps;
PsidXe = PsidXe + eye(ne,ne)*lambda_e;

% Cholesky factorisation
[U,p]=chol(PsidXe);

% Use penalty if ill-conditioned
if p>0
    NegLnLiked=1e4;
else
    % Sum lns of diagonal to find ln(abs(det(Psi)))
    LnDetPsidXe=2*sum(log(abs(diag(U))));

    % Difference vector
    d=ye-rho.*yc(end-ne+1:end);

    % Use back-substitution of Cholesky instead of inverse
    mud=(one'*(U\(U'\d)))/(one'*(U\(U'\one)));
    SigmaSqrd=(d-one.*mud)'*(U\(U'\(d-one.*mud)))/ne;
    NegLnLiked=-1*(-(ne/2)*log(SigmaSqrd)-0.5*LnDetPsidXe);
end
```

A.3. CO-KRIGING REGRESSION FUNCTION

```
%-------------------------------------------------------------------
% Description:
% This script implements the co-kriging regression, adapted from
% Multi-fidelity optimization via surrogate modelling - Forrester,
% Sobester and Keane (2007)
%-------------------------------------------------------------------
% Author: Henrique Cordeiro Novais
%-------------------------------------------------------------------
% Outputs:
%                 ye_co: co-Kriging regression estimator
%                     s: estimated mean-squared error
%-------------------------------------------------------------------
% Inputs:
%               Xc, Yc: cheap data samples
%               Xe, Ye: expensive data samples
```

```
% pc, thetac, lambda_c: hyper-parameters of the cheap data
% pd, thetad, lambda_e: hyper-parameters of the difference model
%                  rho: scaling factor
%                yc_xe: cheap data evaluated at expensive samples
%                xplot: range for the regression
%--------------------------------------------------------------------
function [ye_co, s] = cokriging_regression(Xc,Yc,pc, thetac, ...
    lambda_c,Xe,Ye,pd,thetad,rho,lambda_d,yc_xe,xplot)

% Working with A
Xc = Xc';
[nc, ~] = size(Xc);
PsiC_xc_xc = zeros(nc,nc);
one = ones(nc,1);

for i=1:nc
    for j=1:nc
        PsiC_xc_xc(i,j) = exp(-thetac*(abs(Xc(i) - Xc(j))^pc));
    end
end

Yc = Yc';
mic = (one'*pinv(PsiC_xc_xc + eye(nc,nc)*lambda_c)*Yc) / (one'*pinv ...
    (PsiC_xc_xc + eye(nc,nc)*lambda_c)*one);
sigma2c = ((Yc-one*mic)' * pinv(PsiC_xc_xc + eye(nc,nc)*lambda_c) * ...
    (Yc-one*mic))/(nc);

% Working with B
[ne, ~] = size(Xe);
PsiC_xc_xe = zeros(nc,ne);

for i=1:nc
    for j=1:ne
        PsiC_xc_xe(i,j) = exp(-thetac*(abs(Xc(i) - Xe(j))^pc));
    end
end

% Working with C
for i=1:ne
    for j=1:nc
        PsiC_xe_xc(i,j) = exp(-thetac*(abs(Xe(i) - Xc(j))^pc));
    end
end

% Working with D
for i=1:ne
    for j=1:ne
```

```
        PsiC_xe_xe(i,j) = exp(-thetac*(abs(Xe(i) - Xe(j))^pc));
    end
end

PsiD_xe_xe = zeros(ne,ne);

one = ones(ne,1);

for i=1:ne
    for j=1:ne
        PsiD_xe_xe(i,j) = exp(-thetad*(abs(Xe(i) - Xe(j))^pd));
    end
end

d = Ye - rho.*yc_xe';
mid = (one'*pinv(PsiD_xe_xe + eye(ne,ne)*lambda_d)*d) / (one' ...
    *pinv(PsiD_xe_xe + eye(ne,ne)*lambda_d)*one);
sigma2d = ((d-one*mid)' * pinv(PsiD_xe_xe + eye(ne,ne)*lambda_d) * ...
    (d-one*mid)) / (ne);

% Complete Covariance Matrix Cm = [A B; C D]
A = sigma2c * (PsiC_xc_xc + eye(nc,nc)*lambda_c);
B = rho * sigma2c * (PsiC_xc_xe + [zeros(nc-ne,ne); eye(ne,ne)] * ...
    lambda_c);
C = rho * sigma2c * (PsiC_xe_xc + [zeros(ne,nc-ne) eye(ne,ne)] * ...
    lambda_c);
D = ((rho^2) * sigma2c * (PsiC_xe_xe + eye(ne,ne)*lambda_c)) + ...
    (sigma2d * (PsiD_xe_xe + eye(ne,ne)*lambda_d));
Cm = [A B; C D];

% Expensive estimator Ye(x)
y = [Yc; Ye];
for n=1:length(xplot)
    fprintf('%d / %d \n',n,length(xplot));
    for i=1:nc
        corr1(i,1) = exp(-thetac*(abs(Xc(i) - xplot(n))^pc));
    end

    for i=1:ne
        corr2(i,1) = exp(-thetac*(abs(Xe(i) - xplot(n))^pc));
        corr3(i,1) = exp(-(thetad*(abs(Xe(i) - xplot(n))^pd)));
    end

    above = rho * sigma2c * corr1;
    below = ((rho^2) * sigma2c * corr2) + (sigma2d * corr3);
    c = [above; below];
    mi = (ones(1,length(Cm)) * pinv(Cm) * y) / (ones(1,length(Cm)) * ...
```

```
110          pinv(Cm) * ones(length(Cm),1));
111
112      ye_co(n) = mi + ((c)' * pinv(Cm) * (y - ones(length(Cm),1)*mi));
113      s(n) = abs( ((rho^2)*sigma2c*(1+lambda_c)) + (sigma2d*lambda_d) - ...
114          (c'*pinv(Cm)*c) );
115  end
```